Vector boson pair production at hadron colliders

A thesis presented for the degree of
Doctor of Philosophy
by

Katherine Louise Adamson

Institute for Particle Physics Phenomenology
Department of Physics
University of Durham
September 2002

Abstract

We calculate the contribution of gluon-gluon induced processes to vector boson pair production at hadron colliders, specifically the production of WZ, $W\gamma$ and $Z\gamma$ pairs. We calculate the tree level processes $gg \to WZq\bar{q}$, $gg \to W\gamma q\bar{q}$ and $gg \to Z\gamma q\bar{q}$, and the one loop process $gg \to Z\gamma$. We use the helicity method and include the decay of the W and Z bosons into leptons in the narrow width approximation. We include anomalous triple gauge couplings in all of our vector boson pair production calculations.

In order to integrate over the $q\bar{q}$ final state phase space we use an extended version of the subtraction method to NNLO and cancel collinear singularities explicitly. The general subtraction terms that are obtained apply to all vector boson pair production processes.

Due to the large gluon density at low x, the gluon induced terms of vector boson pair production are expected to be the dominant NNLO QCD correction, relevant at LHC energies. However, we show that due to a cancellation they turn out to provide a rather small contribution, anticipating good stability for the perturbative expansion. This contribution remains small even when anomalous couplings are added, and when one considers energies far above the energies of currently planned hadron colliders.

Declaration

I declare that no material presented in this thesis has previously been submitted for a degree at this or any other university.

The research described in this thesis has been carried out in collaboration with Dr Adrian Signer and Dr Daniel de Florian. Publications corresponding to the work in this thesis are:

- *Gluon induced contributions to WZ and $W\gamma$ production at NNLO.*
  K. L. Adamson, D. de Florian and A. Signer, Phys.Rev. D65, 094041

- *Gluon induced contributions to $Z\gamma$ production at NNLO.*
  K. L. Adamson, D. de Florian and A. Signer, in preparation.

Acknowledgements

First and foremost in any acknowledgements must be my supervisor, Adrian Signer, who has shown immense patience in helping me over all the hurdles of this degree, and has been a fun collaborator. Daniel de Florian deserves credit for carrying out a fruitful collaboration over many thousands of miles – maybe we will meet in person some day!

I would like to thank everyone at the IPPP for making this PhD a good experience, and mention particularly James Stirling for his support in the early stages. My IPPP contemporaries, Jeppe Andersen, Lee Garland and Neil Pomeroy, and James Gregory in the maths department, have been on hand for shared experiences, conversations and mutual commiserations over thesis stress. My CPT friends who finished their PhDs before me deserve credit for being an inspiration, proving that particle physicists are actually capable of getting jobs, and often providing useful places to stay around Europe. Those people who still have years to go have provided a great escape from the stress of the third-year office.

Other people have contributed to my time in Durham, especially Aileen Congreve and all the people from Fonteyn Court (Liz White in particular), who somehow managed to put up with living with me. I'd like to thank everyone who participated in my long-running quiz in GradSoc, especially Stu Cherry for handing over the quiz into my care, and Jon Levell for ably taking over from me this year. I would also like to mention Oona Leppington, Ruth Carey and all of Durham University Belly Dance Society for some seriously relaxing extra curricular activities.

Thanks go to Richard Gregson for proofreading this thesis (the remaining mistakes are all mine) and keeping me sane throughout.

Finally, I would like to thank my family for all their support over the last 24, nearly 25, years. This thesis is dedicated to the memory of my mother.

Contents

List of Figures

Overview

This thesis discusses vector boson pair production at hadron colliders, focussing on the gluon-gluon induced components of WZ, $W\gamma$ and $Z\gamma$ production.

In chapter 1, we discuss the motivations for the thesis topic. The general features of vector boson pair production are described, with reference to the previous literature. We also discuss anomalous couplings and the means of investigating them through the study of vector boson pair production. We explain why one may now wish to focus on the (next-to-next-to-leading order) gluon-gluon induced part of vector boson pair production, and how this may add to previously known results.

In chapter 2, we review the helicity method, and outline the basic method of calculating the helicity amplitudes used in this thesis. The calculation of the helicity amplitudes themselves is given in chapter 3. This covers tree level WZ, $W\gamma$ and $Z\gamma$ production in detail, including electroweak couplings, and the changes that must be made to incorporate anomalous couplings in our results. The required helicity amplitudes are included in Appendix B. We also calculate the one loop gluon-gluon induced production of $Z\gamma$, which consists of a box diagram in the Standard Model, plus a triangle diagram in the anomalous coupling case.

In chapter 4, we discuss the removal of infrared singularities from our amplitudes, by means of the subtraction method. We introduce the principles of the subtraction method, and the particular version that we use, then perform a general calculation that applies to all vector boson pair production processes.

The results of these calculations are presented and investigated in chapter 5. We draw conclusions from this work, as well as suggesting future work, in chapter 6.

Chapter 1

Introduction to vector boson pair production

Vector boson pair production is expected to be a particularly interesting process at future hadron colliders, and is the primary subject of this thesis. In this chapter, we will outline the main motivations for the study of vector boson pair production at hadron colliders, with reference to the literature. In particular, we explain why we choose to calculate the $\mathcal{O}(\alpha_s^2)$ production channel $gg \to V_1 V_2\,(+q\bar{q})$.

We use V_1 and V_2 to represent the two vector bosons, where V_1 and V_2 may be W, Z or γ. These may be accompanied by quark or gluon jets in the final state.

1.1 Motivation for studying vector boson pair production

The study of vector boson pair production is an interesting field, which is expected to become especially relevant in the next few years with results from the Tevatron Run II [1] and especially the LHC [2]. Here we will discuss why vector boson pairs are worth studying and will review the current experimental status, and discuss the developments that are anticipated at the new hadron colliders.

The production of vector boson pairs is interesting both as a process in its own right and as a background for other processes. The most notable feature of vector boson pair production is the presence of a triple gauge vertex. It is possible for two vector bosons to be emitted through coupling to another vector boson in a triple gauge vertex, even at leading order. The fact that this occurs at leading order and not just in higher order corrections makes it easier for the vertex to be probed experimentally.

The triple gauge vertex is interesting because it is a non-abelian vertex that is accessible to experimental study. In testing this vertex, we test the gauge group of the Standard Model, as this vertex is a direct prediction of $SU(3) \times SU(2) \times U(1)$. No variations of this vertex from the Standard Model have yet been detected, but the bounds on possible deviations should be improved by the increased rate of production of vector boson pairs in future experiments. As yet, the triple gauge vertex has been much less precisely measured than, for example, the couplings of gauge bosons to fermions, so it is still a good place to look for non-Standard Model effects.

Any variation of a triple gauge vertex from the Standard Model prediction would suggest the presence of new physics. New physics occurring at a high energy could influence the triple gauge coupling through virtual effects. In section 1.4 we will discuss the parameterisation of a vertex that varies from the Standard Model, and the kinds of new physics that may cause it. It is as a probe of this new physics that vector boson pair production is most exciting.

Vector boson pair production is also relevant as the background to other processes, including the decidedly contemporary topic of Higgs physics. Vector boson pair production becomes an important background to Higgs production when the Higgs is heavy. A Higgs of greater than 180 GeV decays predominantly to WW (branching ratio about 75%) and ZZ (branching ratio about 20%) [3]. $Z\gamma$ is also a comparatively rare decay mode of the Higgs, which is significant between 100 GeV and 160 GeV. It is therefore necessary to have a good Standard Model prediction of vector boson pair production in order to deal with the background to Higgs searches in these regions.

Vector boson pair production is also a possible background for certain supersymmetric processes. The trilepton signal (three leptons plus missing momentum) is considered to be one of the cleanest signals for observing supersymmetric particles in the mSUGRA model [4] [5]. It is clear that the leptonic decay of a WZ pair is a major background to this process.

So, even if evidence for new physics is not seen directly in vector boson pair production, predictions for vector boson pair production are likely to be important as a background to some of the most interesting physics advances of the next few years.

The current experimental knowledge of vector boson pair production processes comes from e^+e^- collisions at LEP and hadron collisions in the Tevatron Run I. As in most processes, e^+e^- colliders and hadron colliders have been complementary in this study, with e^+e^- colliders having the advantage of a precisely known initial state energy, while hadron colliders can reach a higher centre of mass energy.

For the production of vector boson pairs, this high centre of mass energy is very important. It takes a lot of energy for two vector bosons to be produced, especially if they are massive, and this has restricted the number of events that have been studied. The rates of production for vector boson processes will be substantially increased at the new run of the Tevatron, and hugely increased at the LHC.

A number of results concerning vector boson pair production were obtained at LEP, where WW and ZZ production in particular were studied [6]. Limits were set on the triple gauge couplings through these processes [7]: these will be discussed further in section 1.4.

Vector boson pair production has also already been studied in Run I of the Tevatron [1][8] . Here the most studied production channel was $W\gamma$ production, where the W decays into an electron or a muon, with around 100 events for each experiment (CDF and D0). Also studied were WW, WZ and $Z\gamma$, with leptonic decays, and WW and WZ where one of the leptons decayed into jets. It is expected that Run II will improve these results [1]. As well as a substantial increase in rates of production, one can expect that detector upgrades and improved analysis will also lead to better results.

We can also look forward to significantly increased vector boson pair production at future colliders [9]. The LHC will certainly be a useful arena for studying vector boson pair production, much improving Tevatron results. Here, the best means for looking at charged triple gauge couplings is through $W\gamma$ and WZ production [2]. WW production is more difficult to distinguish from the background. Considering only leptonic decays of the W and Z and making appropriate cuts to reduce the background, we would expect to see about 3000 $W\gamma$ and 1200 WZ events for an integrated luminosity of 30 fb^{-1} [2].

Of course, any future linear collider would also improve the results through increased energy and polarisation, and would also have the advantage of a cleaner signal. However, this is likely to be well in the future. For now, we will concentrate on the present and upcoming hadron collider processes.

To summarise, vector boson pair production is valuable both as a probe for new physics and as a background. We have mentioned some of the experimental studies that have been carried out so far, and described some of the physics that may emerge from future ones. We will now discuss the theoretical studies of vector boson pair production, including the motivation for our own theoretical study.

1.2 Previous studies of vector boson pair production

The tree level production of vector boson pairs, $q\bar{q} \to V_1 V_2$, was calculated some time ago for all pairs of vector bosons that we want to look at [10][11][12]. In these calculations, spin states were summed over: the decay of the vector bosons was not included. Similar calculations were then made at the $\mathcal{O}(\alpha_s)$ level. Here, it was sometimes necessary to include loop diagrams as well as tree level, and both possible initial states, $q\bar{q}$ and qg, had to be included. Results were obtained for WW [13][14], ZZ [15][16], $W\gamma$ and $Z\gamma$ [17][18], and WZ [19][20]. Again, spin states were summed over.

We have already mentioned the fact that electroweak couplings are spin dependent. In order to compare theory and experiment, we want to include the decay of the vector bosons, as it is the decay products that we will see in the detector. By including the decay products, we can add arbitrary cuts to the final state and so compare with experiment. We choose to study the decay of the vector bosons into leptons (rather than hadrons) as this process is easier to distinguish experimentally. We also want to retain as much information as possible about the process, including the helicity of the decay products. In order to keep track of the spins of all external particles, we shall calculate amplitudes in the helicity method, as described in chapter 2. This is particularly useful in performing calculations with many external particles.

Calculating vector boson pair production while including decay products can give interesting results. The tree level results for vector boson pair production including decay into leptons were initially given by Gunion and Kunszt [21], where angular correlations in the final state were discussed for the first time.

One loop results including decay into leptons were initially obtained with spin information in the real but not in the virtual part [22][23][24]. Analytic amplitudes including all spin information were given in [25] and these amplitudes were used in the calculation of numerical results in [26] and [27].

All these calculations were carried out with decays included in the narrow width approximation. Here both vector bosons are assumed to be on shell: the diagrams are 'doubly-resonant'. Some available calculations extend this by including singly-resonant as well as doubly-resonant diagrams [28], and by including one loop logarithmic electroweak calculations [29]. However, we will continue to use the narrow width approximation and will not include higher order electroweak terms.

We wish to calculate the process $gg \to V_1V_2\,(+q\bar{q})$, which includes one loop and tree level terms. Some calculations are already available. The loop diagrams for $gg \to Z\gamma$ were calculated long ago [30], but without including decay of the Z into leptons. No loop diagrams are required for gluon-gluon induced WZ or $W\gamma$ production. The general tree level vector boson pair production terms, $gg \to V_1V_2q\bar{q}$, have also been calculated [31] but with the requirement that two jets be seen in the final state. We will generalise this by integrating over the whole phase space for the vector boson pair production process.

1.3 Motivation for the study of gluon-gluon induced terms

The original work presented in this thesis is a calculation of the gluon-gluon contribution to vector boson pair production, $gg \to V_1V_2\,(+q\bar{q})$, where V_1 and V_2 are the two vector bosons. This is calculated for WZ, $W\gamma$ and $Z\gamma$ final states.

The gluon-gluon initial state first contributes to vector boson pair production at NNLO. We explain the motivation for including an NNLO term in the calculation of vector boson pair production, and for selecting the gluon-gluon induced part.

Before we consider adding an NNLO term to the calculation, we have to consider the LO and NLO terms. The papers in which these were calculated have been listed in subsection 1.2. We will look at the qualitative features of plots of the LO and NLO results. In chapter 5 these plots will be discussed again more thoroughly: all details such as cuts and parton distributions are given in the relevant parts of chapter 5.

The leading order term of vector boson pair production is straightforward. The initial state partons can only be $q\bar{q}$ (a gluon would lead to a factor of α_s). The two vector bosons V_1 and V_2 couple directly to the quark line, or come from an intermediate particle via a triple gauge vertex: both options are shown in figure 1.1. Each outgoing vector boson may be a photon, in which case it is treated as an external particle, or a W or Z, with the decay of the particle included. The leading order diagrams for the WZ production process are given in figure 1.1 as an example.

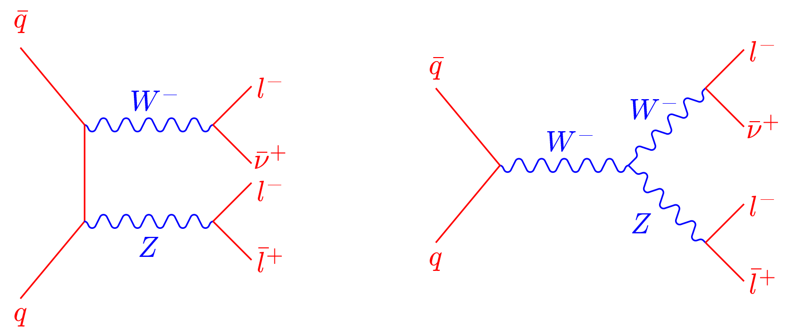

Figure 1.1: Leading order diagrams for WZ production

The NLO terms are slightly more involved. We can decompose the NLO ($\mathcal{O}(\alpha_s)$) contribution to vector boson pair production into two parts.

Firstly, there are the processes with a $q\bar{q}$ initial state: the one loop diagrams for $q\bar{q} \to V_1V_2$, plus the tree-level process with an extra gluon in the final state, $q\bar{q} \to V_1V_2g$.

Secondly, we have a new channel at NLO with the initial state qg, giving the process $qg \to V_1V_2q$. In this qg, q can be either a quark or an antiquark.

The NLO tree level diagrams for WZ production are shown in figure 1.2 for both the qg and $q\bar{q}$ initial states. Two examples of loop diagrams with a $q\bar{q}$ initial state are given in figure 1.3.

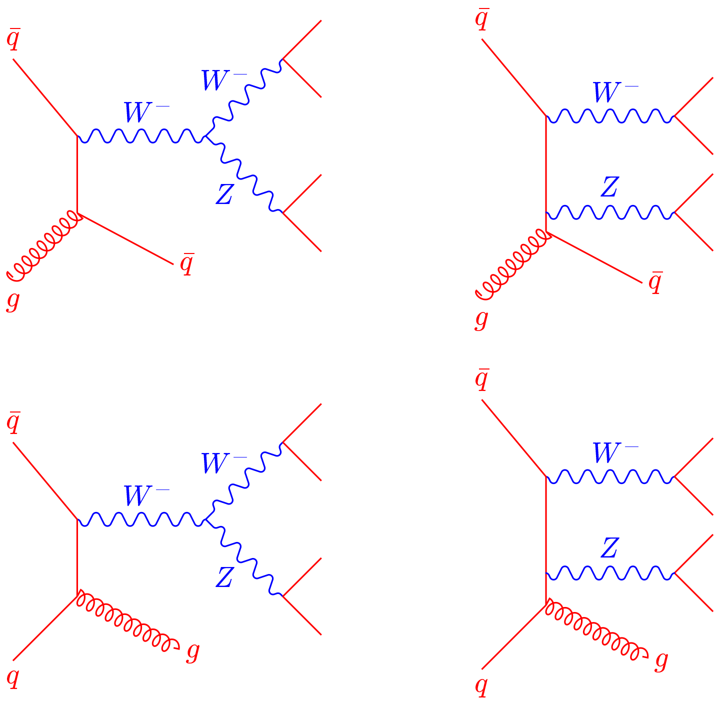

Figure 1.2: Tree level NLO diagrams for WZ production

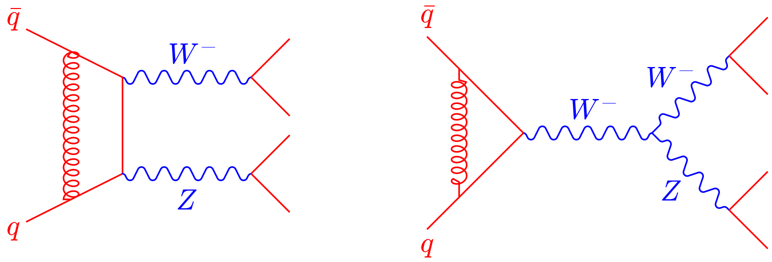

Figure 1.3: Some NLO loop diagrams for WZ production

The numerical contribution of the NLO part proves to be very significant. The correction to the LO result is very large, with the NLO part being considerably larger than the LO contribution in certain regions. For example, regions of high transverse momentum may lead to NLO contributions that are several times the LO result. This can be seen in figure 1.4 (this is the same as figure 5.1 and is further discussed in chapter 5). We show a transverse momentum distribution for WZ production, plotting the p_T of the lepton that results from the decay of the W. This is separated into LO and NLO parts. It can be seen that the NLO part is substantial, especially at high p_T.

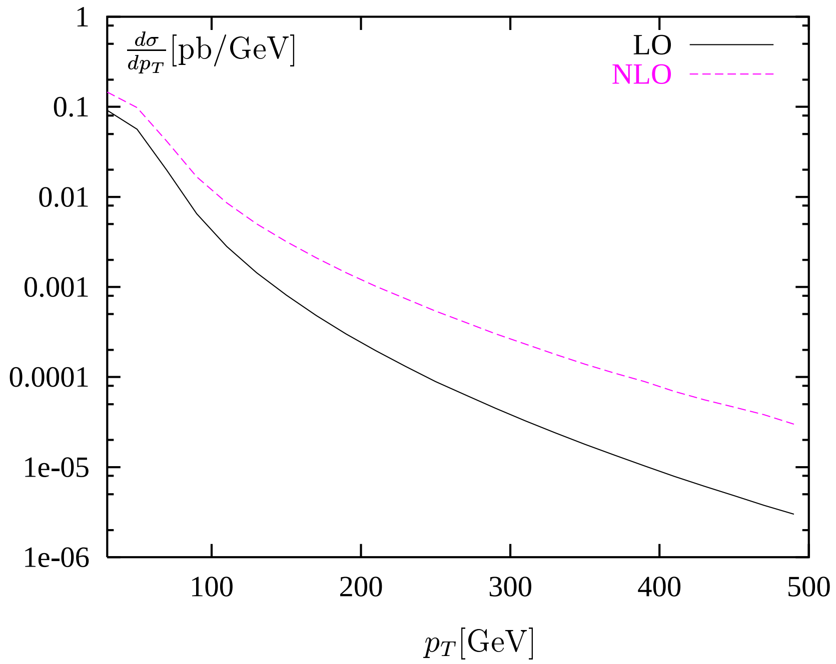

Figure 1.4: Comparing LO and NLO contributions to WZ production

As these regions are also where one might expect to best see the effects of anomalous couplings caused by physics beyond the Standard Model, it is important to have good Standard Model theoretical predictions in order to distinguish these from higher order Standard Model effects (see section 1.4 for a discussion of anomalous couplings and section 5.3 for anomalous coupling results). It is clear that the leading order result is not a good approximation to the overall vector boson pair production, and that including the NLO part is imperative.

An alternative approach to this would be to cut out the NLO term by using a jet veto (cutting out all jets above a certain energy). While this is quite effective in obtaining a result that approximates to the LO result, it also drastically reduces the number of useful events. Including the NLO part and allowing jets seems to be the preferable option.

In calculating the NLO contribution, we may consider the two channels separately, comparing the size of the contribution from the term with the $q\bar{q}$ initial state to that with the qg initial state. These are compared to each other and to the LO term in figure 1.5, which is figure 5.2 of chapter 5 and is further discussed there.

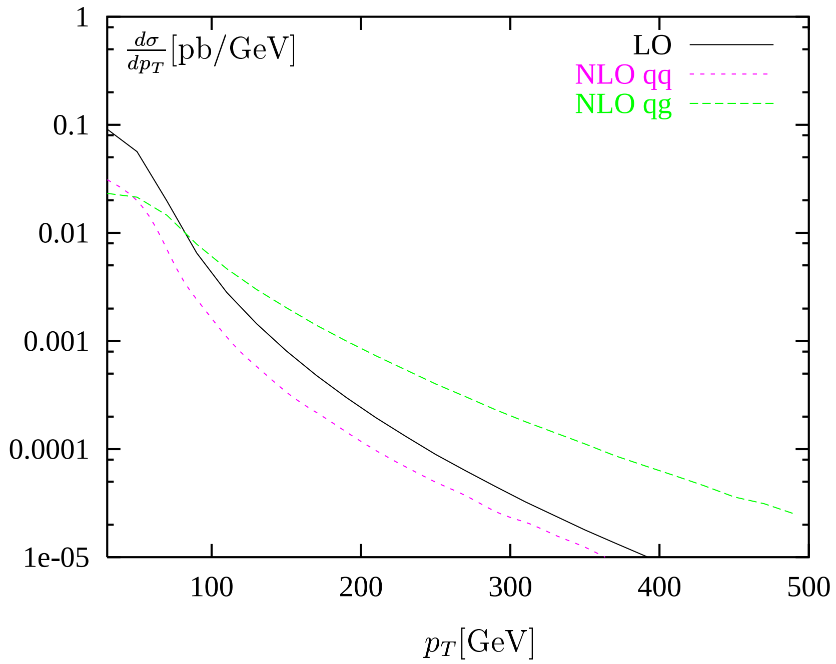

Figure 1.5: Comparing $q\bar{q}$ and qg NLO contributions to WZ production

The contribution from the qg initial state at NLO is substantially bigger than the NLO $q\bar{q}$ initial state. This is because, at the high energies reached at the LHC, the gluon density will become large. The gluon density can enhance the NLO qg term so that it becomes at least as large as the LO term, despite being suppressed by α_s.

The fact that the NLO terms are often of similar size to the LO terms would suggest that calculating to a further order in α_s (a NNLO calculation) would be advisable. It is clear that we do not have the resources to perform a full NNLO calculation. This would include two-loop calculations that are not currently available. As well as loop contributions, a full NNLO calculation would include tree diagrams with quark initial states, $q\bar{q} \to V_1 V_2 gg$, as well as terms with qg and gg initial states.

With this in mind, we therefore choose to make an analogy with the NLO term. In the NLO case, it is the new channel, the qg induced term, that gives a very large result, which can be as big or bigger than the LO term. The $q\bar{q}$ term, in contrast, is quite small, as would normally be expected of a higher order correction. We can see that the new channel with the gluon in the initial state is definitely the dominant term.

Therefore, for the NNLO case we choose to examine the new channel, which has two gluons in the initial state. We make a hypothesis that this term may be important, as the qg term was important at NLO. The gluon density may again be enough to cancel the suppression in α_s^2.

The processes with a gg initial state are $gg \to V_1 V_2$, which does not exist at tree level but may contribute as a loop diagram, and the tree level process $gg \to V_1 V_2 q\bar{q}$.

In this thesis, we will calculate gluon-gluon induced vector boson pair production, with some unexpected results.

1.4 Anomalous couplings and new physics

In the earlier part of this chapter, it was indicated that one of the major motivations for the study of vector boson pair production is the search for new physics through deviations from the Standard Model in triple gauge boson couplings. We will now discuss anomalous (non-Standard Model) triple gauge couplings, and how to use these in a parameterisation of general new physics effects. We will present the relevant Lagrangians and vertices, discuss form factors, and review some previous studies of anomalous couplings in vector boson pair production.

1.4.1 Principles of the anomalous coupling approach

In using the anomalous coupling approach to the detection of new physics effects, we make a number of assumptions. First of all, it is assumed that any new physics only has an effect on the triple gauge couplings. It will always be assumed that while gauge bosons may couple anomalously to each other, all couplings of gauge bosons to quarks and leptons are the normal Standard Model ones. We assume that the new physics is only to be detected through changes in the triple gauge couplings and that new physics will not be seen directly in the production of new particles. The implies that the new physics occurs at an energy much higher that the current experimental scale: we will call this new physics scale Λ.

The basic principle is that high-energy new physics effects can influence lower-energy processes through virtual effects. Deviations from the Standard Model couplings would affect both the overall cross section for the appropriate vector boson pair production and the angular distributions. The fact that new physics is expected to occur at a scale much above the energies that can be measured implies that it is appropriate to take an effective Lagrangian approach. We add new parameters ('anomalous couplings') to the appropriate Lagrangian. The couplings are modified by this but no new particles are introduced.

We will not discuss the principles of effective theories here: instead we will just make use of known effective Lagrangians. All we will therefore need is the appropriate vertices, including the anomalous parameters that describe the variation from the Standard Model.

We will state the appropriate Lagrangians for the triple gauge couplings that we consider. We will also explain how we selected the parameters that we use, and give the vertices that contribute in the Feynman diagram calculation. These vertices and the resulting diagrams are further discussed when we add anomalous couplings to our calculations in chapter 3.

1.4.2 Lagrangians and vertices with anomalous couplings

In this section we will describe the parameterisation of anomalous couplings that we will use. This should be as general as possible, and not dependent on a particular model. We do not know what kind of new physics to expect, because for the effective Lagrangian approach to be appropriate, the new physics will be at an energy that is not directly accessible. Therefore we want to keep as many coupling terms as possible, balancing this with a desire not to overcomplicate the calculation. If we have a great many parameters, it will be more difficult to set bounds for them.

We do make certain restrictions on the possible couplings. Lorentz invariance is always required, as is electromagnetic ($U(1)_{em}$) gauge invariance. We also assume that only the lowest dimension operators will contribute significantly, with higher dimension operators being much suppressed. If the scale of new physics, Λ, is much greater than $\sqrt{\hat{s}}$ – as is required for the effective Lagrangian approach – only the operators of lowest dimension should be important and those of higher dimension can be neglected.

We then have further choices to make when we consider the specific parameterisations of the different triple gauge couplings. We will first consider charged triple gauge boson couplings (WWZ and $WW\gamma$), and then neutral triple gauge boson couplings ($ZZ\gamma$, $Z\gamma\gamma$). There is another neutral triple gauge coupling (ZZZ) but this will not be required in our calculations later in this thesis. The WWZ and $WW\gamma$ couplings will be required for WZ and $W\gamma$ production respectively, and the $ZZ\gamma$ and $Z\gamma\gamma$ couplings for $Z\gamma$ production.

The WWZ and $WW\gamma$ triple couplings already exist in the Standard Model. We modify them by including new parameters, chosen to be as general as possible.

Taking only the operators of lowest dimension, one obtains an effective Lagrangian with 7 parameters. This is as given by Hagiwara et al [32]. We will use their parameterisation throughout our discussion of anomalous couplings. Using V to denote Z or γ, the Lagrangian is:

$$\begin{aligned}\mathcal{L}_{WWV}/g_{WWV} &= ig_1^V(W^*_{\mu\nu}W^\mu V^\nu - W^{*\mu}V^\nu W_{\mu\nu}) + i\kappa^V W^*_\mu W_\nu Z^{\mu\nu} \\ &+\frac{i\lambda^V}{M_W^2}W^*_{\rho\mu}W^\mu_\nu V^{\nu\rho} - g_4^V W^*_\mu W_\nu(\partial^\mu V^\nu + \partial^\nu V^\mu) \\ &+g_5\varepsilon^{\mu\nu\lambda\rho}(W^*_\mu\partial_\lambda W_\nu - \partial_\lambda W^*_\mu W_\nu)V_\rho \\ &+i\tilde{\kappa}_V W^*_\mu W_\nu \tilde{V}^{\mu\nu} + i\frac{\tilde{\lambda}_V}{M_W^2}W^*_{\lambda\mu}W^\mu_\nu\tilde{V}^{\nu\lambda} \qquad (1.1)\end{aligned}$$

Here $V_{\mu\nu} = \partial_\mu V_\nu - \partial_\nu V_\mu$ and $\tilde{V}^{\mu\nu} = \frac{1}{2}\varepsilon_{\mu\nu\alpha\beta}V^{\alpha\beta}$. The overall couplings are straightforward: $g_{WW\gamma} = -e$ and $g_{WWZ} = -e\cot\theta_W$.

When carrying out calculations, we shall not retain all 7 parameters, but instead choose to select parameters by their symmetries. In the above parameterisation of

WWZ and $WW\gamma$ couplings, three of the couplings, g_1^V, κ^V and λ_V, obey both C and P symmetries. $\tilde{\kappa}^V$ and $\tilde{\lambda}^V$ obey C but are P violating. g_4^V violates C but obeys P and g_5^V violates C but is CP invariant.

We shall use only those parameters that are invariant under both C and P. This simply serves to reduce the number of parameters involved and is not a necessary choice.

The $W_\alpha^+(p_+)W_\beta^-(p_-)V_\mu(q)$ vertex that we shall use is [33]:

$$\begin{aligned}\Gamma_{WWV}^{\alpha\beta\mu}(p_+,p_-,q) &= (p_+-q)^\alpha g^{\beta\mu}\frac{1}{2}(g_1^V+\kappa^V+\lambda^V\frac{p_-^2}{M_W^2}) \\ &+(q-p_-)^\beta g^{\alpha\mu}\frac{1}{2}(g_1^V+\kappa^V+\lambda^V\frac{p_+^2}{M_W^2}) \\ &+(p_+-p_-)^\mu(-g^{\alpha\beta}\frac{1}{2}\frac{q^2\lambda^V}{M_W^2}+\frac{\lambda^V}{M_W^2}p_+^\alpha p_-^\beta) \qquad (1.2)\end{aligned}$$

g_1^γ is always 1 by electromagnetic gauge invariance. The other parameters are chosen appropriately. One may make assumptions about relations between these parameters (for example, that they are the same for Z and γ) or choose them freely.

The parameterisation for $ZZ\gamma$ and $Z\gamma\gamma$ couplings is somewhat different. These couplings do not exist at all in the Standard Model. Any triple coupling that does occur is entirely anomalous. These couplings and the use of them are described well in [34].

The Lagrangian for this situation is given below. This is the one used by Ellison and Wudka [8] with a factor of i removed to make the expression hermitian. We need to go to terms of higher dimension than those for WWZ and $WW\gamma$, and we do not restrict the symmetries of the parameters to the same extent.

The Lagrangian is:

$$\begin{aligned}\mathcal{L}_{Z\gamma V} &= -e\Bigg((h_1^V F^{\mu\nu}+h_3^V\tilde{F}^{\mu\nu})Z_\mu\frac{(\Box+m_V^2)}{m_Z^2}V_\nu \\ &+(h_2^V F^{\mu\nu}+h_4^V\tilde{F}^{\mu\nu})Z^\alpha\frac{(\Box+m_V^2)}{m_Z^4}\partial_\alpha\partial_\mu V_\nu\Bigg) \qquad (1.3)\end{aligned}$$

As usual, $\Box=\partial_\mu\partial^\mu$. Again V can be either Z or γ. V is the intermediate particle that decays into Z and γ, and can be off-shell. This Lagrangian is not symmetric between the two Zs, hence this symmetry is also not present in the vertex. In the case of a photon decaying to two Zs, it would be necessary to use a different vertex, which also parameterises the anomalous couplings differently.

All the couplings h_i^V are odd under C. h_1^V and h_2^V violate CP, while h_3^V and h_4^V are CP conserving. We retain all 4 of these couplings: it is no longer possible to have C and P conserving parameters as we did for the WWZ and $WW\gamma$ case.

The resulting $Z_\alpha(q_1)\gamma_\beta(q_2)Z_\mu(p)$ vertex is:

$$\begin{aligned}\Gamma^{\alpha\beta\mu}_{Z\gamma Z}(q_1,q_2,p) \;=\;& \frac{i(p^2-q_1^2)}{M_Z^2}\left(h_1^Z(q_2^\mu g^{\alpha\beta}-q_2^\alpha g^{\mu\beta})+\frac{h_2^Z}{M_Z^2}p^\alpha(p\cdot q_2 g^{\mu\beta}-q_2^\mu p^\beta)\right.\\ &\left.-h_3^Z\varepsilon^{\mu\alpha\beta\nu}q_{2\nu}-\frac{h_4^Z}{M_Z^2}\varepsilon^{\mu\beta\nu\sigma}p^\alpha p_\nu q_{2\sigma}\right) \qquad (1.4)\end{aligned}$$

The vertex for $Z_\alpha(q_1)\gamma_\beta(q_2)\gamma_\mu(p)$ is as in equation (3.24), but with $q_1^2\to 0$ and $h_i^Z\to h_i^\gamma$.

1.4.3 Form factors

One unfortunate result of adding anomalous couplings and their associated new terms is that at high energies these new terms violate unitarity when we get near the scale of the new physics (although of course we should not really approach this scale if our effective theory is to be valid). This is not a problem at an electron-positron collider, where collisions occur at a fixed energy, but is an issue at a hadron collider, where one integrates over a range of energies. The new parameters need to be controlled in some way, so that at very high energies they become the Standard Model couplings, and so obey unitarity.

The method that we will use within this thesis is a conventional one. We introduce a 'form factor' which will control the high-energy behaviour of the new terms. This allows the anomalous parameters to remain fairly constant at low energies, but to approach the Standard Model values at higher energies.

$$AC \to \frac{AC}{(1+\hat{s}/\Lambda^2)^n}, \qquad (1.5)$$

Here AC is any anomalous coupling, Λ is the scale of new physics, and n is a parameter to ensure unitarity.

This approach is quite straightforward and often used, and does produce the required behaviour. However, there are a couple of disadvantages. The form factor depends on the scale of the high-energy beyond the Standard Model behaviour. Making a choice of scale takes away some of the model independent behaviour that we were looking for, by forcing us to add extra parameters in a more or less arbitrary manner. Also, if different values for the scale and the parameter n are used in different publications, it can be hard to compare the results.

Bearing in mind these reservations, we did use the form factor approach, taking a standard scale of 2 TeV for new physics, and putting $n = 2$ in equation (1.5).

An application of a non-form-factor approach, with its advantages and disadvantages, is given in [27].

1.4.4 Previous studies of anomalous couplings in vector boson pair production

A number of theoretical and experimental studies of anomalous couplings in vector boson pair production have been made. These may put limits on the size of anomalous couplings based on known experimental results, or may predict the effect of certain anomalous couplings on vector boson pair production at future colliders. We will briefly mention a few of these studies here.

Anomalous couplings vertices like those in section 1.4.2 have been added to vector boson pair production calculations at LO and NLO.

Anomalous couplings were added to LO Standard Model calculations for WW and WZ [35] and $Z\gamma$ [36] production. It was found that the addition of anomalous couplings tend to increase production, especially at high p_T.

NLO QCD corrections were added along with anomalous coupling effects in a series of papers by Baur, Han and Ohnemus for $W\gamma$ [37], WZ [38], WW [39] and $Z\gamma$ [24].

Some review papers deal with the experimental situation [1] [8]. It is possible to put some limits on the size of anomalous couplings. However, one must be careful when comparing results. Often, only one parameter is varied at a time, leaving others at their Standard Model value. If it turns out that several anomalous parameters contribute at once, it may be that they interfere, and therefore that we require looser bounds.

Some limits on anomalous triple gauge couplings as found at LEP are summarised in [40]. More detailed information on triple gauge couplings at LEP is available from the electroweak gauge couplings working group [1]. The LEP results that are quoted use data from W pair production at all four LEP experiments. It is also possible to set limits on the $WW\gamma$ vertex through single W or single photon production.

For the anomalous WWZ and $WW\gamma$ vertices, the parameterisation is the same as in section 1.4.2, and C, P and CP violating terms are neglected. The WWZ and $WW\gamma$ parameters are related, so that there are only three independent couplings [41]. We already know that $g_1^\gamma = 1$ by electromagnetic gauge invariance. $SU(2)_L \times U(1)_\gamma$ symmetry gives the constraints $\kappa_Z = g_1^Z - (\kappa_\gamma - 1)\tan^2\theta_W$ and $\lambda_Z = \lambda_\gamma$. Then the only independent anomalous couplings are g_1^Z, κ_γ and λ_γ.

The value for the couplings from LEP results are found to be:

$$g_1^Z = 0.990^{+0.023}_{-0.024} \qquad \kappa_\gamma = 0.896^{+0.058}_{-0.056} \qquad \lambda_\gamma = -0.023^{+0.025}_{-0.023}, \tag{1.6}$$

recalling that in the Standard Model, $g_1^Z = 1$, $\kappa_\gamma = 1$ and $\lambda_\gamma = 0$.

Limits on these anomalous couplings should improve substantially at the LHC, improving the sensitivity of some couplings by anywhere up to an order of magnitude [2].

Limits have also been set on neutral triple gauge couplings at LEP. The anomalous parameters, h_i, are not related to each other, but are considered separately. Here we give the 'one-dimensional' limits (where all anomalous parameters other than the one in question are set to zero). There is no evidence as yet for the existence of these couplings. Limits are at the 95% confidence level.

$$\begin{array}{ll} -0.056 < h_1^\gamma < 0.055 & -0.045 < h_2^\gamma < 0.025 \\ -0.049 < h_3^\gamma < 0.008 & -0.001 < h_4^\gamma < 0.034 \\ -0.130 < h_1^Z < 0.130 & -0.078 < h_2^Z < 0.071 \\ -0.200 < h_3^Z < 0.070 & -0.050 < h_4^Z < 0.120 \end{array} \tag{1.7}$$

Again, these will be improved at the LHC.

[1]http://lepewwg.web.cern.ch/LEPEWWG/lepww/tgc/

Of course, the triple gauge boson vertex is not the only area in which one may wish to look for anomalous couplings. Different anomalous couplings arise in the gauge boson four-vertex. These anomalous quartic couplings can be studied through processes which involve the production of three vector bosons, such as $WW\gamma$, $ZZ\gamma$ and $Z\gamma\gamma$ production [42]. These processes have been studied at LEP, with no deviation from the Standard Model being found [43] [44]. The anomalous parameters arising in this case, a_0, a_c and a_n, are less constrained than the triple couplings.

In some of the work to follow in this thesis, we will examine the effect of the appropriate anomalous triple gauge couplings on vector boson pair production. In particular, we will investigate whether anomalous couplings are likely to have a substantial effect on the gluon-gluon induced term of vector boson pair production processes.

Chapter 2

Calculations in the helicity method

In this chapter we shall explore the helicity method and its application to vector boson pair production calculations. We will explain why this method was chosen to carry out our calculations, and introduce the notation that will be used for helicity amplitudes in the rest of the thesis. We will then detail the steps that must be taken in performing a helicity amplitude calculation.

2.1 Principles of the helicity method

The helicity method ([45],[46],[47],[48] and many others) is a means of calculating amplitudes, and therefore cross sections, for QCD processes where all external particles are massless. We use the version as described in [49] and [50]. Articles such as [51] and [52] provide a comprehensive overview of the helicity method.

In the helicity method, amplitudes are calculated for fixed helicities of all external particles, with each possible helicity configuration treated as a separate term. In our calculation, we will obtain colour ordered terms, where the ordering of external quarks and gluons is fixed within each term. These colour ordered terms are separately gauge invariant. The colour ordering means that we can take the colour matrices out of the amplitudes, leaving the 'kinematic part'. Calculating the 'colour part' and the 'kinematic part' individually simplifies the procedure. The calculation as a whole is decomposed by colour and helicity.

Even though we need to calculate for each individual helicity configuration, many of these can be related and hence the overall calculation can be reduced. We can split up the amplitudes into gauge invariant subamplitudes, each of which is composed of a subset of diagrams. Relations between these subamplitudes can be used to reduce the amount of calculation required.

In particular, we have the advantage that the kinematic part of the amplitude is just a complex number, and so the squaring of the amplitude is very easy. When we have many external particles in a process, it is particularly advantageous to use the helicity method. In the traditional mode of performing Feynman diagram calculations, the colour part would be retained within the calculation. This means that squaring an amplitude can lead to lengthy expressions. As the number of Feynman diagrams increases, the intermediate stages of a calculation become much more complicated than the final result, with many diagrams to calculate and many terms within each diagram. In the helicity method, the amplitude will be a number and this, along with the colour matrices, is all that has to be squared.

In the vector boson pair production processes that we are interested in, the helicity method has another advantage in that the helicity information that it retains may be useful to us, as some couplings are spin-dependent. This aspect has been discussed in section 1.2 in relation to previous vector boson pair production calculations.

We will now look at some of the details of performing calculations in the helicity method. We will first consider the technical details of notation and Feynman rules, and then go on to discuss the overall structure of a calculation.

Specific details of vector boson pair production calculations are given in chapter 3.

2.2 The helicity method: notation and conventions

When performing calculations in the helicity method, we will use a specific notation, which will be explained below. We will start with a brief description of the colour part of a Feynman diagram, and then consider the kinematic part in terms of spinors.

The colour part of a helicity method calculation is straightforward. The basic unit of the colour calculation is the generator $(T^a)_{i\bar{\jmath}}$. Quarks and antiquarks have indices $i, \bar{\jmath} = 1 \dots N_c$ and gluons have the adjoint index $a = 1 \dots N_c^2 - 1$. The generators $(T^a)_{i\bar{\jmath}}$ are normalised by $\mathrm{Tr}(T^a T^b) = \delta^{ab}$. This normalisation is the same as that used in helicity method reviews such as Dixon [52] but is a factor of 2 different from the convention of mainstream QCD textbooks such as Ellis, Stirling and Webber [53] (where $\mathrm{Tr}(T^a T^b) = \frac{1}{2}\delta^{ab}$).

The required colour structures are extracted directly from the Feynman diagrams. Each QCD vertex in a Feynman diagram contributes a colour factor: $(T^a)_{i\bar{\jmath}}$ for a gluon-quark-quark vertex and f^{abc} for a triple gluon vertex (with $f^{abe}f^{cde}$ for a pure gluon four-vertex if required). A propagator gives a delta function (δ^{ij} for a fermion propagator, δ^{ab} for a vector propagator).

We can simplify the expression by expanding f^{abc} in terms of T^a:

$$f^{abc} = -\frac{i}{\sqrt{2}} \left(\mathrm{Tr}(T^a T^b T^c) - \mathrm{Tr}(T^a T^c T^b) \right) \tag{2.1}$$

The colour generators can then be manipulated as in normal QCD, remembering the somewhat non-standard normalisation used.

We now calculate the kinematic part of the process. We consider a process where all external particles are massless and have a known helicity and momentum. We shall always work with the unphysical configuration where all particles are outgoing, and so the sum of all external momenta is zero.

An appropriate way to describe the particles involved in this type of process is by means of Weyl spinors and their inner products, the details of which will be explored in this section. Once we can describe the external particles of our process, we go on to use the colour-subtracted Feynman rules of Appendix A to make a full calculation of the kinematic part.

We take our spinor notation from Dixon [52]. Fermions must obey the massless Dirac equation:

$$\not{k}\, \psi(k) = 0, \quad k^2 = 0 \tag{2.2}$$

Here k is the momentum and $\not{k} = \gamma^\mu k_\mu$, where γ^μ is the Dirac gamma matrix.

There are both positive and negative energy solutions to this equation, corresponding to particles and antiparticles, $u(k)$ and $v(k)$. These solutions are identical when particles are massless, as long as we fix the phase between them.

Each particle or antiparticle has two helicity states, and these are given by the chiral projections of $u(k)$ and $v(k)$.

$$\begin{aligned} u_\pm(k) &= \frac{1}{2}(1 \pm \gamma_5)u(k) \\ v_\mp(k) &= \frac{1}{2}(1 \pm \gamma_5)v(k) \end{aligned} \tag{2.3}$$

In the case of the negative energy solution $v(k)$, the *helicity* of the antiparticle is the opposite of its *chirality*. This explains the opposing signs in the equation above.

We define the conjugate momenta:

$$\begin{aligned} \overline{u_\pm(k)} &= \frac{1}{2}(1 \mp \gamma_5)\overline{u(k)} \\ \overline{v_\mp(k)} &= \frac{1}{2}(1 \mp \gamma_5)\overline{v(k)} \end{aligned} \tag{2.4}$$

We then introduce the simple spinor notation as used in [49], [50]. The equivalence of particles and antiparticles is made explicit here.

$$|i^\pm\rangle \equiv |k_i^\pm\rangle \equiv u_\pm(k_i) = v_\mp(k_i), \qquad \langle i^\pm| \equiv \langle k_i^\pm| \equiv \overline{u_\pm(k_i)} = \overline{v_\mp(k_i)} \tag{2.5}$$

where k_i is the momentum of particle i.

These brackets, $|i^\pm\rangle$ and $\langle i^\pm|$, give a concise form to our helicity amplitudes.

Amplitudes are expressed in terms of spinor inner products, combinations of the spinor brackets above.

Spinor products are defined by

$$\langle ij\rangle \equiv \langle i^-|j^+\rangle = \overline{u_-(k_i)}u_+(k_j), \qquad [ij] \equiv \langle i^+|j^-\rangle = \overline{u_+(k_i)}u_i(k_j) \tag{2.6}$$

We can explicitly evaluate the spinor product $\langle ij\rangle$. When both energies, k_i and

k_j, are positive:

$$\langle ij\rangle = \frac{k_i^{(3)} - ik_j^{(2)}}{\sqrt{(k_i^{(3)})^2 + (k_i^{(2)})^2}} \sqrt{(k_i^{(4)} - k_i^{(1)})(k_j^{(4)} + k_j^{(1)})} - (i \leftrightarrow j) \tag{2.7}$$

If one or both of the energies are negative, then we use:

$$\begin{aligned} \langle ij\rangle &= i\langle k_i, -k_j\rangle, \quad k_j^{(4)} < 0 \\ \langle ij\rangle &= i\langle -k_i, k_j\rangle, \quad k_i^{(4)} < 0 \\ \langle ij\rangle &= -\langle -k_i, -k_j\rangle, \quad k_i^{(4)} < 0,\, k_j^{(4)} < 0 \end{aligned} \tag{2.8}$$

It is then possible to obtain $[ij]$, once we know that:

$$\langle ij\rangle[ji] = s_{ij} = (k_i + k_j)^2 = 2k_i \cdot k_j \tag{2.9}$$

The quantity s_{ij} will often appear in amplitudes, along with similar quantities t_{ijl} and u_{ijlm}, where $t_{ijl} = (k_i + k_j + k_l)^2$ and $u_{ijlm} = (k_i + k_j + k_l + k_m)^2$.

The explicit expressions for the spinor products $\langle ij\rangle$ and $[ij]$ should make it clear that the spinor product of a particle with itself is zero,

$$\langle ii\rangle = [ii] = 0 \tag{2.10}$$

The spinor products are asymmetric,

$$\langle ji\rangle = -\langle ij\rangle, \qquad [ji] = -[ij] \tag{2.11}$$

In calculating and simplifying helicity amplitudes, we may also make use of other spinor product identities.

$$\begin{aligned} \langle i^+|\gamma^\mu|j^+\rangle &= \langle j^-|\gamma^\mu|i^-\rangle \\ \langle i^+|\gamma^\mu|j^+\rangle\langle k^+|\gamma_\mu|l^+\rangle &= 2\,[ik]\langle lj\rangle \\ \langle ik\rangle\langle jl\rangle + \langle il\rangle\langle kj\rangle &= \langle ij\rangle\langle kl\rangle \end{aligned} \tag{2.12}$$

A comprehensive treatment of spinor product relations is given in [51].

As stated before, the sum of the momenta in a process is zero, as all particles are outgoing.

$$\sum_{i=1, i \neq j,k}^{n} [ji]\langle ik\rangle = 0 \tag{2.13}$$

where n is the number of particles.

Once we combine spinor products with the $\not{k}$ terms from internal lines ($\not{k} = \gamma^\mu k_\mu$), we may get some very complicated terms. We write them in an abbreviated form:

$$\begin{aligned}
\langle i|l|j\rangle &\equiv \langle k_i^-|\not{k}_l|k_j^-\rangle \\
\langle i|(l+m)|j\rangle &\equiv \langle k_i^-|(\not{k}_l + \not{k}_m)|k_j^-\rangle \\
\langle i|(l+m)(n+r)|j\rangle &\equiv \langle k_i^-|(\not{k}_l + \not{k}_m)(\not{k}_n + \not{k}_r)|k_j^+\rangle \\
[i|\ldots|j] &\equiv \langle i|\ldots|j\rangle, k_{i,j}^{\pm} \to k_{i,j}^{\mp}
\end{aligned} \tag{2.14}$$

These terms and other analogous ones are used in the amplitudes to follow in Appendix B.

Thus far, we have only considered external fermions, which we now know are given as spinors $|i^\pm\rangle$ and $\langle i^\pm|$. However, we also have external bosons: gluons and photons. We can express these too in the spinor formalism, with polarisation vectors constructed from spinor products.

Each outgoing gluon or photon is written as a polarisation vector $\epsilon^\pm(p,k)$ where p is the momentum of the gluon and k is a reference momentum.

$$\epsilon_\mu^\pm(p,k) = \pm\frac{\langle p \pm |\gamma_\mu|k\pm\rangle}{\sqrt{2}\langle k \mp |p\pm\rangle} \tag{2.15}$$

This reference momentum may be chosen at will: a different reference momentum implies a different gauge choice. Clearly the calculation of an individual diagram is not gauge invariant as we include difference reference momenta. However, when the terms from different diagrams are added to obtain a full amplitude or subamplitude, we obtain a gauge invariant expression. By making 'intelligent' choices of reference momenta we may make the calculation easier, even avoiding calculating a number of diagrams altogether.

The following identities may be used to remove terms by the choice of reference momenta.

$$\begin{aligned}
\epsilon^{\pm}(p,k)\cdot k &= 0 \\
\epsilon^{+}(p,k)\cdot \epsilon^{+}(q,k) &= 0 \\
\epsilon^{-}(p,k)\cdot \epsilon^{-}(q,k) &= 0 \\
\epsilon^{+}(p,q)\cdot \epsilon^{-}(q,k) &= 0 \\
\epsilon^{+}(p,k)\cdot \epsilon^{-}(q,p) &= 0 \\
\not{\epsilon}^{\pm}(p,k)|k^{\pm}\rangle &= 0 \\
\langle k^{\pm}|\not{\epsilon}^{\pm}(p,k) &= 0
\end{aligned} \tag{2.16}$$

We now have all the basic tools of the spinor formalism that we will require in making tree-level calculations. Note that the spinor formalism only works in four dimensions.

2.3 A tree level amplitude calculation in the helicity method

We will now consider the method of carrying out a helicity calculation. The basic steps could be described as

1. Drawing all Feynman diagrams
2. Calculating colour and classifying diagrams by colour factor
3. Dividing set of diagrams into gauge invariant subamplitudes
4. Calculating necessary diagrams, using appropriate gauge
5. Using relations between subamplitudes to obtain remaining terms
6. Evaluating amplitudes
7. Squaring and combining with colour and other prefactors to obtain a cross section

To describe these steps more fully, we will use the process $gg \to WZq\bar{q}$ as an illustration. This process will also be discussed comprehensively in section 3.1.

1. Drawing all Feynman diagrams

To calculate the tree level process $gg \to WZq\bar{q}$, we first draw all diagrams. There are four types of diagram – with and without triple gauge vertex, with and without triple gluon vertex. An example of each of these is given in Figure 2.1. The other diagrams are similar to these but with all possible permutations of gluon and vector boson legs. This includes swapping gluon 1 and gluon 2, which are distinct, and exchanging W and Z. We end up with 38 diagrams in all.

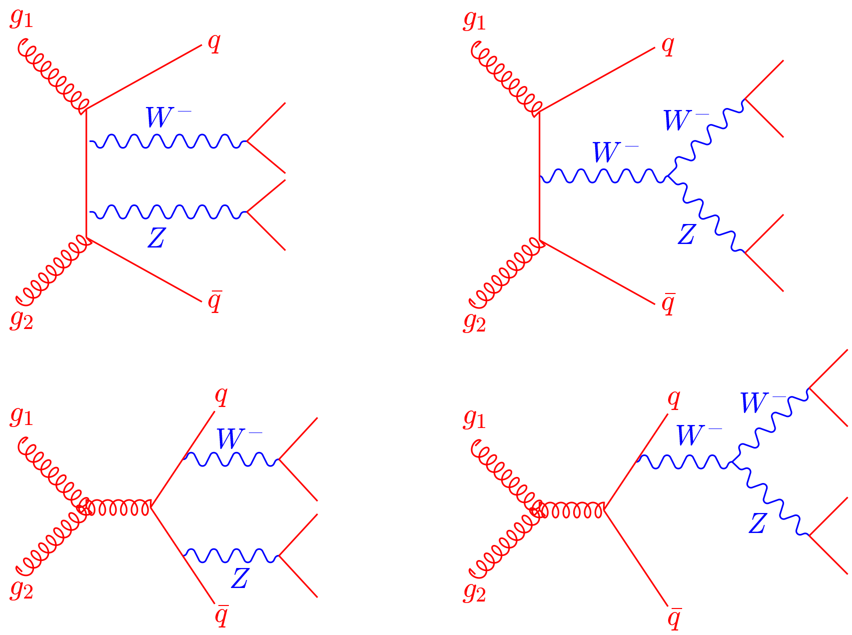

Figure 2.1: Tree level diagrams contibuting to $gg \to WZq\bar{q}$.

2. Calculating colour and classifying diagrams by colour factor

In our case, the colour structures are rather simple as we only have one quark line and two gluons. The colour factors are $(T^{a_1}T^{a_2})_{i\bar{j}}$ for diagrams with gluon ordering g_1g_2 and $(T^{a_2}T^{a_1})_{i\bar{j}}$ for diagrams with ordering g_2g_1. (A diagram with a triple gluon vertex has the sum of both colour factors.) The kinematic part for gluon ordering $g_1 g_2$ is $\mathcal{A}_{12}$, and for gluon ordering $g_2 g_1$ is $\mathcal{A}_{21}$. Each of these is the sum of appropriate diagrams.

At this stage, while we are thinking about colour, we can also anticipate the end of the calculation when the amplitudes are squared to give the cross section. Then we will obtain overall colour factors.

$$\begin{aligned} &|(T^{a_1}T^{a_2})_{i\bar{j}}\mathcal{A}_{12} + (T^{a_2}T^{a_1})_{i\bar{j}}\mathcal{A}_{21}|^2 = \\ &N_c\left(4C_f^2(|\mathcal{A}_{12}|^2 + |\mathcal{A}_{21}|^2) - \frac{2}{3}C_f(\mathrm{Re}|\mathcal{A}_{12}^*\mathcal{A}_{21}| + \mathrm{Re}|\mathcal{A}_{21}^*\mathcal{A}_{12}|)\right) \end{aligned} \tag{2.17}$$

Note the interference terms.

The colour factors are the same for all tree level vector boson pair production processes, as the QCD part of the process never changes.

3. Dividing set of diagrams into gauge invariant subamplitudes

We have already made one step towards dividing into gauge invariant subamplitudes, by classifying by colour part. The amplitudes $\mathcal{A}_{12}$ and $\mathcal{A}_{21}$ are gauge invariant. However, these too can be broken down. The set of diagrams containing a triple gauge vertex is separately gauge invariant from the rest, and the set of diagrams with a chosen ordering of W and Z (with respect to the quarks) is separately gauge invariant from the opposite ordering.

4. Calculating necessary diagrams, using appropriate gauge

In theory, we need to calculate each of these gauge invariant subamplitudes for every possible helicity configuration. In fact only a few of these subamplitudes must be calculated explicitly (they are given in Appendix B.1). When we do have to calculate a subamplitude, we may be able to remove some diagrams by gauge choice. We then sum the remaining diagrams, which are calculated by using colour-subtracted Feynman rules as in Appendix A. Some details of calculation were described in section 2.2.

5. Using relations between subamplitudes to obtain remaining terms

Having calculated the necessary subamplitudes for the required helicity configurations, we then obtain all the other amplitudes and helicities by use of appropriate relations. There are a number of ways to relate amplitudes. We may be able to use discrete group relations like C and P, or gauge relations between amplitudes. There are also relations that are inspired by supersymmetry or string relations [52]. In some cases, going from one amplitude to another may just mean a simple exchange or substitution. Appendix B includes the relations used to obtain the helicity amplitudes that are not given explicitly.

6. Evaluating amplitudes

We give the gauge invariant subamplitudes as helicity amplitudes in the Appendices. On evaluating these, we obtain just a complex number for each, which makes the squaring of the amplitude very easy. It is only necessary to sum the squares of the individual helicity configurations to obtain the full results, as the different helicity amplitudes do not interfere.

7. Squaring and combining with colour and other prefactors to obtain a cross section

Squaring the amplitude is just numerical, although we need to include colour as given in equation (2.17). We also need factors relating to the electroweak part of the amplitude: up till now, we have effectively just calculated in QCD, and now need to add in electroweak factors, changing vertices and propagators as appropriate. For the WZ case, these are given explicitly in section 3.1.3.

The stages given above for WZ are applicable to a general helicity method process and will also be used here for calculating $W\gamma$ and $Z\gamma$ production. These calculations will be carried out in chapter 3, including explicit couplings. The amplitudes themselves can be found in Appendix B.

In practice, we obtained the amplitudes in terms of momenta (spinors) using Feynman rules implemented in Mathematica [54]. We then summed the amplitudes, added couplings and integrated over phase space using a Monte Carlo program written in Fortran 90. Numerical results for all vector boson pairs are given in chapter 5.

Chapter 3

Production of vector boson pairs

In this chapter we will discuss the calculation of helicity amplitudes for the tree level processes $gg \to WZq\bar{q}$, $gg \to W\gamma q\bar{q}$ and $gg \to Z\gamma q\bar{q}$, and for the one loop process $gg \to Z\gamma$. We will also add anomalous couplings and dress with electroweak couplings as appropriate. The helicity amplitudes discussed here and given explicitly in Appendix B were used in calculating the results for pair production as given in [55] and in chapter 5 of this thesis.

3.1 Tree level WZ production

We calculate the helicity amplitudes required for the production of a W^-Z pair. From here onwards, we will just write 'WZ' and assume that the W is always W^-. It is straightforward to use the amplitudes and techniques described to calculate the production of W^+Z: it can also be obtained from the W^-Z case by a CP transformation.

We first calculate a generic set of amplitudes for $gg \to V_1V_2q\bar{q}$, where V_1V_2 could be WW, WZ or ZZ. In this initial calculation, we do not include anomalous couplings or the electroweak couplings of the W and Z. We add anomalous couplings for WZ production in section 3.1.2 and add the correct electroweak couplings in section 3.1.3.

At tree level in the Standard Model, the difference between WZ and WW amplitudes is just in their associated electroweak couplings. ZZ amplitudes are even simpler, as the amplitudes with a triple gauge vertex are not required. To add anomalous terms, diagrams containing a triple gauge vertex would have to be recalculated using the appropriate vertex, which differs between processes.

To calculate $gg \to WWq\bar{q}$ and $gg \to ZZq\bar{q}$, we would also have to calculate the appropriate loop diagrams, and add these contributions to the tree level amplitudes. The potential loop diagrams for WW production are given in figure 3.1, and those for ZZ production have a similar form. Calculation of these loops would proceed in a similar way as for the $Z\gamma$ loops in section 3.4.

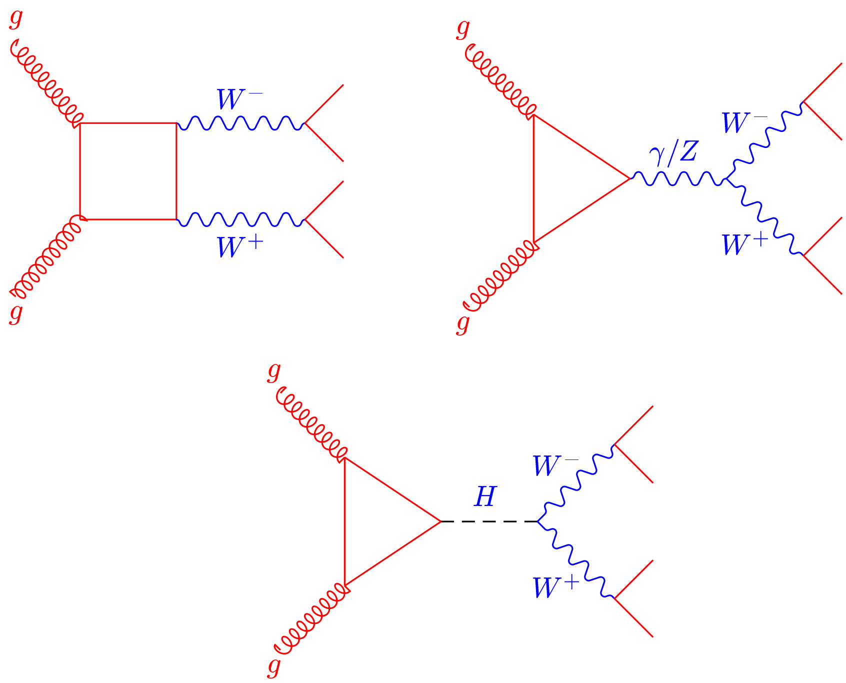

Figure 3.1: Potential loop diagrams for $gg \to WW$

We have not calculated WW or ZZ production in this thesis. WW and ZZ production are less important phenomenologically than $W\gamma$ and $Z\gamma$ production, with more problems with background [2]. However, these calculations may be interesting as future work, especially as they involve extra diagrams that do not exist in the WZ case.

3.1.1 Standard Model amplitudes for WZ

We want to obtain the helicity amplitudes for the process $gg \to WZq\bar{q}$ by carrying out a Feynman diagram calculation as described in the previous chapter.

The types of diagram that contribute to the $gg \to WZq\bar{q}$ process have already been shown in Figure 2.1 on page 26. The remaining diagrams come from ordering the W, Z and gluon legs in every possible way along the quark line, remembering to include the exchange of gluon 1 and gluon 2.

It is reasonably straightforward to separate these diagrams into gauge invariant subsets. Firstly, we can distinguish gluon ordering g_1g_2 from g_2g_1, knowing that these have different colour parts. We can also separate those with a triple gauge vertex from those without. Later on, we will label these as the 'A' amplitudes (not including a triple gauge vertex) and the 'B' amplitudes (including a triple gauge vertex, and thus containing the anomalous part).

In this section we use the labelling $g_1, g_2, l_3, \bar{\nu}_4, \bar{l}'_5, l'_6, q_7, \bar{q}_8$, where g_1 and g_2 are the incoming gluons, l_3 and $\bar{\nu}_4$ are the decay products of the W and $\bar{l}'_5$ and l'_6 are the decay products of the Z.

We need to obtain the helicity amplitudes for all possible helicity configurations. However, it is only necessary to calculate a few of these helicity amplitudes explicitly. The number of helicity configurations is also restricted because some of the particles have their helicity fixed by their couplings. The helicities of leptons 3 and 4 must be $l_3^-, \bar{\nu}_4^+$ as they are fixed by their coupling to the W. Similarly, the quark must be left-handed, giving $q_7^-, \bar{q}_8^+$.

Our amplitudes are calculated for a specific ordering of W and Z (where this is applicable – it does not matter for the case with the triple gauge vertex). They are given for the case where the W is on the same side as the quark, and the Z on the side of the antiquark. To obtain the amplitude with the opposite ordering of WZ we just have to swap the lepton pairs $\{34\} \leftrightarrow \{56\}$. The two orderings have different couplings (as the Z couples to differently flavoured quarks).

In every case, we need to consider the two different gluon orderings, knowing that these have different colour parts.

In expressing the explicit amplitudes, we will suppress all quark and lepton helicities, and calculate with $l_3^-, \bar{\nu}_4^+, \bar{l}'^+_5, l'^-_6, q_7^-, \bar{q}_8^+$, obtaining the other helicities by appropriate relations. The ordering of the W and Z with respect to the quark line is also fixed. So in writing $A_{12}(g_1^+ g_2^+)$, we mean $A_{12}(g_1^+, g_2^+, l_3^-, \bar{\nu}_4^+, \bar{l}'^+_5, l'^-_6, q_7^-, \bar{q}_8^+)$, with the W on the quark side, relative to the Z.

The amplitudes that we need to calculate explicitly are:

$$A_{12}(g_1^+ g_2^+) \quad B_{12}(g_1^+ g_2^+) \quad A_{12}(g_1^+ g_2^-) \quad B_{12}(g_1^+ g_2^-) \quad A_{21}(g_1^+ g_2^-) \quad B_{21}(g_1^+ g_2^-) \tag{3.1}$$

These helicity amplitudes are given in Appendix B.1, along with the operations used to obtain the amplitudes for all other helicity configurations and orderings.

3.1.2 Adding anomalous couplings to WZ

We want to add anomalous couplings to the amplitudes in order to parameterise possible new physics and study the effects of this new physics on couplings and therefore cross sections. The motivation for this has been discussed already in section 1.4, along with the parameterisation to be used.

We use a form of the triple gauge (WWZ) vertex that includes anomalous coupling terms g_1^Z, κ^Z and λ^Z, while retaining Lorentz invariance and C and P invariance. The triple gauge vertex for $W^+_\alpha(p_+)W^-(p_-)_\beta Z_\mu(q)$, including the anomalous terms, is given below, with all momenta outgoing. This was previously discussed in section 1.4.2, where it is equation (1.2).

$$\begin{aligned}
\Gamma^{\alpha\beta\mu}_{WWZ}(p_+, p_-, q) \;=\;& (p_+ - q)^\alpha g^{\beta\mu} \frac{1}{2}(g_1^Z + \kappa^Z + \lambda^Z \frac{p_-^2}{M_W^2}) \\
& + (q - p_-)^\beta g^{\alpha\mu} \frac{1}{2}(g_1^Z + \kappa^Z + \lambda^Z \frac{p_+^2}{M_W^2}) \\
& + (p_+ - p_-)^\mu (-g^{\alpha\beta} \frac{1}{2} \frac{q^2 \lambda^Z}{M_W^2} + \frac{\lambda^Z}{M_W^2} p_+^\alpha p_-^\beta)
\end{aligned} \tag{3.2}$$

Adding anomalous coupling terms to the WZ amplitudes is straightforward. All that is required is that we recalculate all terms with a triple gauge vertex (the B amplitudes), using the anomalous vertex of equation (3.2) instead of the Standard Model vertex. In Appendix B.1 we give the amplitudes including anomalous terms: the Standard Model amplitudes can be obtained by using the Standard Model couplings: $g_1^Z = 1$, $\kappa^Z = 1$, $\lambda^Z = 0$.

3.1.3 Electroweak couplings for WZ

We now add the relevant electroweak couplings to the amplitudes of appendix B.1. The couplings are the same as those given for $q\bar{q}$ and qg induced WZ production in [25], except that we have two colour structures, and must average over initial state gluons rather than quarks. We have already defined the A and B parts of the amplitude (with and without a triple gauge vertex) in the same way as in [25].

We combine individual helicity amplitudes into the two amplitudes $\mathcal{A}_{12}$ and $\mathcal{A}_{21}$, which correspond to the gluon orderings $g_1 g_2$ and $g_2 g_1$ respectively. Each of these is composed of the appropriate A amplitudes without a triple gauge vertex (one for each ordering of the W and Z) and the B amplitude including a triple gauge vertex (where ordering of W and Z is irrelevant). Where there is no triple gauge vertex, the different orderings of the W and Z imply different couplings, as the Z couples to an up- or a down-type quark, depending on its positioning. When the amplitude includes a triple gauge vertex, we have a term associated with the massive propagator: we must replace s_{12} with $s_{12} - M_W^2$ to account for the massive intermediate W. This only occurs in the diagrams with a triple gauge vertex so we have this relative term between the 'A' and the 'B' amplitudes.

$\mathcal{A}_{12}$ and $\mathcal{A}_{21}$ are as follows:

$$\begin{aligned}\mathcal{A}_{12}(g_1^{\pm}, g_2^{\pm}) &= v_{L,d} A_{12}(g_1^{\pm}, g_2^{\pm}) + v_{L,u}[A_{12}(g_1^{\pm}, g_2^{\pm})]_{3456 \to 6543} \\ &\quad - \cot\theta_W \frac{s_{12}}{s_{12} - M_W^2} B_{12}(g_1^{\pm}, g_2^{\pm})\end{aligned} \tag{3.3}$$

$$\begin{aligned}\mathcal{A}_{21}(g_1^{\pm}, g_2^{\pm}) &= v_{L,d} A_{21}(g_1^{\pm}, g_2^{\pm}) + v_{L,u}[A_{21}(g_1^{\pm}, g_2^{\pm})]_{3456 \to 6543} \\ &\quad - \cot\theta_W \frac{s_{12}}{s_{12} - M_W^2} B_{21}(g_1^{\pm}, g_2^{\pm})\end{aligned} \tag{3.4}$$

These add to give a total amplitude $\mathcal{A}^{WZ}$, which includes dressing with the overall electroweak couplings. We then square this and include flux and normalisation factors.

We already know the colour parts: a factor of $(T^{a_1}T^{a_2})_{i\bar{j}}$ for the amplitude $\mathcal{A}_{12}$ and a factor of $(T^{a_2}T^{a_1})_{i\bar{j}}$ for the amplitude $\mathcal{A}_{21}$. The factors arising from the colour part squared have been given in equation (2.17). All of the QCD couplings have already been included.

However, when we performed the Feynman diagram calculations, we calculated everything with QCD-type vertices. This means that we need to change the couplings of the W and Z to the appropriate electroweak coupling. Each W or Z vertex incurs a factor of $\sqrt{2}$ due to our normalisation of the colour matrices. The couplings of the W to fermions are $g_W/\sqrt{2} = e/\sqrt{2}\sin\theta_W$. The couplings of the Z are $ev_{L,e}$ ($ev_{R,e}$) for the left (right) handed coupling of a Z to a lepton and $ev_{L,q}$ ($ev_{R,q}$) for the left (right) handed coupling to a quark, where:

$$v_{L,e} = \frac{-1+2\sin^2\theta_W}{\sin 2\theta_W} \qquad v_{R,e} = \frac{2\sin^2\theta_W}{\sin 2\theta_W} \tag{3.5}$$

$$v_{L,q} = \frac{\pm 1-2Q\sin^2\theta_W}{\sin 2\theta_W} \qquad v_{R,q} = \frac{-2Q\sin^2\theta_W}{\sin 2\theta_W} \tag{3.6}$$

Q is the charge of the quark q and the $\pm$ signs in $v_{L,q}$ are $+$ for up type and $-$ for down type quarks.

We also require to change the propagators. In QCD, these would be massless gluons, giving simple $1/s_{34}$ and $1/s_{56}$ propagator terms. However, we now need to take into account the fact that the propagating W and Z are massive, and change the propagators accordingly to $1/(s_{34}-M_W^2+i\Gamma_W M_W)$ and $1/(s_{56}-M_Z^2+i\Gamma_Z M_Z)$, where Γ_W and Γ_Z are the widths of the W and Z. We should note here that we use the narrow width approximation, which uses only the diagrams with a resonant (on-shell) propagator.

Adding all these factors, we obtain the equation with couplings:

$$\begin{aligned}\mathcal{A}^{WZ}(g_1^\pm, g_2^\pm, l_3^-, \bar{\nu}_4^+, \bar{l'}_5^+, l_6'^-, q_7^-, \bar{q}_8^+) \quad = \quad & 2v_{L,e}V_{ud}\left(\frac{e^2}{\sin\theta_W}\right)^2 \\ & \frac{s_{34}}{s_{34}-M_W^2+i\Gamma_W M_W}\frac{s_{56}}{s_{56}-M_Z^2+i\Gamma_Z M_Z} \\ & [(T^{a_1}T^{a_2})_{i\bar{j}}\mathcal{A}_{12}(g_1^\pm, g_2^\pm) + (T^{a_2}T^{a_1})_{i\bar{j}}\mathcal{A}_{21}(g_1^\pm, g_2^\pm)]\end{aligned} \tag{3.7}$$

We now square this expression. We need to know what happens when we square the propagators in the narrow width approximation.

We use:

$$\int_{-\infty}^{\infty} \frac{d(s_{34})}{(s_{34}-M_W^2)^2+\Gamma_W^2 M_W^2} = \frac{\pi}{M_W \Gamma_W} \tag{3.8}$$

where:

$$\Gamma_W = \frac{1}{B_l(W)} \frac{g_W^2 M_W}{48\pi} = \frac{1}{B_l(W)} \left(\frac{e}{\sin\theta_W}\right)^2 \frac{M_W}{48\pi} \tag{3.9}$$

$B_l(W)$ is the branching ratio for the W decay.

The same applies for the Z propagator:

$$\int_{-\infty}^{\infty} \frac{d(s_{56})}{(s_{56}-M_Z^2)^2+\Gamma_Z^2 M_Z^2} = \frac{\pi}{M_Z \Gamma_Z}. \tag{3.10}$$

$$\Gamma_Z = \frac{1}{B_l(Z)} \frac{g_W^2 M_Z \sin^2\theta_W (v_{L,e}^2 + v_{R,e}^2)}{24\pi} = \frac{1}{B_l(Z)} \frac{e^2 M_Z (v_{L,e}^2 + v_{R,e}^2)}{24\pi} \tag{3.11}$$

We also include a flux factor of $1/2s_{12}$ and average over colours. When we also consider the phase space factors, we obtain a total result of:

$$\begin{aligned} \mathcal{M}^{WZ}(g_1^{\pm}, g_2^{\pm}, l_3^{-}, \bar{\nu}_4^{+}, \bar{l'}_5^{+}, l_6'^{-}, q_7^{-}, \bar{q}_8^{+}) \quad = \quad & B_l(W) B_{l'}(Z) \left(\frac{e^2}{\sin\theta_w}\right)^2 \left(\frac{3}{4\pi}\right)^2 \\ & \frac{M_W^2 M_Z^2 v_{L,e}^2}{4 s_{12} (N_c^2-1)^2 (v_{L,e}^2+v_{R,e}^2)} |V_{ud}|^2 \\ & |(T^{a_1}T^{a_2})_{i\bar{j}} \mathcal{A}_{12}(g_1^{\pm}, g_2^{\pm}) + (T^{a_2}T^{a_1})_{i\bar{j}} \mathcal{A}_{21}(g_1^{\pm}, g_2^{\pm})|^2 \end{aligned} \tag{3.12}$$

It is necessary to sum over all helicity configurations. If the leptons from the Z are $\bar{l}_5'^{-} l_6'^{+}$ rather than $\bar{l}_5'^{-} l_6'^{+}$, the overall coupling $v_{L,e}^2$ will change to $v_{R,e}^2$. Other helicity changes have no effect on the electroweak couplings. Appendix B.1 gives the helicity amplitudes for all possible helicity configurations.

3.2 Tree level $W\gamma$ production

The calculation of $gg \to W\gamma q\bar{q}$ at tree level is very similar to the calculation of $gg \to WZq\bar{q}$ that was described in section 3.1. However, while the W decays into leptons as before, the photon does not decay and is treated as an external particle. This then is a 7 particle process rather than an 8 particle one, and the diagrams calculated are different from the WZ case.

The basic types of diagram are given in figure 3.2. Again, we need to calculate the diagrams for all orderings of legs along the quark line. These divide into subamplitudes, based on the two different colour terms for the two gluon orderings.

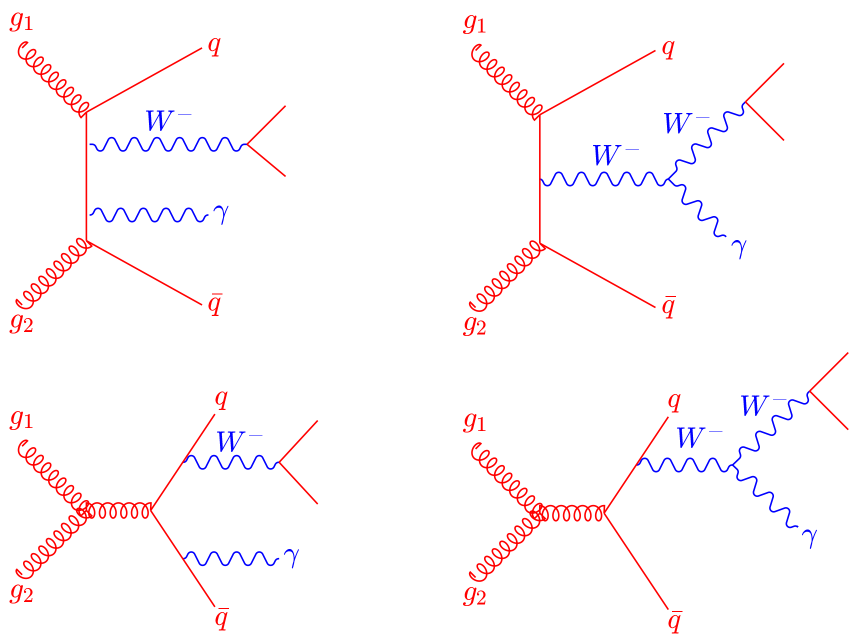

Figure 3.2: Tree level diagrams contibuting to $gg \to W\gamma q\bar{q}$.

The $W\gamma$ production case, despite having one fewer external particle than $gg \to WZq\bar{q}$, is actually slightly more complicated (it requires more independent helicity amplitudes), because the helicity of the photon can vary. In WZ production, while the decay products of the Z could be either $\bar{l}_5'^{+} l_6'^{-}$ or $\bar{l}_5'^{-}\, l_6'^{+}$, these cases were related by a simple exchange. This is not true for the two helicities of the photon in $W\gamma$ production, and more independent amplitudes must be calculated. These are listed in Appendix B.2, both for the Standard Model case and for the case where an anomalous triple gauge vertex is included.

3.2.1 Standard Model amplitudes for $W\gamma$

We use the labelling $g_1, g_2, l_3, \bar{\nu}_4, \gamma_5, q_6, \bar{q}_7$, where g_1 and g_2 are the incoming gluons, l_3 and $\bar{\nu}_4$ are the decay products of the W and γ_5 is the outgoing photon. Note that the quark and antiquark have labels 6 and 7 here, as opposed to 7 and 8 in WZ production.

We can fix the helicities of l_3 and $\bar{\nu}_4$ by their coupling to the W^-. The coupling must be left handed, so the helicities are $l_3^-, \bar{\nu}_4^+$. Similarly, the helicities of the quarks are fixed by the coupling to be $q_6^-, \bar{q}_7^+$. The helicities of the gluons and the photon are free to vary.

The diagrams for the process $gg \to W\gamma q\bar{q}$ consist of two separately gauge invariant subsets, which are labelled A and B. In the A diagrams, the photon is on the $\bar{q}_7$ side of the diagram (when compared with the W) and in the B diagrams the photon is on the q_6 side. Note that these A and B parts are different from the A and B for WZ in section 3.1.

We still have to consider two different gluon orderings, so the diagrams form four basic subsets: A_{12}, A_{21}, B_{12} and B_{21}. Each of these subsets must be calculated for all possible helicity configurations.

Only a few terms need to be calculated explicitly. To get all 32 combinations of helicity, vector boson ordering and gluon ordering, only 8 amplitudes are needed:

$$\begin{array}{llll} A_{12}(g_1^+ g_2^+ \gamma_5^+) & B_{12}(g_1^+ g_2^+ \gamma_5^+) & A_{12}(g_1^+ g_2^+ \gamma_5^-) & B_{12}(g_1^+ g_2^+ \gamma_5^-) \\ A_{12}(g_1^+ g_2^- \gamma_5^+) & B_{12}(g_1^+ g_2^- \gamma_5^+) & A_{21}(g_1^+ g_2^- \gamma_5^+) & B_{21}(g_1^+ g_2^- \gamma_5^+) \end{array} \tag{3.13}$$

Other amplitudes are found by exchanging gluon ordering, or using 'flip' relations. The details of this process, along with the explicit helicity amplitudes, are given in Appendix B.2.

3.2.2 Adding anomalous couplings to $W\gamma$

We now need to add anomalous couplings to the process $gg \to W\gamma q\bar{q}$. Unlike in the WZ case, every one of our Standard Model amplitudes includes diagrams both with and without a triple gauge vertex. Instead of recalculating the amplitudes, we just add extra anomalous terms.

This means that we want to express the anomalous parameters slightly differently. We can immediately use the fact that $g_1^\gamma = 1$ by electromagnetic gauge invariance, so we have only κ^γ and λ^γ to consider (the origin of these terms is discussed in section 1.4). We express κ^γ as $1 + \Delta\kappa^\gamma$, with $\Delta\kappa^\gamma$ being the additional anomalous part (in the Standard Model, $\kappa^\gamma = 1$ and $\lambda^\gamma = 0$). Our triple gauge vertex for $W_\alpha^+(p_+)W^-(p_-)_\beta\gamma_\mu(q)$ is then:

$$\begin{aligned}\Gamma_{WW\gamma}^{\alpha\beta\mu}(p_+, p_-, q) &= \Big((p_+ - q)^\alpha g^{\beta\mu}\frac{1}{2}(2 + \Delta\kappa^\gamma + \lambda^\gamma\frac{p_-^2}{M_W^2}) \\ &\quad +(q - p_-)^\beta g^{\alpha\mu}\frac{1}{2}(2 + \Delta\kappa^\gamma + \lambda^\gamma\frac{p_+^2}{M_W^2}) \\ &\quad +(p_+ - p_-)^\mu(-g^{\alpha\beta}\frac{1}{2}\frac{q^2\lambda^\gamma}{M_W^2} + \frac{\lambda^\gamma}{M_W^2}p_+^\alpha p_-^\beta)\Big) \qquad (3.14)\end{aligned}$$

To calculate the anomalous terms, only the diagrams that contain a triple gauge vertex are calculated, using the vertex above to obtain the additional anomalous part. The anomalous terms are then added to existing amplitudes, combining with the appropriate A and B amplitudes to give the full anomalous amplitudes A^{anom} and B^{anom} as follows:

$$A_{12}^{anom}(g_1^\pm g_2^\pm \gamma_5^\pm) = A_{12}^{SM}(g_1^\pm g_2^\pm \gamma_5^\pm) + \mathcal{A}_{12}^{ac}(g_1^\pm g_2^\pm \gamma_5^\pm) \qquad (3.15)$$

$$B_{12}^{anom}(g_1^\pm g_2^\pm \gamma_5^\pm) = B_{12}^{SM}(g_1^\pm g_2^\pm \gamma_5^\pm) - \mathcal{A}_{12}^{ac}(g_1^\pm g_2^\pm \gamma_5^\pm) \qquad (3.16)$$

The anomalous part is always added to the A amplitude and subtracted from the B amplitude of the same helicity.

In all, we need to calculate only 4 anomalous terms:

$$\mathcal{A}_{12}^{ac}(g_1^+ g_2^+ \gamma_5^+) \quad \mathcal{A}_{12}^{ac}(g_1^+ g_2^+ \gamma_5^-) \quad \mathcal{A}_{12}^{ac}(g_1^+ g_2^- \gamma_5^+) \quad \mathcal{A}_{21}^{ac}(g_1^+ g_2^- \gamma_5^+) \qquad (3.17)$$

These amplitudes are listed explicitly in Appendix B.2.

The full amplitudes, A^{anom} and B^{anom}, obey the same relations as the Standard

Model amplitudes, so the remaining helicity amplitudes can be found in the same way.

3.2.3 Electroweak couplings for $W\gamma$

We now combine the A and B amplitudes, adding appropriate electroweak couplings and colour factors.

For the anomalous case, we use A^{anom} and B^{anom} as given in equations (3.15) and (3.16). If we only want the Standard Model result, we can use the A and B amplitudes without adding in their anomalous parts, which is equivalent to setting the anomalous coupling parameters to their Standard Model values: $\Delta\kappa^{\gamma} = 0$, $\lambda^{\gamma} = 0$.

The A and B amplitudes are combined to give two overall amplitudes $\mathcal{A}_{12}$ and $\mathcal{A}_{21}$, which correspond with the two gluon orderings:

$$\mathcal{A}_{12}(g_1^{\pm}, g_2^{\pm}, \gamma_5^{\pm}) = [Q_7 A_{12}^{anom}(g_1^{\pm}, g_2^{\pm}, \gamma_5^{\pm}) + Q_6 B_{12}^{anom}(g_1^{\pm}, g_2^{\pm}, \gamma_5^{\pm})] \tag{3.18}$$

$$\mathcal{A}_{21}(g_1^{\pm}, g_2^{\pm}, \gamma_5^{\pm}) = [Q_7 A_{21}^{anom}(g_1^{\pm}, g_2^{\pm}, \gamma_5^{\pm}) + Q_6 B_{21}^{anom}(g_1^{\pm}, g_2^{\pm}, \gamma_5^{\pm})] \tag{3.19}$$

Q_6 is the charge of q_6 and Q_7 is the charge of $\bar{q}_7$.

$\mathcal{A}_{12}$ and $\mathcal{A}_{21}$ combine in the total amplitude $\mathcal{A}^{W\gamma}$. Now we also have to take into account their different colour factors, and the appropriate electroweak terms. Again we need to add a factor of $\sqrt{2}$ for each electroweak vertex, and we introduce the W coupling and propagator as before (section 3.1.3). The photon coupling to the quark gives a factor of eQ where Q is the quark charge, and there is a factor of $g_W \cos\theta_W$ from the triple gauge vertex. The total amplitude is:

$$\begin{aligned}\mathcal{A}^{W\gamma}(g_1^{\pm}, g_2^{\pm}, l_3, \bar{\nu}_4, \gamma_5^{\pm}, u_6, \bar{d}_7) \quad = \quad & \sqrt{2}\left(\frac{e^3}{\sin^2\theta_W}\right) V_{ud} \frac{s_{34}}{s_{34} - M_W^2 + i\Gamma_W M_W} \\ & [(T^{a_1}T^{a_2})_{i\bar{j}}\mathcal{A}_{12}(g_1^{\pm}, g_2^{\pm}, \gamma_5^{\pm}) + (T^{a_2}T^{a_1})_{i\bar{j}}\mathcal{A}_{21}(g_1^{\pm}, g_2^{\pm}, \gamma_5^{\pm})]\end{aligned} \tag{3.20}$$

The squared amplitude, including flux and normalisation factors, is

$$\begin{aligned}\mathcal{M}^{W\gamma}(g_1^\pm, g_2^\pm, l_3, \bar{\nu}_4, \gamma_5^\pm, u_6, \bar{d}_7) \quad = \quad & B_l(W)|V_{ud}|^2 \left(\frac{e^3}{\sin\theta_W}\right)^2 \frac{3}{4\pi} \frac{M_W^2}{4s_{12}(N_c^2-1)^2} \\ & |(T^{a_1}T^{a_2})_{i\bar{j}}\mathcal{A}_{12}(g_1^\pm, g_2^\pm, \gamma_5^\pm) + (T^{a_2}T^{a_1})_{i\bar{j}}\mathcal{A}_{21}(g_1^\pm, g_2^\pm, \gamma_5^\pm)|^2\end{aligned} \tag{3.21}$$

This is then summed over all helicity configurations.

3.3 Tree level $Z\gamma$ production

The production of a $Z\gamma$ pair differs from the previously considered cases of WZ and $W\gamma$ production in two significant ways.

Firstly, we can no longer describe the gluon-gluon induced vector boson pair production process in terms of only tree level diagrams. For the $Z\gamma$ case, loop diagrams must also be considered, and we will calculate these in section 3.4.

Secondly, the anomalous coupling vertex required for $Z\gamma$ production is different from the one that was previously used. The $ZZ\gamma$ and $Z\gamma\gamma$ vertices are forbidden in the Standard Model and so no triple gauge vertices are to be found in Standard Model $Z\gamma$ production. These are only added with specific anomalous couplings.

In this section, we calculate the helicity amplitudes for the tree level process $gg \to Z\gamma q\bar{q}$, for both the Standard Model and the anomalous coupling case. We include the decay of the Z into leptons.

We use combinations of the amplitudes found for $gg \to W\gamma$ production to assemble the Standard Model $gg \to Z\gamma$ amplitudes. We then formulate explicit terms for the anomalous $Z\gamma$ amplitudes, with the new helicity amplitudes being listed in appendix B.3.

3.3.1 Standard Model tree amplitudes for $Z\gamma$

In calculating the amplitudes for $Z\gamma$ production, we will always use the labelling $g_1, g_2, l_3, \bar{l}_4, \gamma_5, q_6, \bar{q}_7$ where g_1 and g_2 are the initial state gluons, l_3 and $\bar{l}_4$ are the leptons resulting from the decay of the Z, γ_5 is the photon and q_6 and $\bar{q}_7$ are the quarks in the final state.

Any of these particles can have either '+' or '−' helicity. We also need to consider the two possible orderings of the gluons, which produce the two possible colour terms.

The amplitudes for $W\gamma$ production, which are already known and were given in Appendix B.2, can be used to assemble the Standard Model $Z\gamma$ amplitudes where the quark and lepton helicities are $l_3^-, \bar{l}_4^+, q_6^-, \bar{q}_7^+$. We make a symmetric combination of the 'A' and 'B' $W\gamma$ amplitudes from section 3.2.1 (in the $W\gamma$ amplitudes, the ordering of the vector bosons matters, so we have 'A' and 'B' amplitudes depending on which side of the W the photon is on).

To combine the $W\gamma$ amplitudes, we have:

$$A_{12}^{Z\gamma,SM}(g_1^\pm, g_2^\pm, \gamma_5^\pm) = A_{12}(g_1^\pm, g_2^\pm, \gamma_5^\pm) + B_{12}(g_1^\pm, g_2^\pm, \gamma_5^\pm) \tag{3.22}$$

$$A_{21}^{Z\gamma,SM}(g_1^\pm, g_2^\pm, \gamma_5^\pm) = A_{21}(g_1^\pm, g_2^\pm, \gamma_5^\pm) + B_{21}(g_1^\pm, g_2^\pm, \gamma_5^\pm) \tag{3.23}$$

This allows us to obtain for $Z\gamma$ all the helicity configurations that apply to $W\gamma$ production. The combination of 'A' and 'B' amplitudes cancels out those diagrams with a triple gauge vertex, as required – these diagrams do not exist for $Z\gamma$ in the Standard Model.

To obtain the remaining helicity configurations, with $l_3^+, \bar{l}_4^-$ and/or $q_6^+, \bar{q}_7^-$ rather than $l_3^-, \bar{l}_4^+, q_6^-, \bar{q}_7^+$, just requires some simple relations. To go from $l_3^-, \bar{l}_4^+$ to $l_3^+, \bar{l}_4^-$ we exchange $3 \leftrightarrow 4$ in the amplitudes, and to go from $q_6^-, \bar{q}_7^+$ to $q_6^+, \bar{q}_7^-$ we exchange $6 \leftrightarrow 7$.

3.3.2 Adding anomalous couplings to $Z\gamma$

In adding anomalous terms to our expressions for $Z\gamma$ production, we introduce new vertices. The $ZZ\gamma$ and $Z\gamma\gamma$ triple gauge vertices are not present in the Standard Model at tree level.

New diagrams now contribute to the tree level amplitudes. The diagrams that include a triple gauge vertex are included, where they were omitted in the Standard Model case. The new anomalous amplitudes can be calculated separately from the Standard Model amplitudes and then added as appropriate. This process is analogous to adding anomalous couplings to $W\gamma$ in section 3.2.

We need an anomalous parameterisation where $ZZ\gamma$ and $Z\gamma\gamma$ are allowed. Using anomalous couplings $h_1^{Z/\gamma}$, $h_2^{Z/\gamma}$, $h_3^{Z/\gamma}$ and $h_4^{Z/\gamma}$ as introduced in section 1.4 and taking the form of the vertex from [34], the $Z_\alpha(q_1)\gamma_\beta(q_2)Z_\mu(p)$ vertex is:

$$\begin{aligned}\Gamma^{\alpha\beta\mu}_{Z\gamma Z}(q_1, q_2, p) \;=\; & \frac{i(p^2 - q_1^2)}{M_Z^2}\left(h_1^Z (q_2^\mu\, g^{\alpha\beta} - q_2^\alpha\, g^{\mu\beta}) + \frac{h_2^Z}{M_Z^2} p^\alpha (p\cdot q_2\, g^{\mu\beta} - q_2^\mu\, p^\beta) \right. \\ & \left. - h_3^Z \varepsilon^{\mu\alpha\beta\nu} q_{2\nu} - \frac{h_4^Z}{M_Z^2} \varepsilon^{\mu\beta\nu\sigma} p^\alpha p_\nu\, q_{2\sigma} \right)\end{aligned} \tag{3.24}$$

The vertex for $Z_\alpha(q_1)\gamma_\beta(q_2)\gamma_\mu(p)$ is as in equation (3.24), but with $q_1^2 \to 0$ and $h_i^Z \to h_i^\gamma$.

Once we have the form of the vertex, we can carry out amplitude calculations as before. In expressing the amplitudes in Appendix B.3, we shall work with $\tilde{h}_i^{Z/\gamma}$, where we redefine the parameters to include the factors of $\frac{1}{M_Z^2}$ inside the couplings:

$$\tilde{h}_1^{Z/\gamma} = \frac{h_1^{Z/\gamma}}{M_Z^2}; \quad \tilde{h}_2^{Z/\gamma} = \frac{h_2^{Z/\gamma}}{M_Z^4}; \quad \tilde{h}_3^{Z/\gamma} = \frac{h_3^{Z/\gamma}}{M_Z^2}; \quad \tilde{h}_4^{Z/\gamma} = \frac{h_4^{Z/\gamma}}{M_Z^4} \tag{3.25}$$

As was the case for $W\gamma$ production in section 3.2.2, it is not necessary to calculate many independent amplitudes in order to obtain the amplitudes with anomalous couplings for all helicity configurations. Suppressing the lepton and quark helicities, which are $l_3^-, \bar{l}_4^+, q_6^-, \bar{q}_7^+$, the four independent terms required are:

$$\mathcal{A}_{12}^{Z/\gamma,ac}(g_1^+, g_2^+\gamma_5^+) \quad \mathcal{A}_{12}^{Z/\gamma,ac}(g_1^+g_2^+\gamma_5^-) \quad \mathcal{A}_{12}^{Z/\gamma,ac}(g_1^+g_2^-\gamma_5^+) \quad \mathcal{A}_{21}^{Z/\gamma,ac}(g_1^+g_2^-\gamma_5^+) \tag{3.26}$$

$\mathcal{A}^{Z,ac}$ has an intermediate Z (a $ZZ\gamma$ vertex) while $\mathcal{A}^{\gamma,ac}$ has an intermediate photon (a $Z\gamma\gamma$ vertex). The amplitudes obtained are the same, because the difference between the $ZZ\gamma$ and $Z\gamma\gamma$ vertices obtained above cancels the change in propagator between the intermediate photon and intermediate Z.

The explicit helicity amplitudes for the four necessary anomalous terms are given in Appendix B.3, along with details of the method that is used to obtain amplitudes for all helicity configurations from the amplitudes listed above These other helicity configurations can be obtained by use of 'flip' relations or simple exchanges, just as they were in the Standard Model case.

3.3.3 Electroweak couplings for $Z\gamma$

We now combine the known amplitudes to give the complete amplitudes and cross-sections for tree level $gg \to Z\gamma q\bar{q}$. Here we shall give the full result, including anomalous couplings. To obtain the Standard Model result, it is only necessary to omit the relevant terms, $\mathcal{A}^{\gamma,ac}$ and $\mathcal{A}^{Z,ac}$. Terms with a triple gauge vertex do not exist at all for $Z\gamma$ production and we may use just the Standard Model amplitudes that we obtained from $W\gamma$ amplitudes in section 3.3.1.

We shall first assemble the overall $Z\gamma$ amplitudes, $\mathcal{A}_{12}^{Z\gamma}$ and $\mathcal{A}_{21}^{Z\gamma}$. We need to take into account the relative couplings resulting from the diagrams with and without a triple gauge vertex.

Once again we shall suppress the helicities of the leptons and quarks, using $l_3^-, \bar{l}_4^+, q_6^-, \bar{q}_7^+$. We can then calculate the remaining helicities in the usual way.

For the Standard Model part of the amplitudes, we use $\mathcal{A}_{12}^{Z\gamma,SM}$ and $\mathcal{A}_{21}^{Z\gamma,SM}$ as given in equations (3.22) and (3.23). Adding the anomalous terms, taking into account the relative couplings, we obtain:

$$\begin{aligned}\mathcal{A}_{12}^{Z\gamma}(g_1^\pm, g_2^\pm, \gamma_5^\pm) &= Qv_{L,q}\mathcal{A}_{12}^{Z\gamma,SM}(g_1^\pm, g_2^\pm, \gamma_5^\pm) \\ &+ Q\mathcal{A}_{12}^{\gamma,ac}(g_1^\pm g_2^\pm \gamma_5^\pm) + v_{L,q}\mathcal{A}_{12}^{Z,ac}(g_1^\pm g_2^\pm \gamma_5^\pm)\end{aligned} \tag{3.27}$$

$$\begin{aligned}\mathcal{A}_{21}^{Z\gamma}(g_1^\pm, g_2^\pm, \gamma_5^\pm) &= Qv_{L,q}\mathcal{A}_{21}^{Z\gamma,SM}(g_1^\pm, g_2^\pm, \gamma_5^\pm) \\ &+ Q\mathcal{A}_{21}^{\gamma,ac}(g_1^\pm g_2^\pm \gamma_5^\pm) + v_{L,q}\mathcal{A}_{21}^{Z,ac}(g_1^\pm g_2^\pm \gamma_5^\pm)\end{aligned} \tag{3.28}$$

Here Q is the quark charge. $v_{L,q}$ and $v_{R,q}$ are the left- and right-handed couplings of the Z to the quark line and $v_{L,e}$ and $v_{R,e}$ are the couplings of the Z to leptons.

In combining the amplitudes $\mathcal{A}_{12}^{Z\gamma}$ and $\mathcal{A}_{21}^{Z\gamma}$ to give a cross section, we need to include the two colour factors, $(T^{a_1}T^{a_2})_{i\bar{j}}$ and $(T^{a_2}T^{a_1})_{i\bar{j}}$.

We add electroweak vertex factors and propagators as in the previous sections. Adding $\mathcal{A}_{12}^{Z\gamma}$ and $\mathcal{A}_{21}^{Z\gamma}$ along with their colour factors and electroweak couplings gives:

$$\begin{aligned}\mathcal{A}^{Z\gamma}(g_1^\pm, g_2^\pm, l_3^-, \bar{l}_4^+, \gamma_5^\pm, q_6^-, \bar{q}_7^+) &= e^3 v_{L,e}\frac{s_{34}}{s_{34} - M_Z^2 + i\Gamma_Z M_Z} \\ &\quad [(T^{a_1}T^{a_2})_{i\bar{j}}\mathcal{A}_{12}^{Z\gamma}(g_1^\pm, g_2^\pm, \gamma_5^\pm) + (T^{a_2}T^{a_1})_{i\bar{j}}\mathcal{A}_{21}^{Z\gamma}(g_1^\pm, g_2^\pm, \gamma_5^\pm)]\end{aligned} \tag{3.29}$$

We then square and add flux and normalisation factors. The total cross section is:

$$\begin{aligned}\mathcal{M}^{Z\gamma}(g_1^\pm, g_2^\pm, l_3^-, \bar{l}_4^+, \gamma_5^\pm, q_6^-, \bar{q}_7^+) &= B_l(Z)e^4\left(\frac{3}{4\pi}\right)\frac{M_Z^2 v_{L,e}^2}{2s_{12}(N_c^2-1)^2(v_{L,e}^2 + v_{R,e}^2)} \\ &\quad |(T^{a_1}T^{a_2})_{i\bar{j}}\mathcal{A}_{12}^{Z\gamma}(g_1^\pm, g_2^\pm, \gamma_5^\pm) + (T^{a_2}T^{a_1})_{i\bar{j}}\mathcal{A}_{21}^{Z\gamma}(g_1^\pm, g_2^\pm, \gamma_5^\pm)|^2\end{aligned} \tag{3.30}$$

$B_l(Z)$ is the branching ratio of the Z to leptons.

When we exchange the helicities of the leptons from $l_3^-, \bar{l}_4^+$ to $l_3^+, \bar{l}_4^-$, we must change the $v_{L,e}^2$ coupling in the numerator to $v_{R,e}^2$, as well as exchanging 3 and 4 in the amplitudes.

To exchange helicities of the quarks from $q_6^-, \bar{q}_7^+$ to $q_6^+, \bar{q}_7^-$, we exchange 6 and 7 and change the $v_{L,q}^2$ coupling in the numerator to $v_{R,q}^2$.

In this way, it is simple to obtain the tree level results for all helicities. In the next section, we will add the loop terms.

3.4 Production of $Z\gamma$ at one-loop level

Having calculated the tree diagrams that are required for $Z\gamma$ production, we now add the loop diagrams for $gg \to Z\gamma$.

The loop diagrams that are required in the Standard Model and in the anomalous coupling case differ entirely, with box diagrams contributing only to the Standard Model, and triangles only to the anomalous contribution.

The types of loop diagram that one could imagine for the process $gg \to Z\gamma$ are given in figure 3.3.

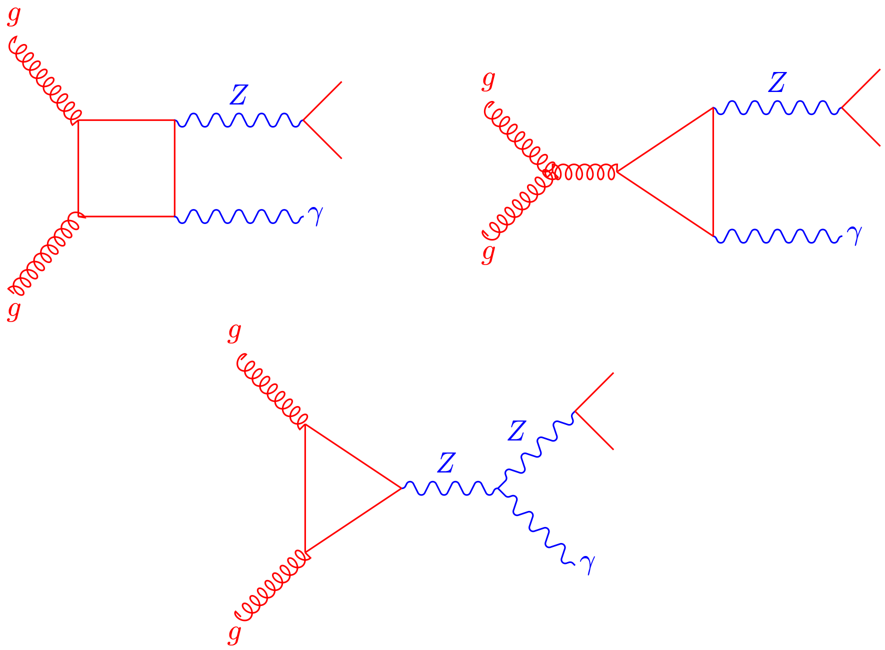

Figure 3.3: Potential loop diagrams for $gg \to Z\gamma$

Each of the diagrams in figure 3.3 is an example of a set of diagrams, the others being found by a reordering of legs. The three types of loop diagram are

- box diagrams,
- triangle diagrams with triple gluon vertex,
- triangle diagrams with triple gauge boson vertex.

One type of diagram can be eliminated immediately. Any loop diagram for $Z\gamma$ production that includes a triple gluon coupling cannot contribute. For this diagram there is only one gluon coupling to the quark loop, so the colour part is just the trace of a single colour matrix and hence disappears.

It is clear that the triangle diagram with the triple gauge boson vertex is allowed only in the anomalous case: the triple gauge vertex itself is forbidden in the Standard Model. We will consider this anomalous coupling contribution in section 3.4.2.

But for now it is apparent that only the box diagrams can contribute to the Standard Model production of $Z\gamma$ pairs. This is what we will calculate in section 3.4.1.

3.4.1 Box diagram contributions to Standard Model $Z\gamma$ production

In figure 3.3, we showed an example of a box diagram that contributes to $gg \to Z\gamma$. The other box diagrams that we require just differ by a reordering of legs around the loop. These box diagrams were originally calculated some time ago [30] [56] [57] but were summed over helicities and did not include the decay of the Z.

We would expect to calculate the diagrams for both the vector and the axial vector couplings of the Z, with the vector and axial vector parts being separately gauge invariant. However, only the vector part contributes in this case.

We consider all quarks except the top to be massless. The top is taken to be massive, but instead of a full calculation, we consider only an expansion in $1/m_t^2$. We will do this for all loop contributions. This approach is most appropriate for small energies, where we may expect that $\sqrt{\hat{s}} < m_t$. This may not be the case in LHC collisions. However, we expect the effect of the approximation to be a small one. The calculation of the $Z\gamma$ box loop by van der Bij and Glover [56] shows that the difference between a calculation using $m_t = 0$ and one with $m_t = \infty$ is small.

In analogy with our other helicity amplitudes, we label the gluons g_1 and g_2, the leptons produced by the Z decay l_3 and $\bar{l}_4$, and the photon γ_5. All amplitudes will be given for $l_3^+, \bar{l}_4^-$. It is straightforward to reverse the helicities of these leptons by exchanging $3 \leftrightarrow 4$ in the amplitudes. To reverse all helicities, we use $\langle ab\rangle \leftrightarrow -[ab]$.

There is only one colour structure for these diagrams, the trace $\mathrm{Tr}(T^{a_1}T^{a_2})$ where

T^{a_1} and T^{a_2} are the colour matrices of gluons 1 and 2.

The structure for the amplitude of the box is simple.

$$\mathcal{A}^{box}(g_1, g_2, l_3, \bar{l}_4, \gamma_5) = \frac{i}{N_c}\mathcal{B}_{tr}^{N_F}(g_1, g_2, l_3, \bar{l}_4, \gamma_5) \tag{3.31}$$

This applies when the circulating quark is massless.

$\mathcal{B}_{tr}^{N_F}$ is a straightforward sum of the $\mathcal{B}^{N_F}$ terms as given below. The helicities given for the $\mathcal{B}^{N_F}$ terms are those for the gluons and the photon: $\mathcal{B}_{tr}^{N_F}(+,+,+) = \mathcal{B}_{tr}^{N_F}(g_1^+, g_2^+, \gamma_5^+)$.

The $\mathcal{B}^{N_F}$ terms come from Signer [58], equations (5.24) – (5.26). We must be very careful in labelling here, as in Signer the photon is labelled 3 rather than 5. Changing all 3s to 5s to correspond with our notation, we have:

$$\mathcal{B}_{tr}^{N_F}(+,+,+) = 2\mathcal{B}^{N_F}(+,+,+) \tag{3.32}$$

$$\mathcal{B}_{tr}^{N_F}(-,+,+) = \mathcal{B}^{N_F}(-,+,+) + (\mathcal{B}^{N_F}(-,+,+))_{2\leftrightarrow 5} \tag{3.33}$$

$$\mathcal{B}_{tr}^{N_F}(+,-,+) = \mathcal{B}^{N_F}(+,-,+) + (\mathcal{B}^{N_F}(+,-,+))_{1\leftrightarrow 5} \tag{3.34}$$

$$\mathcal{B}_{tr}^{N_F}(+,+,-) = \mathcal{B}^{N_F}(+,+,-) + (\mathcal{B}^{N_F}(+,+,-))_{1\leftrightarrow 2} \tag{3.35}$$

Results for the remaining helicity configurations can be found using the usual relations.

It is now necessary to add electroweak couplings to this amplitude. This is much the same as for previous amplitudes. We need to add the appropriate couplings to the electroweak vertices, each of these also incurring a factor of $\sqrt{2}$ when we go from a QCD to an electroweak vertex, due to our normalisation. The coupling of the photon to the loop is $e\,Q_f$, and is summed over all the quarks in the loop. As usual, the Z propagator must be changed from s_{34} to $s_{34} - M_Z^2 + i\Gamma_Z M_Z$ and we use the narrow width approximation.

For the Z coupling to the loop, instead of splitting the coupling into left and right handed parts, we instead have to split the coupling into vector and axial vector parts, ev_v and ev_{ax}. For the box, we need just the vector term, v_v, where

$$v_v = \frac{\frac{1}{2} - 2Q_f \sin^2\theta_W}{\sin 2\theta_W} \tag{3.36}$$

This is summed over all the quarks.

Adding these factors to equation (3.31) gives:

$$\begin{aligned}\mathcal{A}(g_1, g_2, l_3^+, \bar{l}_4^-, \gamma_5) &= 2\sqrt{2}\, e \sum Q_f\, e\, v_{R,e}\, e\, v_v \frac{s_{34}}{s_{34} - M_Z^2 + i\Gamma_Z M_Z} \\ &\quad \mathrm{Tr}(T^{a_1}T^{a_2})\mathcal{A}^{box}(g_1, g_2, l_3^+, \bar{l}_4^-, \gamma_5)\end{aligned} \tag{3.37}$$

If we change from $l_3^+, \bar{l}_4^-$ to $l_3^-, \bar{l}_4^+$, we have to change $v_{R,e}$ to $v_{L,e}$ as well as changing the amplitudes.

We then square this expression, using the narrow width approximation, and adding flux and normalisation factors.

$$\begin{aligned}\mathcal{M}^{box}(g_1, g_2, l_3^+, \bar{l}_4^-, \gamma_5) &= B_l(Z) e^4 \left(\frac{3}{4\pi}\right) \frac{M_Z^2 \sum Q_f^2 v_{R,e}^2 v_v^2}{2 s_{12}(N_c^2 - 1)^2 (v_{L,e}^2 + v_{R,e}^2)} \\ &\quad |\mathrm{Tr}(T^{a_1}T^{a_2})\mathcal{A}^{box}(g_1, g_2, l_3^+, \bar{l}_4^-, \gamma_5)|^2\end{aligned} \tag{3.38}$$

The result above applies only for massless quarks.

For the top quark, we take the same approach as in Bern, Dixon and Kosower in [59], where e^+e^- to four partons is calculated. We expand in $\frac{1}{m_t}$ where m_t is the top mass, and then neglect terms of $\mathcal{O}(\frac{1}{m_t^4})$, keeping only terms of $\mathcal{O}(\frac{1}{m_t^2})$ The diagram that we want is a collinear limit of the one of the diagrams discussed in [59]. The relevant part of the paper is section 11, where they discuss amplitudes where the Z couples directly to the fermion loop. Here it is found that the contribution of the top loop decouples rapidly and there are no terms in $\frac{1}{m_t^2}$, the highest terms being in $\frac{1}{m_t^4}$, so in this case we can ignore the top contribution. Hence we now have all the information we need to calculate $gg \to Z\gamma$ at one loop in the Standard Model.

To find the explicit form of the $gg \to Z\gamma$ box amplitude given in equation (3.31), we used the results for $q\bar{q} \to gg\gamma$ that are given in Signer [58]. We are able to use these results as the coupling of the Z to the loop is only a vector coupling. Therefore the box loop for $gg \to Z\gamma$ has exactly the same form as the box for $q\bar{q} \to gg\gamma$, and we need only to change the couplings, after selecting the appropriate box part of the $q\bar{q} \to gg\gamma$ expression from the other terms that are present.

The process $q\bar{q} \to gg\gamma$ is more complicated than $gg \to Z\gamma$ as more diagrams are involved. There is more of a QCD part to deal with. Instead of only box diagrams, there are also triangle diagrams where a photon can be emitted from the external quark rather than from the loop, or where a triple gluon coupling is involved. The types of diagrams involved in $q\bar{q} \to gg\gamma$ are given in figure 3.4. We tend to put the gluons to the left to make the analogy to $gg \to Z\gamma$ more apparent: as we calculate with all momenta outgoing, we do not have to distinguish between the incoming and the outgoing particles.

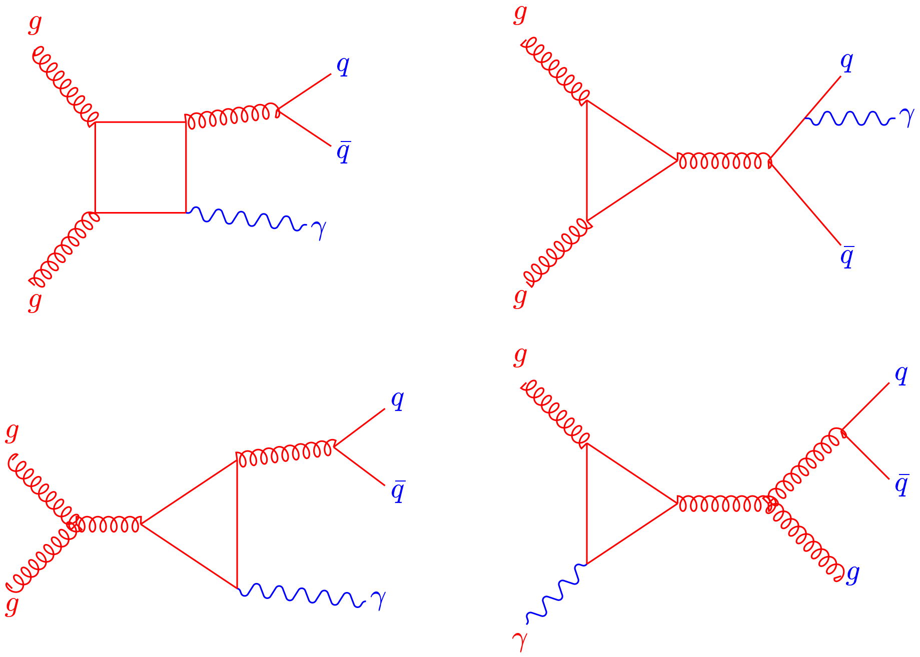

Figure 3.4: Loop diagrams for $q\bar{q} \to gg\gamma$

Despite the number of diagrams involved, it is quite straightforward to pick out the terms that contribute to $gg \to Z\gamma$. We know that the relevant terms are box diagrams with the photon coupling directly to the loop. We also know that the colour part of $gg \to Z\gamma$ is always $\mathrm{Tr}(T^{a_1}T^{a_2})$.

The colour factor allows us to make an initial selection. Only the diagrams on the upper line of figure 3.4 have the correct colour factor. The total amplitude for $q\bar{q} \to gg\gamma$ is the sum of two terms with different colour factors.

$$\mathcal{A}^{(1)}(q,1,2,\gamma,\bar{q}) = g^2\sqrt{2}e_q\left(\frac{g}{4\pi}\right)^2 \left[\sum_{P(1,2)}(T^{a_1}T^{a_2})_{q\bar{q}}b_{12}(q,1,2,\gamma,\bar{q}) + \mathrm{Tr}(T^{a_1}T^{a_2})\delta_{a_1a_2}b_{tr}(q,1,2,\gamma,\bar{q})\right] \tag{3.39}$$

This is equation (3.6) of Signer [58] with a slight simplification of notation. It includes the factors in g, which we tend to leave till later, and also has a factor of $\sqrt{2}e_q$ which comes from the coupling of the photon to the quark (we wrote e_q as eQ_f).

We can ignore the term with the colour factor $(T^{a_1}T^{a_2})_{q\bar{q}}$, which is $b_{12}(q,1,2,\gamma,\bar{q})$. We need only consider the term $b_{tr}(q,1,2,\gamma,\bar{q})$, which can be expanded as:

$$b_{tr}(q,1,2,\gamma,\bar{q}) = i\frac{N_F}{N_C}\mathcal{B}_{tr}^{N_F}(q,1,2,\gamma,\bar{q}) + i\mathcal{B}_{tr}(q,1,2,\gamma,\bar{q}). \tag{3.40}$$

This is equation (5.69) of [58].

We still need to separate the diagrams that we want, where the photon couples directly to the quark loop, from the unwanted diagrams. We can do this simply by looking at the couplings of $\mathcal{B}_{tr}^{N_F}$ and $\mathcal{B}_{tr}$. We find that $\mathcal{B}_{tr}$ contains the terms in which the photon couples to the external quark line, while $\mathcal{B}_{tr}^{N_F}$ contains the terms in which the photon couples to the loop. These are easily separated as the notation of [58] distinguishes between the coupling to the external quark e_q and the coupling to the loop e_{Loop} (e_{Loop} is the coupling summed over all quarks in the loop).

We can select just the term $\mathcal{B}_{tr}^{N_F}(q,1,2,\gamma,\bar{q})$ from the $q\bar{q} \to gg\gamma$ amplitude, knowing that this is just the box amplitude that we require. We select the correct colour part and photon coupling, and need just to change the electroweak couplings to give us the result for the $gg \to Z\gamma$ box.

3.4.2 Triangle contribution to $Z\gamma$ production with anomalous couplings

As we have already discussed, the box diagram is the only loop to contribute to $Z\gamma$ production in the Standard Model. However, this situation changes when we include anomalous couplings. Anomalous couplings emerge through a triple gauge coupling: the triple $ZZ\gamma$ or $Z\gamma\gamma$ coupling was forbidden in the Standard Model, but contributes in the anomalous terms. The presence of this triple coupling means that any contributing loop diagram must be a triangle rather than a box. It is in fact the third diagram of figure 3.3.

For the triangle with two gluon legs and a vector boson leg to exist, it is necessary that at least one of the legs be off-shell: the on-shell case is zero by Yang's theorem [60], which forbids the decay of a spin-one particle into two massless photons, and similarly restricts the couplings of gluons. Even the triangle $gg \to Z \to$ leptons is zero. However, the anomalous coupling that is present here leads to a non-zero result for our triangle diagram.

The triangle diagram in which all couplings are vector couplings vanishes by Furry's theorem (charge conjugation). Therefore we can eliminate the diagrams with an intermediate photon or a vector coupling of the Z, and only have to think about the axial coupling of the Z, where Furry's theorem does not apply. For each helicity configuration, there is only one diagram, which is therefore gauge invariant. The diagrams are also infrared and ultraviolet finite.

We require to calculate the diagrams with all possible quarks in the loop. However, we find that in the case of a triangle with an axial coupling, contributions from a massless isodoublet cancel. As we consider only the top quark to be massive, and all other quarks to be massless, we can neglect the $\{u, d\}$ and $\{s, c\}$ isodoublets and consider only the massless b quark and massive t quark in the loop.

In examining the triangle integral, we made use of the paper of Hagiwara et al [61], in which the triangle is studied.

In calculating the triangle, we use the notation of figure 3.5.

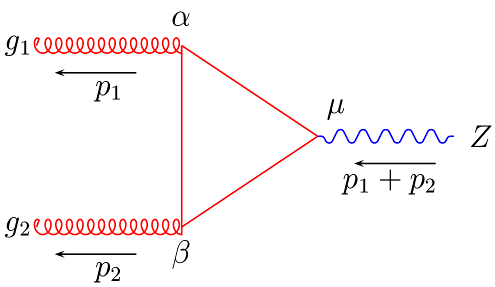

Figure 3.5: Notation for triangle calculation

Then the general expression for the vertex $T_{\mu\alpha\beta}$ is:

$$\begin{aligned} T_{\mu\alpha\beta} &= f_1(p_1^2\,\varepsilon_{\mu\alpha\beta\rho}\,p_2^\rho + p_{1\alpha}\,[p_1p_2]_{\mu\beta}) + f_2(p_2^2\,\varepsilon_{\mu\alpha\beta\rho}\,p_1^\rho + p_{2\beta}\,[p_1p_2]_{\mu\alpha}) \\ &\quad + f_3(p1+p2)_\mu\,[p_1p_2]_{\alpha\beta} + f_4(p1-p2)_\mu\,[p_1p_2]_{\alpha\beta} \end{aligned} \tag{3.41}$$

Here $[p_1p_2]_{\alpha\beta} = \varepsilon_{\alpha\beta\rho\sigma}\,p_1^\rho\,p_2^\sigma$ and $\varepsilon_{\alpha\beta\rho\sigma}$ is the totally antisymmetric tensor. Equation (3.41) is equation (2.8) of Hagiwara et al [61] with a change of notation for the gluon momenta.

This is a general expression and does not just apply at one-loop. Hagiwara et al give the functions f_i for the one loop case in terms of Feynman parameters. We will only need to calculate the term in f_3.

In calculating our triangle diagram as in figure 3.5, the first thing we do is to consider the gluons as external particles. As the gluons are on-shell, we can remove the terms in p_1^2 and p_2^2. We contract our remaining expression for the vertex with gluons $\epsilon^\alpha(p_1)$ and $\epsilon^\beta(p_2)$. This removes the remaining coefficients of f_1 and f_2 as $\epsilon(p_1)\cdot p_1 = \epsilon(p_2)\cdot p_2 = 0$. We are left with only terms in f_3 and f_4. The term in f_4 is antisymmetric and so vanishes: the expression must be symmetric on exchange of gluons. We need only calculate the function f_3.

Here we should note that f_3 is *not* calculated in the paper of Hagiwara et al. This is because they assumed conservation of the axial vector current. The fact that this current is not necessarily conserved is well known (see, for example, chapter 19 of Peskin and Schroeder [62]). We shall assume that current conservation need not be obeyed, allowing us to use the f_3 term.

Our simple expression for our vertex is now:

$$T_{\mu\alpha\beta} = f_3(p_1 + p_2)_\mu \, [p_1 p_2]_{\alpha\beta} \tag{3.42}$$

The term $[p_1 p_2]_{\alpha\beta}$ contracts with the external gluon terms $\epsilon^\alpha(p_1)$ and $\epsilon^\beta(p_2)$. We will write this as

$$T_{\mu\alpha\beta} = f_3(p_1 + p_2)_\mu \, \varepsilon(\epsilon_1, \epsilon_2, p_1, p_2) \tag{3.43}$$

where $\varepsilon(p_1, p_2, \epsilon_1, \epsilon_2) = \varepsilon_{\alpha\beta\rho\sigma} \, \epsilon^\alpha(p_1) \, \epsilon^\beta(p_2) \, p_1^\rho \, p_2^\sigma$.

As well as looking at the general expression from Hagiwara et al, we also calculated this structure, starting from all possible terms and substituting for the relevant integrals. This allowed us to achieve this same structure from a different direction.

The integral for f_3 is given in Hagiwara et al. The general expression for f_3, when all particles are off-shell and there is a mass in the loop, is:

$$f_3 = -\frac{1}{\pi^2} \int [dz] \, \frac{z_1 z_3}{m^2 - z_1 z_2 p_1^2 - z_2 z_3 p_2^2 - z_1 z_3 (p_1 + p_2)^2} \tag{3.44}$$

where z_1, z_2, z_3 are Feynman parameters, m is the mass in the loop, and

$$\int [dz] = \int_0^1 dz_1 \, dz_2 \, dz_3 \, \delta(1 - z_1 - z_2 - z_3) \tag{3.45}$$

This is equation (2.11) of [61].

This expression will always be simplified considerably in our case, as $p_1^2 = p_2^2 = 0$. In the massless case the integral becomes trivial. With $m = 0$, we simply have:

$$f_3 = \frac{1}{\pi^2} \frac{1}{(p_1 + p_2)^2} \int [dz] = \frac{1}{\pi^2 \, s_{12}} \int [dz] \tag{3.46}$$

and $\int [dz] = \frac{1}{2}$, so we have an overall

$$f_3 = \frac{1}{2\pi^2 s_{12}} \tag{3.47}$$

For the massive case, the situation is a bit more complicated. The expression for f_3 including the mass circulating in the loop is:

$$f_3 = -\frac{1}{\pi^2}\int [dz]\, \frac{z_1 z_3}{m_t^2 - z_1 z_3 (p_1+p_2)^2} \tag{3.48}$$

This then has to be integrated over the Feynman parameters, leading to a more complicated expression.

$$\begin{aligned} f_3 \;=\; & -\frac{1}{\pi^2}\left(\frac{1}{s_{12}^2}\left(-\frac{s_{12}}{2} + m_t^2\,\mathrm{Li}_2\left[\frac{2s_{12}}{s_{12}-\sqrt{s_{12}^2-4m_t^2 s_{12}}}\right]\right.\right. \\ & \left.\left. + m_t^2\,\mathrm{Li}_2\left[\frac{2s_{12}}{s_{12}+\sqrt{s_{12}^2-4m_t^2 s_{12}}}\right]\right)\right) \end{aligned} \tag{3.49}$$

We however just require the term that is leading in $1/m_t^2$.

We find that:

$$f_3 = -\frac{1}{\pi^2}\frac{1}{24\, m_t^2} + \mathcal{O}\left(\frac{1}{m_t^4}\right) \tag{3.50}$$

Our entire vertex term is then:

$$T_{\mu\alpha\beta} = \left(-\frac{1}{24\,\pi^2\, m_t^2} - \frac{1}{2\pi^2 s_{12}}\right)\varepsilon(\epsilon_1,\epsilon_2,p_1,p_2)(p_1+p_2)_\mu \tag{3.51}$$

With the triangle part of the diagram known, we need to add the triple gauge vertex and outgoing particles.

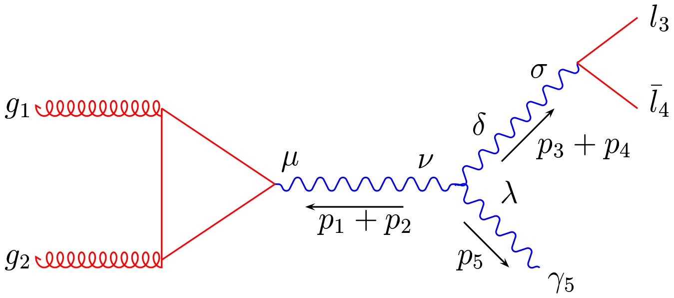

Figure 3.6: Triangle diagram including triple gauge vertex

We discussed possible anomalous couplings in section 1.4. The anomalous triple gauge vertex in figure 3.6 is parameterised as:

$$\Gamma^{\delta\lambda\nu}_{Z\gamma Z}(p_3+p_4,p_5,p_1+p_2) = \frac{i((p_1+p_2)^2-(p_3+p_4)^2)}{M_Z^2}\Big(h_1^Z(p_5^\nu\, g^{\delta\lambda}-p_5^\delta\, g^{\nu\lambda})$$
$$+\frac{h_2^Z}{M_Z^2}(p_1+p_2)^\delta((p_1+p_2)\cdot p_5\, g^{\nu\lambda}-p_5^\nu(p_1+p_2)^\lambda)$$
$$-h_3^Z\,\varepsilon^{\nu\delta\lambda\xi}\,p_{5\xi}-\frac{h_4^Z}{M_Z^2}\,\varepsilon^{\nu\lambda\xi\rho}\,(p_1+p_2)^\delta\,(p_1+p_2)_\xi\,p_{5\rho}\Big) \tag{3.52}$$

When we contract the anomalous coupling vertex of equation (3.52) with a factor of $(p_1+p_2)_\mu$ from the triangle and $g_{\mu\nu}$ from the propagator, the coefficients of h_2 and h_4 cancel immediately and we are left with just terms in h_1 and h_3.

We need to calculate the diagram for both helicities of the photon. We choose to set l_3^-, l_4^+ initially, but exchanging these just entails setting $3 \leftrightarrow 4$ in the amplitudes and changing the coupling to the Z appropriately.

The helicity amplitudes obtained are rather simple. When we just combine the anomalous vertex term and the external particles with the $(p_1+p_2)_\mu$ from the triangle, we get

$$\mathcal{A}^{tri}(g_1,g_2,l_3^-,\bar{l}_4^+,\gamma_5^+) = \frac{(h_1-ih_3)}{M_z^2}\frac{[45]^2}{2[34]} \tag{3.53}$$

$$\mathcal{A}^{tri}(g_1,g_2,l_3^-,\bar{l}_4^+,\gamma_5^-) = \frac{(h_1-ih_3)}{M_z^2}\frac{\langle 35\rangle^2}{2\langle 34\rangle} \tag{3.54}$$

We then add in the extra terms from the triangle vertex.

$$\mathcal{A}^{tri}(g_1,g_2,l_3^-,\bar{l}_4^+,\gamma_5^+) = \left(-\frac{1}{24\,\pi^2\,m_t^2}-\frac{1}{2\pi^2 s_{12}}\right)\varepsilon(\epsilon_1,\epsilon_2,p_1,p_2)\frac{(h_1-ih_3)}{M_z^2}\frac{[45]^2}{2[34]} \tag{3.55}$$

$$\mathcal{A}^{tri}(g_1,g_2,l_3^-,\bar{l}_4^+,\gamma_5^-) = \left(-\frac{1}{24\,\pi^2\,m_t^2}-\frac{1}{2\pi^2 s_{12}}\right)\varepsilon(\epsilon_1,\epsilon_2,p_1,p_2)\frac{(h_1-ih_3)}{M_z^2}\frac{\langle 35\rangle^2}{2\langle 34\rangle} \tag{3.56}$$

We then add electroweak couplings as before. We have two Z propagators to worry about, but the propagator in s_{12} just removes the prefactor term given by the vertex. (We change from s_{12} to $s_{12}-M_Z^2$ in the propagator by multiplying by $\frac{s_{12}}{s_{12}-M_Z^2}$.

This cancels with the existing factor of $\frac{s_{12}-s_{34}}{s_{12}}$ in the vertex.) So the situation is very similar to the box, adding in one Z propagator and the electroweak couplings. Again, we have to divide the coupling of Z to a quark into vector and axial parts, this time keeping the axial part, which is very simple, $v_{ax} = 1/2\sin 2\theta_W$.

$$\begin{aligned} A(g_1, g_2, l_3^-, \bar{l}_4^+, \gamma_5) &= 2\sqrt{2}\, e^3 v_{L,e} v_{ax} \frac{s_{34}}{s_{34} - M_Z^2 + i\Gamma_Z M_Z} \\ &\quad \mathrm{Tr}(T^{a_1}T^{a_2}) A^{tri}(g_1, g_2, l_3^-, \bar{l}_4^+, \gamma_5) \end{aligned} \tag{3.57}$$

This then squares to give:

$$\begin{aligned} \mathcal{M}^{tri}(g_1, g_2, l_3^-, \bar{l}_4^+, \gamma_5) &= B_l(Z) e^4 \left(\frac{3}{4\pi}\right) \frac{M_Z^2 v_{L,e}^2 v_{ax}^2}{2 s_{12}(N_c^2 - 1)^2 (v_{L,e}^2 + v_{R,e}^2)} \\ &\quad |\mathrm{Tr}(T^{a_1}T^{a_2}) A^{tri}(g_1, g_2, l_3^-, \bar{l}_4^+, \gamma_5)|^2 \end{aligned} \tag{3.58}$$

We can add this anomalous triangle to the existing Standard Model loop term, which comes from the box of section 3.4.1.

$$\begin{aligned} \mathcal{M}^{total}(g_1, g_2, l_3^+, \bar{l}_4^-, \gamma_5) &= B_l(Z) e^4 \left(\frac{3}{4\pi}\right) \frac{M_Z^2 v_{R,e}^2}{2 s_{12}(N_c^2 - 1)^2 (v_{L,e}^2 + v_{R,e}^2)} \\ &\quad |\mathrm{Tr}(T^{a_1}T^{a_2}) \{Q_f v_v \mathcal{A}^{box}(g_1, g_2, l_3^+, \bar{l}_4^-, \gamma_5) + v_{ax} \mathcal{A}^{tri}(g_1, g_2, l_3^+, \bar{l}_4^-, \gamma_5)\}|^2 \end{aligned} \tag{3.59}$$

Note that as the box term and the triangle term have the same colour factor, there will be an interference term when this expression is squared.

Chapter 4

Cancellation of singularities by the subtraction method

We now have a method for calculating Feynman diagrams and combining them into amplitudes and cross sections. So we have much of the information that we need for a calculation of vector boson pair production. However, it is important that when we perform this calculation we end up with a physically relevant result: one that contains no divergences. Hence we have to consider the possible divergences in the QCD calculation and how they can be removed. In many ways, this is the core part of the vector boson pair production calculation.

There are two types of divergences in QCD: infrared and ultraviolet. Infrared divergences arise from the low momentum limit of the integrals in the calculation, and ultraviolet divergences from the high momentum limit. Ultraviolet divergences are removed by the usual process of renormalisation. In this chapter we deal with infrared divergences and how they are removed, first for the general case and then for our specific cases of vector boson pair production.

In treating the infrared singularities, we need only consider the QCD parts of the Feynman diagrams for much of the time, with the electroweak parts being irrelevant. The exception to this is when we have an external photon: this case is discussed in section 4.4. For the photon, we will use an isolation procedure to avoid singular regions, rather than using the subtraction method that we use to cancel singularities in the QCD parts. Apart from the singularities that could potentially be caused by the photon, the structure of singularities for each pair production process is identical. Thus we shall initially neglect the electroweak part of the calculation, and just consider the incoming gluons and outgoing quarks.

Almost everything we shall say is relevant to all vector boson pair production processes. Where we have to be specific, we will use as an example the process $gg \to WZq\bar{q}$. Therefore the explicit equations given will be for an 8 particle process. However, it is straightforward to translate to the 7 particle case of $W\gamma$ or $Z\gamma$ production, again because the electroweak particles do not contribute to the structure of infrared divergences that we are discussing.

4.1 Introduction to infrared singularities

In this section, we will discuss the issue of infrared singularities, where they come from and how they can be eliminated. We will include a discussion of different types of IR singularities, and will mention the KLN (Kinoshita-Lee-Nauenberg) theorem and the factorisation theorem in QCD, which will be required later.

Two basic types of infrared singularity arise in QCD. Firstly, there is the 'soft' singularity. Here a final state particle becomes of very low energy: all components of its momentum go to zero. This soft particle cannot be detected in the final state. Secondly, we may have a 'collinear' singularity. A particle may emerge at so close an angle to another particle that they are indistinguishable. It is convenient to divide collinear singularities into two categories: final state collinear singularities, where both of the collinear particles are outgoing, and initial state collinear singularities, where an outgoing particle becomes collinear to an incoming particle. Soft singularities are always in the final state by definition: it would not make physical sense for an incoming particle to disappear.

We know that a physical quantity must be finite so somehow the inherent singularities in QCD must be eliminated.

We differentiate between initial and final state singularities when eliminating singularities. Final state singularities cancel between the real and virtual terms in the cross section (section 4.1.1). Initial state singularities can be removed by absorbing them into the parton distribution functions (we will use the subtraction method to do this in section 4.1.2 and subsequent sections).

Because of this distinction, we now have to start separating incoming and outgoing particles, whereas in previous chapters we treated all particles as outgoing to simplify the amplitude calculations.

4.1.1 Cancellation of real and virtual singularities

We will now start to discuss the cancellation of infrared divergences. We will consider the cancellation of singularities between the real and virtual parts, and also introduce the idea of infrared safety and the factorisation theorem.

First, we consider a soft photon (the same argument applies for a gluon). The photon is massless, and becomes soft by its 4-momentum going to zero. This causes a soft divergence. We cannot distinguish a physical state with a soft photon from the state without a soft photon, so the relevant physical process may have any number of soft photons.

When we are only dealing with soft divergences within QED (where divergences are much less complicated than in QCD), these divergences cancel when we add the relevant virtual processes to the processes with real emission of soft photons. This is the essence of the Bloch-Nordsieck theorem [63]. The cancellation is shown explicitly in chapter 6 of Muta [64].

In QCD, we also have to deal with collinear singularities. In QED, these only occur when the external particles are massless. In QCD, they can occur even if the external quarks are massive, as the triple gluon vertex means that we have the additional possibility of massless gluons becoming collinear to each other.

A pair of collinear particles is indistinguishable from the appropriate single particle. We need to consider all states with an indefinite number of collinear gluons, in order to obtain the physical process, and remove the collinear divergence.

We extend the Bloch-Nordsieck theorem to the Kinoshita-Lee-Nauenberg (KLN) theorem [65], [66]. The KLN theorem states that we must include all indistinguishable initial states as well as all the final state processes. The final state processes may be real or virtual, and may contain soft or collinear gluons.

Quantities that obey the KLN theorem are *infrared safe*. This is to say that what they measure does not change with the addition of soft or collinear gluons.

Infrared safety is required for the factorisation properties of a calculation. A useful discussion of factorisation theorems is given in [67]. Here we shall just briefly mention the principles of factorisation: the process of separating the long distance (hadronic) from the short distance (partonic) part of a calculation.

In QCD calculations, it is assumed that we can separate interactions that occur at the parton level – the hard scattering process – from events that occur at the hadronic level.

We make the assumption that, in the hard scattering, each hadron is composed of fixed partons, each of which possesses a known fraction of the hadron's momentum. We will call this fraction of momentum x, where $0 \leq x \leq 1$. The parton content of a hadron is given by the parton distribution function: $f_{a/A}(x_A)$ is the probability of parton a being found in hadron A with momentum fraction x_A. This can then be used to express an interaction of hadrons in terms of the hard scattering cross section.

The general form of a differential cross section is:

$$d\sigma_{AB}(k_A, k_B) = \sum_{ab} \int dx_A \, dx_B \; f_{a/A}(x_A) f_{b/B}(x_B) \, d\hat{\sigma}_{ab}(x_A k_A, x_B k_B) \,, \tag{4.1}$$

where A and B are hadrons, a and b are partons and $f_{a/A}$ and $f_{b/B}$ are the parton distribution functions.

The partonic cross section given in this expression is $d\hat{\sigma}_{ab}$, the subtracted partonic cross section. This is the hard scattering cross section when the divergences have been removed. Final state soft and collinear divergences can be removed by cancelling with the divergences in the virtual part (the KLN theorem). In the sections to come, we will examine how initial state divergences may be removed: we will use the subtraction method to do this.

We calculate the subtracted cross section for the vector boson pair production processes that we wish to examine. Then we add in the parton distribution functions and integrate over phase space, in order to obtain a physical result.

4.1.2 Removing initial state singularities: the subtraction method

We have already mentioned the factorisation theorem and our need to be able to calculate initial state collinear singularities. These need to be removed by absorbing them into the parton distribution function.

Though IR singularities always cancel or can be absorbed, to give finite physical quantities, this does not happen automatically. We cannot numerically integrate over soft or collinear regions. Instead, we must separate these regions and calculate them analytically, before integrating the finite result.

This can be done in several ways. We will just mention two: the phase space slicing method, and the subtraction method. In later parts of this chapter, we will use the subtraction method to remove initial state collinear singularities from the vector boson pair production calculation.

One way of removing singular regions is to 'cut them out' of the calculation, replacing them by their limits. This is known as the phase space slicing method [68] [69] [70]. Here, and for the subtraction method, the one-dimensional example given in Kunszt [71] will be used for illustration.

In the phase space slicing method, singular regions are cut out and replaced with their limits, with the integration in the excluded area performed analytically. The boundary is defined by a small parameter, here δ.

Our one-dimensional example has the domain $0 \leq x \leq 1$ and a simple pole at $x = 0$. The integration region is sliced into two parts, with the boundary being δ. The part surrounding the pole, $0 < x < \delta$, is replaced by its limit, and the finite part $\delta < x < 1$ remains. It is necessary for δ to be much smaller than 1.

The integration is then:

$$\begin{aligned} I &\sim \lim_{\epsilon \to 0} \left\{ F(0) \int_0^\delta \frac{dx}{x} x^\epsilon + \int_\delta^1 \frac{dx}{x} x^\epsilon F(x) - \frac{1}{\epsilon} F(0) \right\} \\ &= F(0) \ln(\delta) + \int_\delta^1 \frac{dx}{x} F(x) \,. \end{aligned} \tag{4.2}$$

This is equation (32) of [71]. The remaining integral can be evaluated by normal numerical integration.

Alternatively, we can use the subtraction method: this is the choice we will make in this chapter. We use a version of the subtraction method as introduced by Ellis, Ross and Terrano [72] and developed by Kunszt and Soper [73].

The singular behaviour is a simple pole with a known residue. We subtract the integral at the pole and then add it on again. We shall see in the next section how this works in practice.

For our one-dimensional example, we have

$$\begin{aligned} I &= \lim_{\epsilon \to 0} \left\{ \int_0^1 \frac{dx}{x} x^\epsilon [F(x) - F(0)] + F[0] \int_0^1 \frac{dx}{x} x^\epsilon \right\} \\ &= \int_0^1 [F(x) - F(0)] + \frac{1}{\epsilon} F(0) \,. \end{aligned} \tag{4.3}$$

Again, this results in a term that can be integrated numerically.

In section 4.2 we will show how we use the subtraction method in order to give counterterms that cancel out our initial state singularities, resulting in the subtracted cross section that we require.

4.1.3 Infrared singularities at NLO and NNLO

Infrared singularities first arise at NLO. As previously discussed, these can be either soft (a particle becoming low-energy) or collinear (two particles becoming close in angle).

We will discuss the overall structure of these soft or collinear singularities. The behaviour of infrared divergences is universal: it does not depend on the particular process being considered.

We will mention the presence of soft and collinear singularities at NLO, then consider the NNLO case, where singularities can occur in combination, resulting in a much more complicated phase space.

First, consider what happens when a single final state particle in a n particle process becomes soft. When the momentum of the soft particle goes to zero, this reduces the number of particles by one. So as long as this soft particle is of low enough energy, the amplitude may be written as the $n-1$ particle amplitude, multiplied by a soft factor. This soft factor is normally called the eikonal factor.

If s is the soft gluon and a and b are its neighbouring particles (remembering that the amplitude is colour ordered), then:

$$\mathcal{A}_n(\ldots,a,s,b,\ldots) \xrightarrow{k_s\to 0} \frac{\langle ab\rangle}{\langle as\rangle\langle sb\rangle}\mathcal{A}_{n-1}(\ldots,a,b,\ldots)\,. \tag{4.4}$$

The eikonal factor is the term $\frac{\langle ab\rangle}{\langle as\rangle\langle sb\rangle}$ (or $\frac{[ab]}{[as][sb]}$, depending on the gluon helicity). This depends on the momenta of the soft gluon and its adjacent particles.

The other simple infrared singularity is the collinear case. Here a pair of particles become so close in angle that they can be replaced by a single particle, which is capable of splitting into the pair. Again this mean that the number of particles is reduced by one. We rewrite the original n particle amplitude as a $n-1$ particle amplitude, with the multiplying factor here being a splitting function.

If a and b are the two particles that are becoming collinear, we introduce c, which may split into the collinear pair, and substitute c into the amplitude in their place.

$$\mathcal{A}_n(\ldots,a,b,\ldots) \xrightarrow{a||b} S_{ac}(x)\mathcal{A}_{n-1}(\ldots,c,\ldots)\,. \tag{4.5}$$

The splitting function $S_{ac}(x)$ corresponds to particle c producing particle a with a momentum fraction x. As $k_c = k_a + k_b$, we know that $k_a = xk_c$ and $k_b = (1-x)k_c$. If the splitting is an unphysical one then the splitting function is zero. $|S_{ac}|^2 = P_{ac}$, where P_{ac} is the Altarelli-Parisi splitting function.

The only splitting function that is required in our vector boson pair production calculation is the function for a gluon splitting into a quark-antiquark pair. This is the function $P_{qg}(x)$. It is independent of the flavour of quark produced, and is the same for production of an antiquark as it is for a quark. The leading-order splitting function is:

$$|S_{qg}|^2 = P_{qg}(x) = \frac{1}{2}\{x^2 + (1-x)^2\}\,. \tag{4.6}$$

We can use this as long as we have summed over the helicities of the particles involved. If we have particles of specific helicity, the splitting function can be decomposed into S_{qg} terms of different helicities, which are used in the amplitudes. These are then squared to give the overall P_{qg} splitting function above.

The splitting function must obey some momentum restrictions. The quark pair must always be $q^+, \bar{q}^-$ or $q^-, \bar{q}^+$: it is not possible for the quark and the antiquark to have the same helicity.

In a NLO amplitude, it is only possible to have one soft singularity, or one collinear singularity. For each of these cases, we will calculate the amplitude as the leading order amplitude, multiplied by the appropriate prefactor.

When we start to examine the NNLO case, we see that the situation becomes much more complicated. The singularities are no longer restricted to those involving just a single particle. A simple soft or collinear singularity will reduce the number of partons in the process to $n-1$, meaning that we calculate an NLO process, multiplied by a prefactor. However, we know that NLO quantities can themselves have singularities, so therefore there may be a further soft or collinear factor. These singularities can occur in several different combinations, making the situation at NNLO much more complicated than it was at NLO.

The new types of singularity that arise at NNLO are

- double soft – two separate particles each become soft.
- soft-collinear – both a soft and a collinear singularity occur.
- double-collinear – two pairs of particles separately become collinear.
- triple-collinear – three particles all become collinear to each other, giving a splitting into three rather than two particles.

The behaviour of tree level and one loop amplitudes in these limits has been studied in [74],[75],[76],[77],[78],[79],[80],[81],[82],[83]. The new singularities lead to a very complicated phase space, and therefore many difficulties with integrating over the phase space.

However, we are very fortunate in our calculation of $gg \to WZq\bar{q}$, and other vector boson pair production processes. The singularities that occur in our case are straightforward and controllable.

Firstly, there are no soft singularities. Only a final state gluon can become soft, and our gluons are in the initial state. If a quark becomes soft, the amplitude does not develop a singularity as it does in the case of the gluon. Instead the amplitude just decreases to zero, as the process without the final state quark does not exist (we would have a single quark rather than a quark pair, which would make no sense).

We only need to consider collinear singularities. The collinear singularities are of a particular type. It is possible for a final state (anti)quark to become collinear to an initial state gluon, causing a collinear singularity, but there is no such singularity if a final state quark and antiquark become collinear to each other. Hence we have no final state singularities, only initial state.

We have single collinear singularities where either quark 7 or antiquark 8 becomes collinear to gluon 1 or gluon 2 – a total of 4 different scenarios.

An example of a relevant single collinear process is given schematically in figure 4.1.

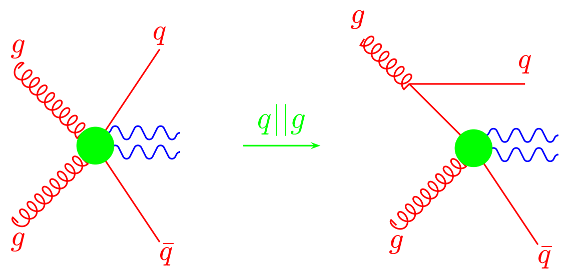

Figure 4.1: A single collinear limit of a gluon induced amplitude

This shows that the collinear limit of an 8-particle diagram is the appropriate 7-particle diagram multiplied by a splitting function, which in this case is that of a gluon splitting to a quark pair.

We also have double collinear singularities, where the quark and antiquark each become collinear to an initial state gluon, to form two separate collinear pairs. We may have quark 7 || gluon 1 and antiquark 8 || gluon 2, or the same but with gluons exchanged. There is no singularity where both quark and antiquark become collinear to the same gluon.

A schematic representation of a double collinear singularity, with two splitting functions, is given in figure 4.2.

To express the singular terms, we need only use the splitting function as in equation (4.6). If two particles become collinear, we just use it twice. As it is not possible for the two final state partons to become collinear to the same initial state parton simultaneously, we can just treat the process as two separate splittings.

These single and double collinear terms will come up in the calculation and as

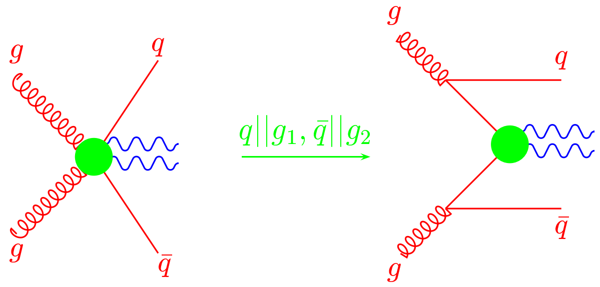

Figure 4.2: A double collinear limit of a gluon induced amplitude

collinear counterterms in the subtraction method. They also allow us to perform checks on our NNLO amplitudes by relating them to the known LO and NLO amplitudes, making sure that the collinear limits are correct.

Now we proceed to subtract the initial state singularities and to obtain a finite result for vector boson pair production. We will explain the particular form of the subtraction method that we are using, and how it is applied to the calculation.

4.2 The subtraction method in practice

Here we will use the subtraction method to remove initial state collinear singularities. These are not process dependent, so we can discuss a general case before turning to the specifics of vector boson pair production in section 4.3.

From the factorisation theorem, the general form of a differential cross section is as discussed before:

$$d\sigma_{AB}(k_A, k_B) = \sum_{ab} \int dx_A \, dx_B \; f_{a/A}(x_A) f_{b/B}(x_B) \, d\hat{\sigma}_{ab}(x_A k_A, x_B k_B) \,. \tag{4.7}$$

This relates the partonic calculation to the hadron-level result. It describes a cross section as a subtracted cross section convoluted with parton density functions.

Here we can make use of the universal nature of QCD. Not only does equation (4.7) apply to the partons in a hadron (the chance of finding each parton being determined by the parton distribution function), but the equation can also be rewritten as the chance of finding a parton within another parton (QCD allows us to make this formal substitution).

Here the incoming partons for our hard scattering, a and b, may come via a splitting function from initial partons c and d.

$$d\sigma_{cd}(k_1, k_2) = \sum_{ab} \int dx_1\, dx_2\, f_{a/c}(x_1) f_{b/d}(x_2)\, d\hat{\sigma}_{ab}(x_1 k_1, x_2 k_2)\,. \tag{4.8}$$

Now we will assign the incoming partons c and d the momenta k_1 and k_2 respectively, as these will later become our incoming gluons 1 and 2.

We already know the unsubtracted cross sections for our vector boson pair production processes. These are just the hard scattering terms that we have already calculated. When we consider the parton level expression, we find that we also know the parton distribution functions. The probability of getting a parton from another parton is simply a splitting function at the appropriate order. To calculate the subtracted cross section, we need the unsubtracted hard scattering cross sections and the parton distributions at the correct order in QCD. We shall perform this calculation both at NLO and at NNLO.

4.2.1 General subtraction terms at NLO

Infrared singularities first occur at NLO, so this is the simplest case in which we can discuss the subtraction method. The calculation that we want to perform at NNLO is just an extension of this.

To calculate the subtracted cross section at NLO, we need the NLO unsubtracted cross section, which we shall assume we know, and a NLO parton distribution. The NLO parton distribution is just a delta function (the probability of finding exactly the same particle with the same energy) plus an Altarelli-Parisi splitting function as described earlier, with the resulting parton having a fraction x of the energy of the parton that it originates from.

The expression for the NLO parton distribution is:

$$f_{a/c}(x) = \delta_{ac}\delta(1-x) - \frac{\alpha_s}{2\pi}\left(\frac{1}{\bar{\epsilon}} P_{ac}(x,0) - K_{ac}(x)\right) + \mathcal{O}(\alpha_s^2)\,. \tag{4.9}$$

$P_{ac}(x, 0)$ is the Altarelli-Parisi splitting function for $\epsilon = 0$ (4 dimensions). From now on, we will suppress the zero, and use $P_{ac}(x)$. The splitting function depends on the types of parton involved, and on the momentum fraction. $1/\bar{\epsilon}$ is defined by $1/\bar{\epsilon} \equiv 1/\epsilon - \gamma_E + \log 4\pi$.

The term K_{ad} is dependent on which factorisation scheme is used. We will work in $\overline{\mathrm{MS}}$, where $K_{ad} \equiv 0$. The fact that we have to make a choice indicates that the result will be dependent on the factorisation scheme. We must consider this dependence and whether it will affect the overall result. This is especially relevant later, when we calculate the NNLO gg induced vector boson pair production. However, when we calculate the gg term, we have already made an approximation in selecting only this one term from all possible NNLO terms. We assume that any effect due to scheme dependence will be less than the effect resulting from choosing only gg.

Substituting the parton distribution of equation (4.9) into equation (4.8), we obtain an expression that relates subtracted and unsubtracted cross sections.

$$\begin{aligned} d\sigma_{cd}(k_1,k_2) &= \sum_{ab}\int dx_1 dx_2 \left[\delta_{ac}\delta(1-x_1) - \frac{\alpha_s}{2\pi}\frac{1}{\bar{\epsilon}}P_{ac}(x_1)\right] \\ &\quad \left[\delta_{bd}\delta(1-x_2) - \frac{\alpha_s}{2\pi}\frac{1}{\bar{\epsilon}}P_{bd}(x_2)\right] d\hat{\sigma}_{ab}(x_1k_1, x_2k_2)\,. \end{aligned} \tag{4.10}$$

On expanding this expression, and retaining terms only up to NLO, we obtain:

$$\begin{aligned} d\sigma_{cd}(k_1,k_2) &= d\hat{\sigma}_{cd}(k_1,k_2) - \frac{\alpha_s}{2\pi}\sum_a \int dx_1 \frac{1}{\bar{\epsilon}}P_{ac}(x_1) d\hat{\sigma}_{ad}(x_1k_1,k_2) \\ &\quad - \frac{\alpha_s}{2\pi}\sum_b \int dx_2 \frac{1}{\bar{\epsilon}}P_{bd}(x_2) d\hat{\sigma}_{cb}(k_1,x_2k_2) + \mathcal{O}(\alpha_s^2)\,. \end{aligned} \tag{4.11}$$

Each term can then be broken up into the sum of its leading order and NLO parts, calling these $d\sigma^{(0)}$ and $d\sigma^{(1)}$ respectively ($d\hat{\sigma}^{(0)}$ and $d\hat{\sigma}^{(1)}$ for the subtracted cross section). This allows us to equate terms order by order in α_s.

At leading order there are no divergences, and therefore no need for subtraction, meaning that $d\hat{\sigma}^{(0)}$ is just the same as $d\sigma^{(0)}$.

At NLO, we rearrange equation (4.11), using the fact that $d\hat{\sigma}^{(0)} = d\sigma^{(0)}$, to give an expression for the NLO subtracted cross section in terms of unsubtracted quantities.

$$\begin{aligned} d\hat{\sigma}^{(1)}_{cd}(k_1,k_2) &= d\sigma^{(1)}_{cd}(k_1,k_2) + \frac{\alpha_s}{2\pi}\sum_a \int dx_1 \frac{1}{\bar{\epsilon}} P_{ac}(x) d\sigma^{(0)}_{ad}(x_1 k_1, k_2) \\ &\quad + \frac{\alpha_s}{2\pi}\sum_b \int dx_2 \frac{1}{\bar{\epsilon}} P_{bd}(x,0) d\sigma^{(0)}_{cb}(k_1, x_2 k_2)\,. \end{aligned} \tag{4.12}$$

The leading order terms that add to the unsubtracted terms are the collinear counterterms that are required to obtain a finite result. All that we need at NLO is these two counterterms. At NNLO it will be more complicated. We must then add a explicit $\mathcal{O}(\alpha_s^2)$ term to equation (4.9) as well as including another order in the cross section.

4.2.2 General subtraction terms at NNLO

Now that we have discussed the subtraction method at NLO, it is time to turn to the situation at NNLO, which is the case that we will need when discussing gluon-gluon induced vector boson pair production. This is just an extension of the NLO calculation with more complicated expressions, and a greater number of possible singularities. We will follow the same procedure as in the previous section to give us the general counterterms for NNLO. In section 4.3 we will translate the general particles into our incoming gluons and outgoing quarks.

Again we use equation (4.8), substituting in appropriate parton distributions. However, we now have to add an extra term to the distribution of equation (4.9): we can no longer ignore terms of $\mathcal{O}(\alpha_s^2)$. The new expression for the parton distribution function in $\overline{\text{MS}}$ is:

$$f_{a/c} = \delta_{ac}\delta(1-x) - \frac{\alpha_s}{2\pi}\frac{1}{\bar{\epsilon}}P_{ac}(x) - \left(\frac{\alpha_s}{2\pi}\right)^2\left(\frac{1}{\bar{\epsilon}}\right)^2 Q_{ac}(x) + \mathcal{O}(\alpha_s^3)\,. \tag{4.13}$$

$P_{ac}(x)$ is the one-loop Altarelli-Parisi splitting function in 4 dimensions, while $Q_{ac}(x)$ is the next order contribution, including two-loop splitting functions.

Substituting into equation (4.8):

$$\begin{aligned} d\sigma_{cd}(k_1,k_2) &= \sum_{ab}\int dx_1 dx_2 \left[\delta_{ac}\delta(1-x_1) - \frac{\alpha_s}{2\pi}\frac{1}{\bar{\epsilon}}P_{ac}(x_1) - \left(\frac{\alpha_s}{2\pi}\right)^2\left(\frac{1}{\bar{\epsilon}}\right)^2 Q_{ac}(x_1)\right] \\ &\left[\delta_{bd}\delta(1-x_2) - \frac{\alpha_s}{2\pi}\frac{1}{\bar{\epsilon}}P_{bd}(x_2) - \left(\frac{\alpha_s}{2\pi}\right)^2\left(\frac{1}{\bar{\epsilon}}\right)^2 Q_{bd}(x_2)\right] d\hat{\sigma}_{ab}(x_1k_1, x_2k_2)\,. \end{aligned} \tag{4.14}$$

Expanding this expression and retaining terms up to $\mathcal{O}(\alpha_s^2)$, we get

$$\begin{aligned} d\sigma_{cd}(k_1,k_2) &= d\hat{\sigma}_{cd}(k_1,k_2) \\ &- \frac{\alpha_s}{2\pi}\sum_a\int dx_1 \left(\frac{1}{\bar{\epsilon}}P_{ac}(x_1) + \frac{\alpha_s}{2\pi}\left(\frac{1}{\bar{\epsilon}}\right)^2 Q_{ac}(x_1)\right) d\hat{\sigma}_{ad}(x_1k_1,k_2) \\ &- \frac{\alpha_s}{2\pi}\sum_b\int dx_2 \left(\frac{1}{\bar{\epsilon}}P_{bd}(x_2) + \frac{\alpha_s}{2\pi}\left(\frac{1}{\bar{\epsilon}}\right)^2 Q_{bd}(x_2)\right) d\hat{\sigma}_{cb}(k_1,x_2k_2) \\ &+ \left(\frac{\alpha_s}{2\pi}\right)^2\sum_{ab}\int dx_1dx_2 \left(\frac{1}{\bar{\epsilon}}P_{ac}(x_1)\right)\left(\frac{1}{\bar{\epsilon}}P_{bd}(x_1)\right) d\hat{\sigma}_{ab}(x_1k_1,x_2k_2) \\ &+ \mathcal{O}(\alpha_s^3)\,. \end{aligned} \tag{4.15}$$

We expand the cross sections and compare terms order by order.

$$d\sigma_{cd} = d\sigma_{cd}^{(0)} + d\sigma_{cd}^{(1)} + d\sigma_{cd}^{(2)} \tag{4.16}$$

$$d\hat{\sigma}_{cd} = d\hat{\sigma}_{cd}^{(0)} + d\hat{\sigma}_{cd}^{(1)} + d\hat{\sigma}_{cd}^{(2)} \tag{4.17}$$

Once again, at leading order, $d\sigma_{cd}^{(0)} = d\hat{\sigma}_{cd}^{(0)}$. We will use this equality later. At $\mathcal{O}(\alpha_s)$, we have the same result as was found in the previous section:

$$\begin{aligned} d\hat{\sigma}_{cd}^{(1)}(k_1,k_2) &= d\sigma_{cd}^{(1)}(k_1,k_2) \\ &+ \frac{\alpha_s}{2\pi}\sum_a\int dx_1\left(\frac{1}{\bar{\epsilon}}P_{ac}(x_1)\right) d\hat{\sigma}_{ad}^{(0)}(x_1k_1,k_2) \\ &+ \frac{\alpha_s}{2\pi}\sum_b\int dx_2\left(\frac{1}{\bar{\epsilon}}P_{bd}(x_2)\right) d\hat{\sigma}_{cb}^{(0)}(k_1,x_2k_2)\,. \end{aligned} \tag{4.18}$$

This gives us an expression for the NLO subtracted cross section in terms of the

NLO unsubtracted cross section plus leading order counterterms.

At $\mathcal{O}(\alpha_s^2)$ there are clearly more terms involved. A simple expansion of equation (4.15) gives:

$$\begin{aligned}
d\sigma_{cd}^{(2)}(k_1,k_2) \;=\;& d\hat{\sigma}_{cd}^{(2)}(k_1,k_2) \\
&- \frac{\alpha_s}{2\pi}\sum_a \int dx_1 \left(\frac{1}{\bar{\epsilon}}P_{ac}(x_1)\right) d\hat{\sigma}_{ad}^{(1)}(x_1k_1,k_2) \\
&- \frac{\alpha_s}{2\pi}\sum_b \int dx_2 \left(\frac{1}{\bar{\epsilon}}P_{bd}(x_2)\right) d\hat{\sigma}_{cb}^{(1)}(k_1,x_2k_2) \\
&- \left(\frac{\alpha_s}{2\pi}\right)^2 \sum_a \int dx_1 Q_{ac}(x_1) d\hat{\sigma}_{ad}^{(0)}(x_1k_1,k_2) \\
&- \left(\frac{\alpha_s}{2\pi}\right)^2 \sum_b \int dx_2 Q_{bd}(x_2) d\hat{\sigma}_{cb}^{(0)}(k_1,x_2k_2) \\
&+ \left(\frac{\alpha_s}{2\pi}\right)^2 \sum_{ab} \int dx_1 dx_2 \left(\frac{1}{\bar{\epsilon}}P_{ac}(x_1)\right)\left(\frac{1}{\bar{\epsilon}}P_{bd}(x_2)\right) d\hat{\sigma}_{ab}^{(0)}(x_1k_1,x_2k_2) \\
&+ \mathcal{O}(\alpha_s^3)\,.
\end{aligned} \tag{4.19}$$

We then use the expressions that we already have for $d\hat{\sigma}^{(0)}$ and $d\hat{\sigma}^{(1)}$ and substitute in to get the whole $\mathcal{O}(\alpha_s^2)$ equation with all counterterms given explicitly.

$$\begin{aligned}
d\hat{\sigma}_{cd}^{(2)}(k_1,k_2) \;=\;& d\sigma_{cd}^{(2)}(k_1,k_2) \\
&+ \frac{\alpha_s}{2\pi}\sum_a \int dx_1 \left(\frac{1}{\bar{\epsilon}}P_{ac}(x_1)\right) d\sigma_{ad}^{(1)}(x_1k_1,k_2) \\
&+ \frac{\alpha_s}{2\pi}\sum_b \int dx_2 \left(\frac{1}{\bar{\epsilon}}P_{bd}(x_2)\right) d\sigma_{cb}^{(1)}(k_1,x_2k_2) \\
&+ \left(\frac{\alpha_s}{2\pi}\right)^2 \sum_{yz} \int dx_1 dx_2 \left(\frac{1}{\bar{\epsilon}}P_{yc}(x_1)\frac{1}{\bar{\epsilon}}P_{zy}(x_2)\right) d\sigma_{zd}^{(0)}(x_1x_2k_1,k_2) \\
&+ \left(\frac{\alpha_s}{2\pi}\right)^2 \sum_{yz} \int dx_1 dx_2 \left(\frac{1}{\bar{\epsilon}}P_{yd}(x_1)\frac{1}{\bar{\epsilon}}P_{zy}(x_2)\right) d\sigma_{cz}^{(0)}(k_1,x_1x_2k_2) \\
&+ \left(\frac{\alpha_s}{2\pi}\right)^2 \sum_a \int dx_1 Q_{ac}(x_1) d\sigma_{ad}^{(0)}(x_1k_1,k_2) \\
&+ \left(\frac{\alpha_s}{2\pi}\right)^2 \sum_b \int dx_2 Q_{bd}(x_2) d\sigma_{cb}^{(0)}(k_1,x_2k_2)
\end{aligned}$$

$$+\left(\frac{\alpha_s}{2\pi}\right)^2 \sum_{ab} \int dx_1 dx_2 \left(\frac{1}{\bar{\epsilon}} P_{ac}(x_1)\right) \left(\frac{1}{\bar{\epsilon}} P_{bd}(x_2)\right) d\sigma^{(0)}_{ab}(x_1 k_1, x_2 k_2)\,. \tag{4.20}$$

This is the general expression for removing the initial state collinear singularities from a NNLO quantity by using collinear counterterms. One would expect to be able to expand the terms explicitly and remove the singularities analytically. It can be seen that some of the poles are explicit and some are 'hidden' inside (N)NLO cross sections.

4.3 Applying the subtraction method to vector boson pair production

We now have a general expression for the counterterms required to subtract initial state collinear singularities from an NNLO cross section: this is equation (4.20). We now want to apply this to the specific case of vector boson pair production. To do this, we need to consider only the two initial state gluons and the final quark-antiquark pair.

For the first half of this section, while establishing the counterterms, the expressions will be appropriate for any vector boson pair production process. In the second half, the finite terms for a calculation of $gg \to WZq\bar{q}$ will be calculated, and we will indicate how to convert the result into $W\gamma$ or $Z\gamma$ production.

We need to substitute actual particles for the generic a, b, c, d of equation (4.20). Our initial particles, c and d, are now specified as the two initial state gluons g_1 and g_2. These may be substituted for c and d in either order, but for now we will just call them both g. A σ_{gg} term is the NNLO cross section including both gluon orderings.

The particles a and b are particles which the initial gluons may split into. In theory, these may be either quarks or gluons. However, we have to remember that they are also the incoming particles for the vector boson pair production hard scattering process. The incoming particles for LO vector boson pair production can only be $q\bar{q}$, in either ordering. For NLO vector boson pair production, we can also have

qg or $\bar{q}g$, again in either ordering. These restrictions on the hard scattering process limit the number of counterterms.

First we substitute gluons for the initial state partons c and d in equation (4.20). This gives us:

$$\begin{aligned} d\hat{\sigma}^{(2)}_{gg}(k_1,k_2) &= d\sigma^{(2)}_{gg}(k_1,k_2) \\ &+ \frac{\alpha_s}{2\pi}\sum_a \int dx_1 \left(\frac{1}{\bar{\epsilon}}P_{ag}(x_1)\right) d\sigma^{(1)}_{ag}(x_1k_1,k_2) \\ &+ \frac{\alpha_s}{2\pi}\sum_b \int dx_2 \left(\frac{1}{\bar{\epsilon}}P_{bg}(x_2)\right) d\sigma^{(1)}_{gb}(k_1,x_2k_2) \\ &+ \left(\frac{\alpha_s}{2\pi}\right)^2 \sum_{yz} \int dx_1dx_2 \left(\frac{1}{\bar{\epsilon}}P_{yg}(x_1)\frac{1}{\bar{\epsilon}}P_{zy}(x_2)\right) d\sigma^{(0)}_{zg}(x_1x_2k_1,k_2) \\ &+ \left(\frac{\alpha_s}{2\pi}\right)^2 \sum_{yz} \int dx_1dx_2 \left(\frac{1}{\bar{\epsilon}}P_{yg}(x_1)\frac{1}{\bar{\epsilon}}P_{zy}(x_2)\right) d\sigma^{(0)}_{gz}(k_1,x_1x_2k_2) \\ &+ \left(\frac{\alpha_s}{2\pi}\right)^2 \sum_a \int dx_1 Q_{ag}(x_1) d\sigma^{(0)}_{ag}(x_1k_1,k_2) \\ &+ \left(\frac{\alpha_s}{2\pi}\right)^2 \sum_b \int dx_2 Q_{bg}(x_2) d\sigma^{(0)}_{gb}(k_1,x_2k_2) \\ &+ \left(\frac{\alpha_s}{2\pi}\right)^2 \sum_{ab} \int dx_1dx_2 \left(\frac{1}{\bar{\epsilon}}P_{ag}(x_1)\right)\left(\frac{1}{\bar{\epsilon}}P_{bg}(x_2)\right) d\sigma^{(0)}_{ab}(x_1k_1,x_2k_2)\,. \end{aligned} \tag{4.21}$$

Examining this expression, we find some impossible terms – we cannot have a leading order vector boson pair production cross section with a gluon in the initial state. Therefore all terms including $d\sigma^{(0)}_{xg}$ or $d\sigma^{(0)}_{gx}$ can be removed. The remaining terms are:

$$\begin{aligned} d\hat{\sigma}^{(2)}_{gg}(k_1,k_2) &= d\sigma^{(2)}_{gg}(k_1,k_2) \\ &+ \frac{\alpha_s}{2\pi}\sum_a \int dx_1 \left(\frac{1}{\bar{\epsilon}}P_{ag}(x_1)\right) d\sigma^{(1)}_{ag}(x_1k_1,k_2) \\ &+ \frac{\alpha_s}{2\pi}\sum_b \int dx_2 \left(\frac{1}{\bar{\epsilon}}P_{bg}(x_2)\right) d\sigma^{(1)}_{gb}(k_1,x_2k_2) \end{aligned}$$

$$+\left(\frac{\alpha_s}{2\pi}\right)^2 \sum_{ab} \int dx_1 dx_2 \left(\frac{1}{\bar{\epsilon}} P_{ag}(x_1)\right) \left(\frac{1}{\bar{\epsilon}} P_{bg}(x_2)\right) d\sigma^{(0)}_{ab}(x_1 k_1, x_2 k_2)\,. \tag{4.22}$$

Now we may substitute q or $\bar{q}$ for each a or b. This gives us a LO term with a $q\bar{q}$ initial state and a NLO term with qg or $\bar{q}g$ initial state: these terms are all allowed. The counterterms result from the single and double collinear singularities as detailed in section 4.1.3, with all splitting functions as required.

With these substituted in all possible ways, we get the expression:

$$\begin{aligned}
d\hat{\sigma}^{(2)}_{gg}(k_1, k_2) &= d\sigma^{(2)}_{gg}(k_1, k_2) \\
&+ \frac{\alpha_s}{2\pi} \int dx_1 \left(\frac{1}{\bar{\epsilon}} P_{qg}(x_1)\right) d\sigma^{(1)}_{qg}(x_1 k_1, k_2) + \frac{\alpha_s}{2\pi} \int dx_1 \left(\frac{1}{\bar{\epsilon}} P_{\bar{q}g}(x_1)\right) d\sigma^{(1)}_{\bar{q}g}(x_1 k_1, k_2) \\
&+ \frac{\alpha_s}{2\pi} \int dx_2 \left(\frac{1}{\bar{\epsilon}} P_{qg}(x_2)\right) d\sigma^{(1)}_{gq}(k_1, x_2 k_2) + \frac{\alpha_s}{2\pi} \int dx_2 \left(\frac{1}{\bar{\epsilon}} P_{\bar{q}g}(x_2)\right) d\sigma^{(1)}_{g\bar{q}}(k_1, x_2 k_2) \\
&+ \left(\frac{\alpha_s}{2\pi}\right)^2 \int dx_1 dx_2 \left(\frac{1}{\bar{\epsilon}} P_{qg}(x_1)\right) \left(\frac{1}{\bar{\epsilon}} P_{\bar{q}g}(x_2)\right) d\sigma^{(0)}_{q\bar{q}}(x_1 k_1, x_2 k_2) \\
&+ \left(\frac{\alpha_s}{2\pi}\right)^2 \int dx_1 dx_2 \left(\frac{1}{\bar{\epsilon}} P_{\bar{q}g}(x_1)\right) \left(\frac{1}{\bar{\epsilon}} P_{qg}(x_2)\right) d\sigma^{(0)}_{\bar{q}q}(x_1 k_1, x_2 k_2)\,.
\end{aligned} \tag{4.23}$$

These are all the necessary counterterms to produce a finite result. We now have to substitute in more explicit expressions for the terms themselves, and cancel the singularities. This is a lengthy procedure, so here we will just give the final result. This will be a finite expression that can be integrated numerically, and will use LO, NLO and NNLO cross sections for vector boson pair production.

In calculating these terms we use the same conventions and parameterisation as Frixione, Kunszt and Signer [84], expressing momenta in terms of energy and angle variables. The incoming gluons are labelled g_1 and g_2. We shall label the outgoing quark and antiquark as q_7 and $\bar{q}_8$, and the final electroweak decay particles as particles 3 to 6. Of course, this assumes that we have an 8 particle process, as in $gg \to WZq\bar{q}$. For $W\gamma$ or $Z\gamma$ production, we just have to remove one of particles $3-6$ and relabel the remaining particles, which is straightforward.

In the partonic centre of mass frame, incoming gluons 1 and 2 have momenta:

$$k_1 = \frac{\sqrt{s_{12}}}{2}(1, \vec{0}, 1) \tag{4.24}$$

$$k_2 = \frac{\sqrt{s_{12}}}{2}(1, \vec{0}, -1) \tag{4.25}$$

The outgoing quarks have momenta parameterised as:

$$k_7 = \frac{\sqrt{s_{12}}}{2}\xi_7 \left(1, \sqrt{1-y_7^2}\,\vec{e}_T, y_7\right) \tag{4.26}$$

$$k_8 = \frac{\sqrt{s_{12}}}{2}\xi_8 \left(1, \sqrt{1-y_8^2}\,\vec{e}_T, y_8\right) \tag{4.27}$$

where $\vec{e}_T$ is a $D-2$ dimensional unit vector in transverse momentum space, $y_i = \cos\theta_i$ so that $-1 \leq y_i \leq 1$, and $0 \leq \xi_i \leq 1$. s_{12} is the partonic centre of mass energy.

This parameterisation makes the soft and collinear limits apparent. The soft limit results from taking the energy variable to zero, $\xi_i \to 0$. The collinear limit where one of the outgoing quarks becomes collinear to one of the incoming gluons occurs when the angle variable y becomes the same as that of one of the gluons, $y_i \to \pm 1$.

We then follow a procedure similar to that in [84] to cancel singularities explicitly, giving us a finite term.

This is the sum of three separately finite pieces.

$$d\hat{\sigma}_{gg}^{(2)} = d\sigma^{(\text{fin},6)} + d\sigma^{(\text{fin},7)} + d\sigma^{(\text{fin},8)} \tag{4.28}$$

$d\sigma^{(\text{fin},6)}$ is the term containing the 6 particle LO amplitudes. $d\sigma^{(\text{fin},7)}$ contains the 7 particle NLO amplitudes, and $d\sigma^{(\text{fin},8)}$ contains the 8 particle NNLO amplitudes.

We should note here that only the 4-dimensional matrix elements need to be used, despite the fact that the subtraction calculation takes place in $D = 4 - 2\epsilon$ dimensions. We must be careful to make sure that in only using 4-dimensional matrix elements, we do not lose extra finite pieces that may result from calculating in D dimensions.

We need to consider both the initial state collinear singularities, which are absorbed into the parton distributions, and the final state collinear and soft singularities, which cancel with the singularities from the virtual part.

Our version of the subtraction method deals with the latter situation by dividing the matrix element into a 4-dimensional part and a $1/\epsilon$-term. Around the pole we have a reduced matrix element multiplied by a splitting function, as we explained earlier in this chapter. The reduced matrix element is subtracted from the full matrix element, and then added again separately and integrated analytically. There is a universal finite part associated with each $1/\epsilon$ pole. In this process of subtracting and the adding on the pole part, any finite part that may be associated with the pole is also subtracted and added, meaning that we do not miss any terms in just taking the 4-dimensional part.

Initial state collinear singularities are absorbed into the parton distributions. When doing this, we only use 4 dimensional splitting functions in, for example, equations (4.9) and (4.13). We do this because we work in the $\overline{\mathrm{MS}}$ scheme: a different choice of splitting function would imply the use of a different scheme. As we already stated in section 4.2.1, our result is scheme dependent, but the scheme dependence is not important at the level of accuracy of our calculation.

We now give the finite terms explicitly.

The explicit form of $d\sigma^{(\mathrm{fin},8)}$ is given by

$$\begin{aligned} d\sigma^{(\mathrm{fin},8)} &= (1-y_7^2)(1-y_8^2)\mathcal{M}_{gg}^{(8)}\left(k_1,k_2,\{k_i\}_{3,6},k_7,k_8\right)\frac{s_{12}^2}{64(2\pi)^6}\xi_7\,\xi_8\,\mathcal{P}(y_7)\,\mathcal{P}(y_8) \\ & \quad d\xi_7\,d\xi_8\,dy_7\,dy_8\,d\varphi_7\,d\varphi_8\,d\Phi_{(3-6)}\,. \end{aligned} \tag{4.29}$$

$d\Phi_{(3-6)}$ is the phase-space integration over the vector-boson decay products.

$\mathcal{M}_{gg}^{(8)}$ is the squared amplitude summed (averaged) over helicities, including the flux factor $1/(2s_{12})$. This is just the $\mathcal{M}^{WZ}$ of equation (3.12).

We have also included the distribution $\mathcal{P}(y_i)$, where i is 7 or 8. This is given by:

$$\mathcal{P}(y_i) \equiv \frac{1}{2}\left[\left(\frac{1}{1-y_i}\right)_{\delta_I} + \left(\frac{1}{1+y_i}\right)_{\delta_I}\right]. \tag{4.30}$$

The distributions $\left(\frac{1}{1\pm y_i}\right)_{\delta_I}$ have been introduced in [84] and are defined for an arbitrary test function $f(y_i)$ through

$$\left\langle \left(\frac{1}{1\pm y_i}\right)_{\delta_I}, f(y_i) \right\rangle = \int_{-1}^{1} dy_i \, \frac{f(y_i) - f(\mp 1)\theta(\mp y_i - 1 + \delta_I)}{1 \pm y_i} \,. \tag{4.31}$$

The two $\mathcal{P}$ distributions in equation (4.29) perform the subtraction of single and double collinear singularities in the 8-particle NNLO amplitudes.

The expression for the 7 particle finite part is somewhat more complicated.

$$\begin{aligned} d\sigma^{(\mathrm{fin},7)} \;=\; & \frac{\alpha_s}{2\pi}\left(\mathcal{L}_7 P^{<}_{qg}(1-\xi_7) - P'^{<}_{qg}(1-\xi_7)\right)(1-y_8^2) \\ & \left\{ \mathcal{M}^{(7)}_{\bar{q}g}\left((1-\xi_7)k_1, k_2, \{k_i\}_{3,6}, k_8\right) + \mathcal{M}^{(7)}_{g\bar{q}}\left(k_1, (1-\xi_7)k_2, \{k_i\}_{3,6}, k_8\right) \right\} \\ & \frac{s_{12}}{8(2\pi)^3}\, \xi_8\, \mathcal{P}(y_8)\, d\xi_7\, d\xi_8\, dy_8\, d\varphi_8\, d\Phi_{(3-6)} \\ & + \frac{\alpha_s}{2\pi}\left(\mathcal{L}_8 P^{<}_{\bar{q}g}(1-\xi_8) - P'^{<}_{\bar{q}g}(1-\xi_8)\right)(1-y_7^2) \\ & \left\{ \mathcal{M}^{(7)}_{qg}\left((1-\xi_8)k_1, k_2, \{k_i\}_{3,6}, k_7\right) + \mathcal{M}^{(7)}_{gq}\left(k_1, (1-\xi_8)k_2, \{k_i\}_{3,6}, k_7\right) \right\} \\ & \frac{s_{12}}{8(2\pi)^3}\, \xi_7\, \mathcal{P}(y_7)\, d\xi_7\, d\xi_8\, dy_7\, d\varphi_7\, d\Phi_{(3-6)} \,. \end{aligned} \tag{4.32}$$

Most of these terms are familiar. $\mathcal{M}^{(7)}_{\bar{q}g}$ and similar terms are the NLO squared amplitudes for WZ production as stated in [25]. We also have the $\mathcal{P}$ distribution defined in equation (4.30), which subtracts the single collinear singularity present in the 7 particle amplitude.

We have also used the functions $\mathcal{L}_7$ and $\mathcal{L}_8$, which are defined by

$$\mathcal{L}_7 = \log \frac{s_{12}\, \delta_I\, \xi_7^2}{2\mu^2} \qquad \mathcal{L}_8 = \log \frac{s_{12}\, \delta_I\, \xi_8^2}{2\mu^2} \tag{4.33}$$

s_{12} is the centre of mass energy. δ_I is an arbitrary quantity that is present in all the finite terms, and cancels when they are summed to give the total finite cross section. ξ_7 and ξ_8 relate to the energy of q_7 and $\bar{q}_8$, and μ is the factorisation scale.

We divide the unregularized Altarelli-Parisi splitting function into the 4-dimensional piece, $P^{<}_{ad}$, and the piece proportional to ϵ, $P'^{<}_{ad}$. Explicitly,

$$P^{<}_{qg}(1-\xi_i) \;=\; \frac{1}{2}(1 - 2\xi_i + 2\xi_i^2) \tag{4.34}$$

$$P'^{<}_{qg}(1-\xi_i) \;=\; \xi_i(\xi_i-1)\,. \tag{4.35}$$

Finally, the 6 parton case is reasonably simple, and only uses quantities that have already been defined above.

$$\begin{aligned} d\sigma^{(\mathrm{fin},6)} \;=\; & \left(\frac{\alpha_s}{2\pi}\right)^2 \left(\mathcal{L}_7 P^{<}_{qg}(1-\xi_7) - P'^{<}_{qg}(1-\xi_7)\right) \left(\mathcal{L}_8 P^{<}_{\bar{q}g}(1-\xi_8) - P'^{<}_{\bar{q}g}(1-\xi_8)\right) \\ & \Big\{ \mathcal{M}^{(6)}_{\bar{q}q}\left((1-\xi_7)k_1, (1-\xi_8)k_2, \{k_i\}_{(3,6)}\right) \\ & \quad + \mathcal{M}^{(6)}_{q\bar{q}}\left((1-\xi_8)k_1, (1-\xi_7)k_2, \{k_i\}_{(3,6)}\right) \Big\}\, d\xi_7\, d\xi_8\, d\Phi_{(3-6)}\,. \end{aligned} \tag{4.36}$$

We then implement all these finite terms in a numerical integration. We already mentioned the quantity δ_I, which occurs in all the finite terms, but is cancelled when the terms are added. This provides a good check on our calculation: it must be invariant under a change in δ_I.

As already mentioned, we have the necessary amplitudes for WZ production in [25] and Appendix B of this thesis. To calculate $W\gamma$ or $Z\gamma$ production, we use the appropriate 5, 6 and 7 particle amplitudes from [25] and Appendix B and relabel as necessary. Otherwise the subtraction process is the same.

These terms are then implemented in a numerical integration over phase space, using `VEGAS` [85].

4.4 Treatment of photons in $W\gamma$ and $Z\gamma$ production

We have already dealt with all the infrared singularities that arise in the case of $gg \to WZq\bar{q}$. In this case we were only concerned about quarks and gluons and could totally neglect the electroweak particles and their decay products when it came to thinking about singularities.

This would still be the case if we were calculating, for example, production of a WW pair or a ZZ pair. The final state leptons could not become soft, or collinear to the final state quarks. However, if we have an external photon in the final state, as in the $W\gamma$ and $Z\gamma$ production processes, we have a new scenario. It is possible for a photon to become collinear to a quark, as a quark may emit a photon: this is known as fragmentation. We have to consider new singularities due to the photon behaviour.

To treat these singularities properly, it would be necessary to add fragmentation contributions to our photon production. The calculation would be divided in to direct and fragmentation contributions, with the fragmentation term being a non-perturbative term. However, the photon fragmentation is not known at this order (it is not even known at NLO for the process of interest).

To get round this problem it is possible to use an isolation procedure that restricts the angle of the photon and does not allow it to become collinear to the quark or antiquark. It also removes the possibility of the photon being 'faked' by a quark jet. The easiest way to isolate the photon is to impose a cone round the photon, completely excluding all hadrons in this region. However, this complete exclusion within a cone is not infrared safe, nor is it realistic as far as the detector is concerned. Therefore the normal way to deal with the photon is to allow a small hadronic energy, $E_T < E_{T\,\mathrm{max}}$, in the vicinity of the photon.

An infrared-safe photon isolation procedure was introduced by Frixione [86]. This also allows only a certain small hadronic energy in the neighbourhood of the photon, but this energy varies with the distance from the photon. The energy must be zero at the photon itself, and then grows with the distance from the photon until it reaches a specified cut-off.

The hadronic momentum deposited in a cone of size R_0 around the momentum of the photon must obey the condition:

$$\sum_i p_{Ti}\theta(R - R_{i\gamma}) \leq p_{T\gamma}\left(\frac{1-\cos R}{1-\cos R_0}\right) , \tag{4.37}$$

for all $R \leq R_0$. p_{Ti} are the hadronic momenta present within the cone, and $p_{T\gamma}$ is the photon momentum.

The distance, $R_{i\gamma}$ in pseudorapidity η and azimuthal angle ϕ is given by

$$R_{i\gamma} = \sqrt{(\eta_i - \eta_\gamma)^2 + (\phi_i - \phi_\gamma)^2} . \tag{4.38}$$

Then only soft partons can be emitted close to the photon, and we can eliminate the possibility of troublesome collinear singularities.

This procedure is the one that we use in calculating the results given in chapter 6.

Frixione's procedure has been found to produce very similar results to the standard cone isolation. This is fortunate because, although Frixione's method is theoretically preferable to other cone isolations, it is still not clear whether it is experimentally practical to implement.

Chapter 5

Results

The helicity amplitudes of chapter 3 and the subtraction method of chapter 4 allow us to calculate numerical results for gluon-gluon induced vector boson pair production at the LHC. In this chapter, we study these results, illustrating them with the appropriate plots. In particular, we compare the gg induced terms to the $q\bar{q}$ and qg parts. All contributions are calculated using standard cuts, scales, parton distributions and so on, allowing us to make direct and fair comparisons between different terms. The relevant helicity amplitudes for the $q\bar{q}$ and qg induced terms are given in [25], and we have already calculated the helicity amplitudes for gg production within this thesis.

We show transverse momentum plots for each production process, separating the total production into the contributions of the different initial states. We are particularly interested in the high p_T region. This is where one might expect to see anomalous couplings most easily, so it is an interesting and important region to look at. It is also where the large size of the NLO term compared with the LO term may be seen most clearly.

We find that the real gg term in vector boson pair production often gives a small and negative contribution to the cross section. Even at high p_T, the gg term does not become significant in the overall cross section. This had not been previously anticipated. We also find the one loop gg induced term in $Z\gamma$ production to be smaller than in previous calculations, though it appears that the use of up-to-date parton distributions is responsible.

We briefly look at the scale dependence of the transverse momentum results.

In section 5.2, we improve our understanding of the transverse momentum results by considering at the hard scattering part and the parton distributions separately, before they are convoluted together.

Having presented our results in the Standard Model initially, in section 5.3 we go on to look at the possible anomalous terms. We use some sample values of anomalous couplings to see what effect they are likely to have on production at the LHC. While one might hope that anomalous couplings would enhance the gg induced contribution to vector boson pair production, it was actually found that the effect on $q\bar{q}$ and qg induced terms is much more substantial than the effect on the gg induced term. Thus the gg term is responsible for an even smaller proportion of the total cross section than before. We were unable to find allowed values for the anomalous couplings that would provide a substantial increase in the gg contribution at LHC energies.

As a final investigation, we studied vector boson pair production at a hypothetical Very Large Hadron Collider or VLHC, imagined to have a centre of mass energy of 200 TeV. This was to see whether a very much higher energy would cause the gg term to become important. We found that gg contributions were not substantially enhanced even at this huge energy. In fact, in no circumstances throughout our different investigations did we find a significant gg term: the gg contribution was always at the 1% level.

It should be noted that throughout this chapter we shall mostly make use of results for WZ production, comparing to $W\gamma$ and $Z\gamma$ where appropriate. Generally, these results are very similar. The choice of WZ to show most features was simply a matter of convenience for the author.

5.1 Numerical results: p_T distributions

Before we go on to give explicit results for vector boson pair production, we must set some of the necessary parameters. These will be used throughout this chapter unless otherwise specified.

The MRST 2001 parton distributions [87] are used throughout, with the one-loop expression for the coupling constant ($\alpha_s(M_Z) = 0.119$). This is used even for the leading order results. We use the NLO parton distribution functions and coupling constant. NNLO parton distributions are not fully available yet, and are not expected to make much change to the results or alter our overall conclusions.

The scales used routinely, where μ_F is the factorisation scale and μ_R the renormalisation scale, are:

- for WZ production, $\mu_F = \mu_R = \sqrt{\frac{1}{2}(M_W^2 + M_Z^2) + \frac{1}{2}(p_{TW}^2 + p_{TZ}^2)}$.
- for $W\gamma$ production, $\mu_F = \mu_R = \sqrt{M_W^2 + p_{T\gamma}^2}$.
- for $Z\gamma$ production, $\mu_F = \mu_R = \sqrt{M_Z^2 + p_{T\gamma}^2}$.

These are chosen to suit both the total cross section and the transverse momentum distributions.

The masses of the vector bosons used are $M_Z = 91.187$ GeV and $M_W = 80.41$ GeV. We do not include electroweak corrections, choosing α and $\sin^2(\theta_W)$ in the spirit of the improved Born approximation [88], [89]. For couplings of vector bosons with the quarks we use $\alpha = \alpha(M_Z) = 1/128$ and for the coupling of the photon we use $\alpha = 1/137$.

We neglect contributions from external b and t quarks, assuming that these will be suppressed by the large top mass. The values for the CKM matrix elements that we use are $|V_{ud}| = |V_{cs}| = 0.975$, $|V_{us}| = |V_{cd}| = 0.222$.

We do not include branching ratios for the decay of the vector bosons. These depend on the decay that takes place, and must be added to the final result.

The standard cuts, which we use throughout, are $p_T > 20$ GeV and $\eta < 2.5$ for charged leptons, where p_T is the transverse momentum of the lepton and η is the rapidity. For photons, we also require that $p_T > 20$ GeV, and use $R_0 = 1$ in the isolation prescription in section 4.4. If there is a neutrino in the final state, the required missing momentum , p_T^{miss}, is also at least 20 GeV.

The energy of the LHC collisions, $\sqrt{s}_{LHC}$, is always assumed to be 14 TeV, and the energy of the hypothetical VLHC is taken to be 200 TeV.

We start our numerical investigation of vector boson pair production by looking at transverse momentum distributions. We want to separate the contributions to vector boson pair production that come from different initial states. We can then see the relative sizes of these different terms.

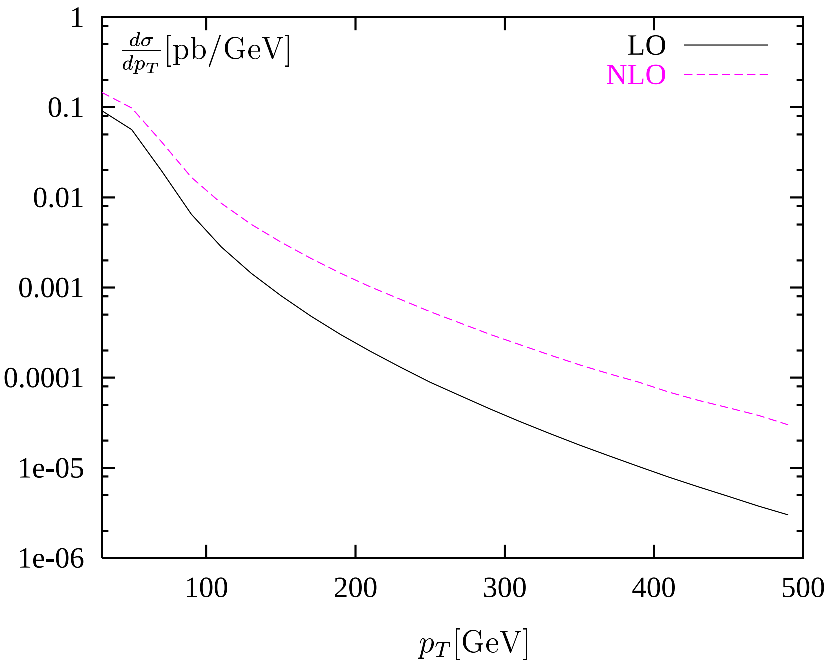

Figure 5.1: Comparing LO and NLO contributions to WZ production at the LHC

Figure 5.1 shows the results that were known previously, for LO and NLO contributions to vector boson pair production. In this figure, we show WZ production. The p_T that is plotted is the p_T of the lepton that results from the decay of the W. We plot the differential cross section $\frac{d\sigma}{dp_T}$ against p_T. The LO contribution is a black solid line and the NLO contribution is a purple dashed line. It can be seen that the NLO term is of the same order as the LO term, and is considerably greater than LO at high transverse momentum (the y scale is logarithmic). This was mentioned previously in section 1.3 as a motivation for the study of a further order in α_s and the plot shows it explicitly.

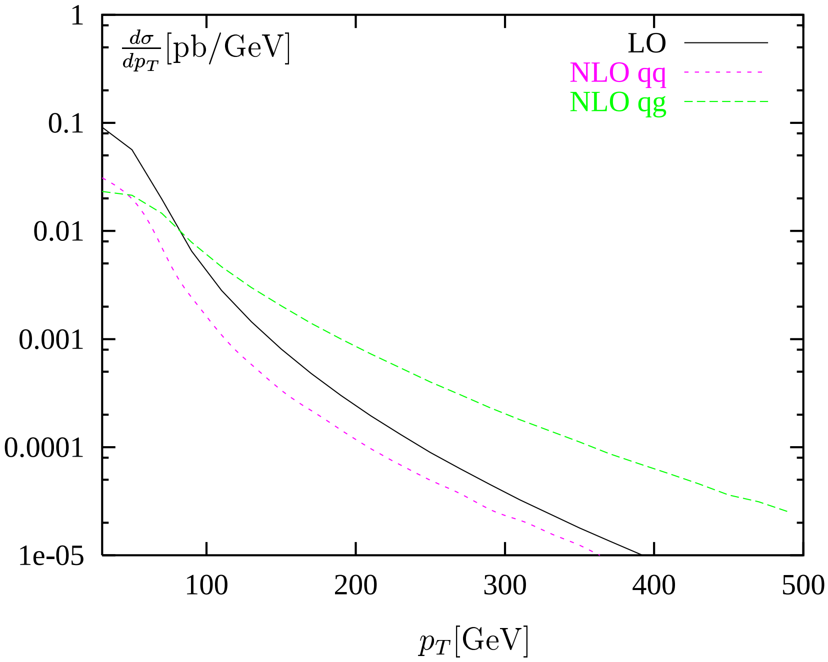

Figure 5.2: Comparing $q\bar{q}$ and qg NLO contributions to WZ production

Next, we break the NLO term into its two constituent parts: a $q\bar{q}$ induced term and a qg induced term. These different contributions are compared to LO in Figure 5.2 (for WZ production). The LO term, plotted as a solid black line, is exactly the same as that given in figure 5.1. However, the NLO contribution is divided into a $q\bar{q}$ induced part (purple dotted) and a qg induced part (green dashed). These individual parts can be compared to the LO term.

We see that the new channel qg is responsible for the large NLO corrections. The qg NLO contribution is larger than LO except at low p_T, while the $q\bar{q}$ NLO term is smaller than NLO at all times, as would normally be expected of a higher order term. In the case of the qg induced part, the large gluon density compensates for the order in α_s and makes this term of similar size to, or bigger than, the LO part.

From now on, we will break down results by initial state. Rather than separating LO from NLO, we separate $q\bar{q}$ from qg. The $q\bar{q}$ induced term is the sum of the LO term and the $q\bar{q}$ induced part at NLO. We have the qg induced NLO term as before.

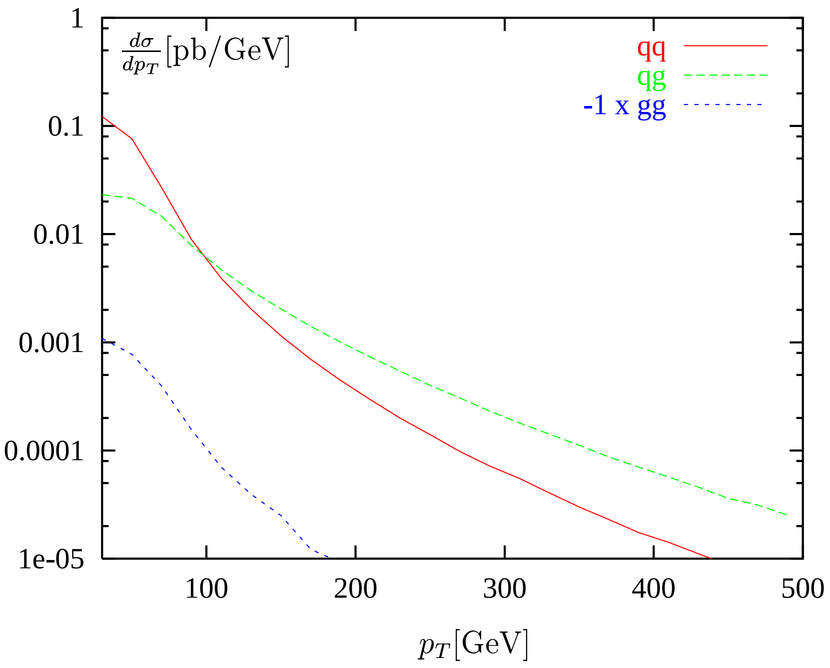

Figure 5.3: Adding gg induced NNLO term in WZ

In figure 5.3, we add our newly calculated gg induced result, which is part of NNLO. We use a convention that $q\bar{q}$ is plotted in red (solid), qg in green (dashed) and gg in blue (dotted).

Figure 5.3 shows the somewhat surprising result of adding the gg induced term. Earlier in this thesis (section 1.3), we speculated that the gg induced term would be large, due to the large gluon densities that are present at the LHC. In analogy with the qg induced term, we expected a situation where the suppression in α_s was counterbalanced by the effects of the gluon density.

However, it can be seen from Figure 5.3 that the resulting gg term is actually small and negative (it should be noted that the gg term plotted has been multiplied by -1, and that Figure 5.3 is a logarithmic plot). Neither the size nor the change of sign was something that was anticipated in advance, and both are worthy of note.

Figure 5.4 shows the corresponding results for $W\gamma$ production. It can be seen that small and negative behaviour is not specific to WZ production but also occurs in this gg induced term, with the plots having a very similar shape.

The situation for $Z\gamma$ production is shown in Figure 5.5. Here the gg induced

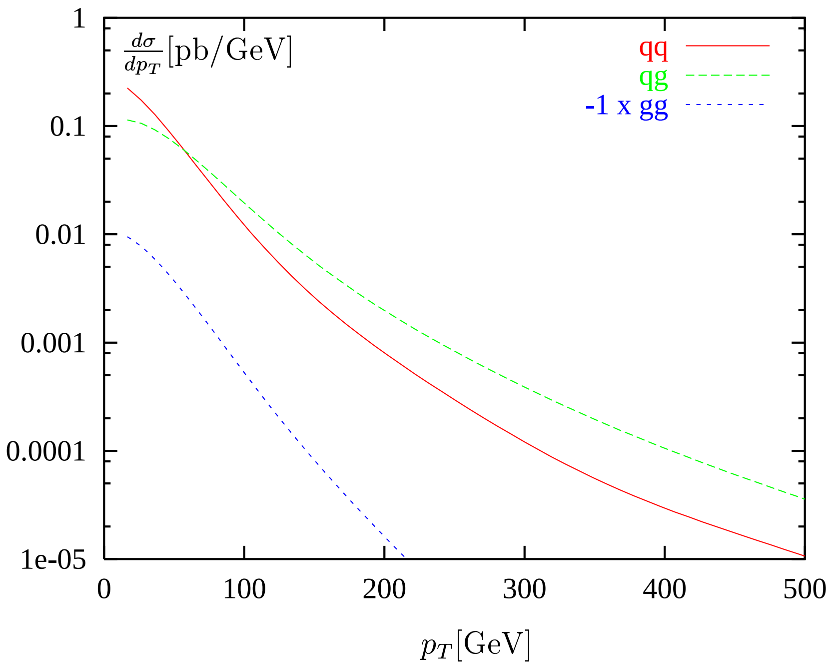

Figure 5.4: Adding gg induced NNLO term in $W\gamma$

term shows some different features from those in the WZ and $W\gamma$ cases. This is because the gg induced term in $Z\gamma$ production consists of both the tree level term and a one loop contribution (see sections 3.3 and 3.4). Figure 5.5 shows the total gg induced term compared to the $q\bar{q}$ and qg induced terms. We can see that the gg induced term is rather larger than previously, and that it is positive rather than negative.

In Figure 5.6, we decompose the gg induced term of $Z\gamma$ into its constituent part, showing the tree level and one loop parts separately. The tree level part is very much like the gg induced parts of WZ and $W\gamma$, being similarly small and negative.

The one loop part is somewhat larger and positive. Though more significant than the tree level part, it is not quite as big as one might expect from results in the literature, in particular van der Bij and Glover [56]. However, when we compare to [56], using the same centre of mass energy and parton distribution functions, we reproduce their result. This result becomes smaller on changing from their Duke and Owens parton distributions [90] to our MRST [87].

The interesting part of the gg term is still the tree level part, as its shape and size

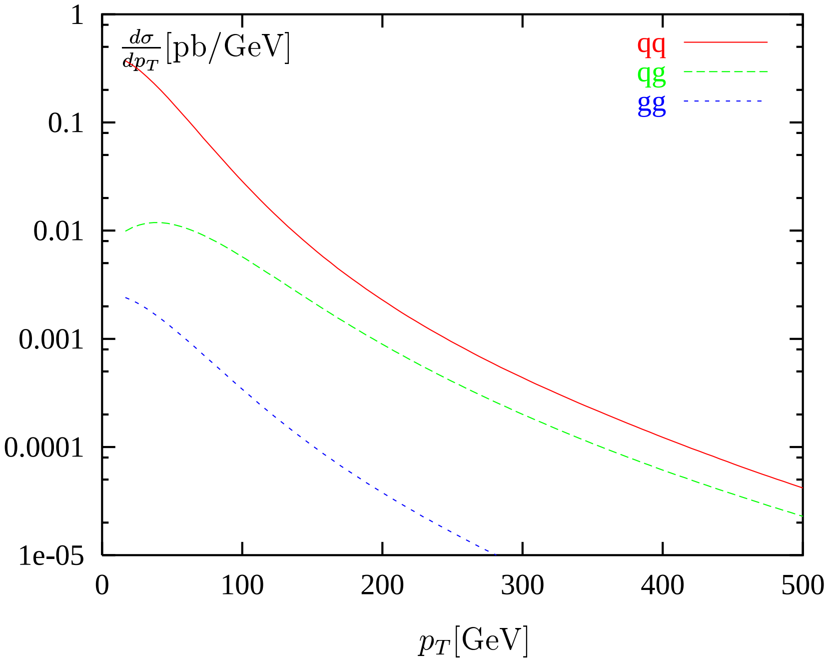

Figure 5.5: Adding full gg induced NNLO term in $Z\gamma$

came as a surprise. This term is investigated more thoroughly in section 5.2, where we separate the hard scattering part from the parton distributions, in an attempt to find out what causes the particular behaviour of the gg contribution.

For the last investigation of this section, we examine the scale dependence of our results. In figure 5.7, we plot once again the transverse momentum distribution for WZ production, with the $q\bar{q}$ induced part in red, the qg part in green and the gg part in blue. However, this time we do so for three different scales. For each of these, the factorisation scale is the same as the renormalisation scale, $\mu = \mu_F = \mu_R$. $\mu = \mu_{st}$ is the normal scale $\mu_{st} = \sqrt{\frac{1}{2}(M_W^2 + M_Z^2) + \frac{1}{2}(p_{TW}^2 + p_{TZ}^2)}$. This is plotted as a solid line. The dashed line represents the scale $\mu = 2\mu_{st}$ and the dotted line represents $\mu = \frac{1}{2}\mu_{st}$. Figure 5.7 shows that the results are similar for these different scales.

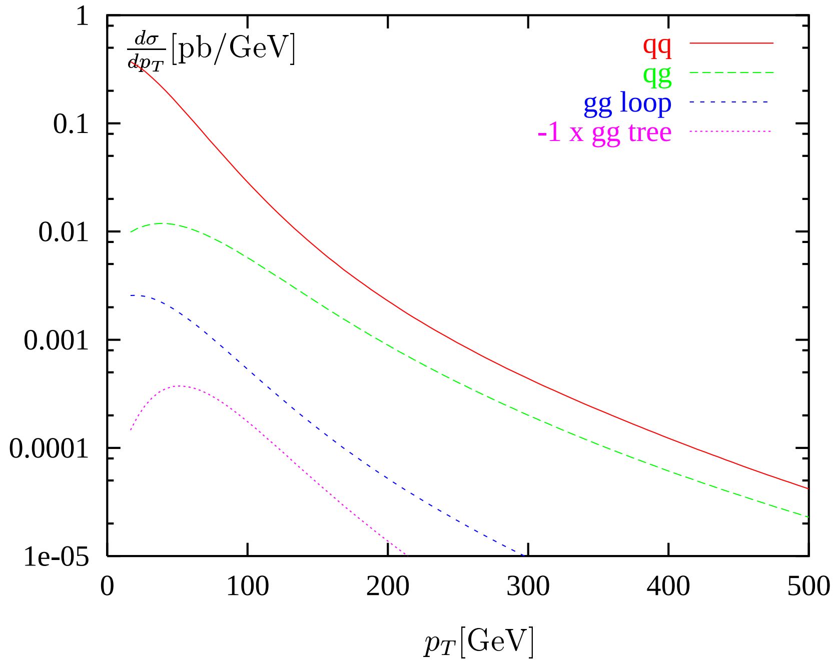

Figure 5.6: Separating tree level and one loop terms in the gg induced contribution to $Z\gamma$ production

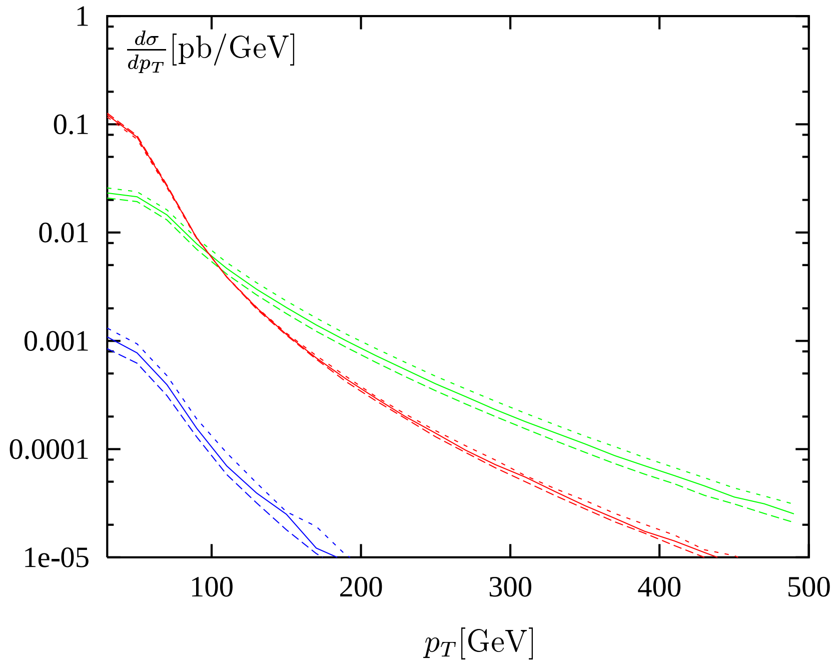

Figure 5.7: Comparing p_T results at different scales: $2\mu_{st}$ (dashed), μ_{st} (solid), $\frac{1}{2}\mu_{st}$ (dotted), for $q\bar{q}$ (red), qg (green) and gg (blue) induced terms.

5.2 Understanding the gg contribution: hard scattering plots

We noted in the previous section that the gluon-gluon induced contribution to vector boson pair production tends to be small and negative. We now wish to further explore the properties of the gg term.

It had been anticipated that the gluon parton distributions would have a large effect on this term, enhancing it to something comparable to the other terms. However, this proved not to be the case. To investigate the causes of the observed behaviour, we remove the parton distributions (that is, we set them to 1 everywhere) and look at the partonic hard scattering part of the results.

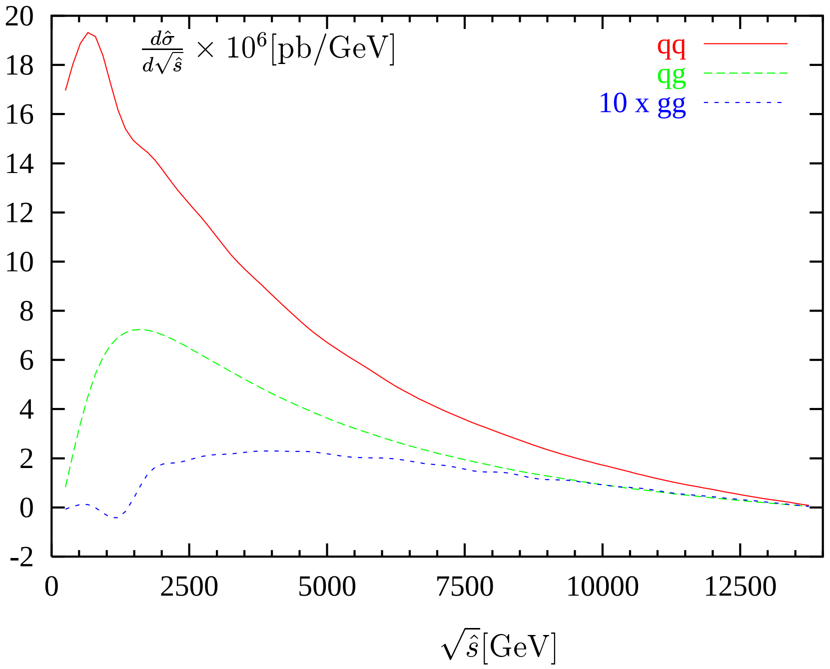

Figure 5.8: $q\bar{q}$, qg and gg partonic (hard scattering) cross sections for WZ

The partonic hard scattering cross section of the WZ process is shown in Figure 5.8.

The gg contribution has been multiplied by 10, and all cross sections have also been multiplied by 10^6.

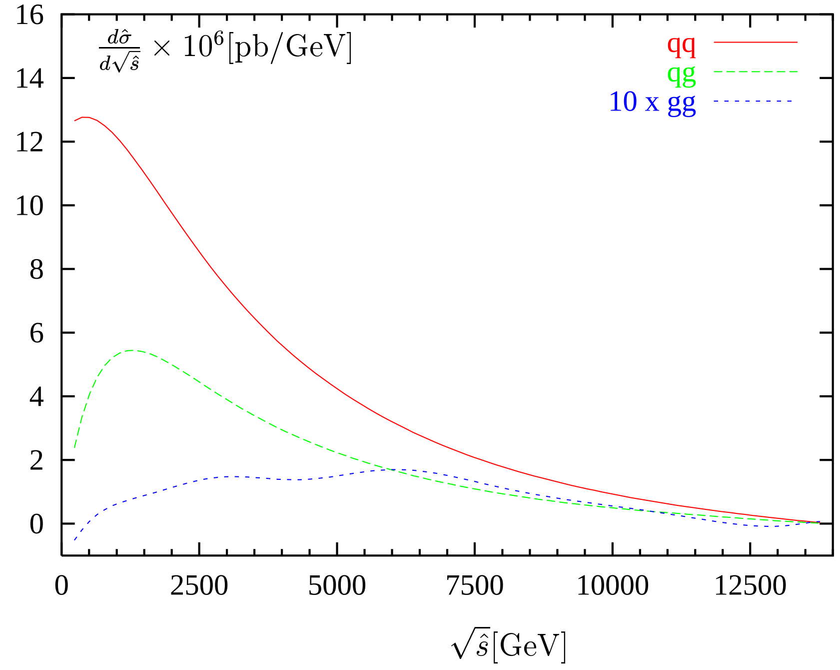

Figure 5.9: Hard scattering for $W\gamma$

It can be seen that the gg induced NNLO term is unlike the other terms in that it is negative at small $\hat{s}$. It is unexpectedly small in this region, while at high values of $\hat{s}$ the size and shape of the curve is more as expected, with reasonably good perturbative convergence.

This also applies to $W\gamma$ and $Z\gamma$ production, with the $W\gamma$ result being given in figure 5.9.

We examine the negative part of the gg induced term more closely in figure 5.10 where we magnify the low $\hat{s}$ region of figure 5.8. Here we can see exactly where the gg term turns from negative to positive. The gg term is small and negative in the important region where the gluon density is largest, turning positive only at a level where the gluon density is not so important and does not significantly enhance the process.

Considering the hard scattering plots and parton distributions separately enables us to understand the overall shape that results when we convolute them. This is useful in helping us to understand both why the qg induced term is larger than one would expect from its order in α_s, and why the gg induced term is smaller than

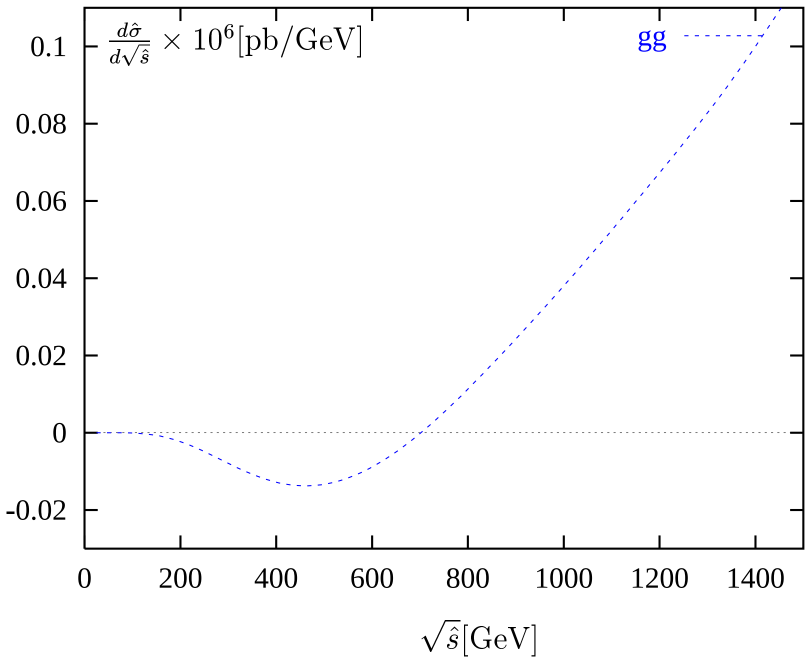

Figure 5.10: Hard scattering for WZ at low $\sqrt{\hat{s}}$

expected.

The qg and gg induced luminosities are both steep functions of the momentum fraction carried by the initial partons. This is mostly due to the fact that the gluon distribution $g(x)$ increases sharply as the momentum fraction x decreases.

When looking at results as a function of partonic energy $\hat{s}$, as we do in this section, we know that the partonic cross section is very often much less than the hadronic cross section. The average value of the partonic cross section, $\langle\hat{s}\rangle$ is much less than the hadronic cross section s as the momentum fractions x_1 and x_2 are involved, $\langle\hat{s}\rangle = \langle x_1 x_2\rangle s$.

As $\hat{s}$ tends to be low, the behaviour of the qg and gg induced production cross sections is dominated by the behaviour of the hard scattering cross section at low $\hat{s}$.

In the case of qg, the partonic cross section reaches a maximum at low $\hat{s}$. Hence this large result dominates and the overall hadronic contribution from the qg initial state is large.

The gg case is very different as the partonic cross section is small at low $\hat{s}$ and also has a negative part. The negative and positive contributions will tend to balance out, and the terms are already small. Therefore the hadronic contribution of the gg initial state remains small despite the high gluon density.

We have seen how the smallness of the hard scattering part translates into a very small contribution when convoluted with parton densities. However, one may ask whether the smallness of the hard scattering part is due to numerically small matrix elements or to a large cancellation within the subtraction process.

The answer to this can be found by examining a previous calculation of the gluon-gluon induced term at NNLO. Baur and Glover [31] calculated the processes $gg \to ZZq\bar{q}$, $qg \to ZZqg$ and $q\bar{q} \to ZZgg$, which are all of the same order. Here, the singularities caused by the final state partons becoming collinear or soft were avoided by requiring the presence of two well-separated, energetic jets in the final state. Under these conditions, it was found that the $ZZjj$ cross section was dominated by the qg induced term, with the $q\bar{q}$ term contributing about 30% and the gg term at the level of $5 - 10\%$.

It seems that the gg induced contribution to vector boson pair production is essentially small and does not become enhanced by the inclusion of singular regions. The particular shape of the gg term means that even the large gluon densities at LHC energies do not produce a significant gg induced contribution to the overall cross section.

5.3 Further results: anomalous couplings and VLHC

So far we have considered vector boson pair production at LHC energies and in the Standard Model, and have compared the terms caused by different initial states. We found that the gg induced term in vector boson pair production is likely to be small, and so one would expect good perturbative stability in a Standard Model vector boson pair production result.

However, we also want to investigate the effects that non-standard couplings may have on vector boson pair production. We will now determine whether a change in the couplings has any dramatic effect on the results.

We will also briefly look at the question of a hypothetical VLHC to see whether gluon-gluon terms could become significant at energies much higher than that of the LHC, or whether they will always be suppressed.

In Figure 5.11, we plot the transverse momentum distribution for WZ production at the LHC if anomalous couplings are included. The anomalous couplings are

$$g_1^\gamma = 1; \quad g_1^Z = 1.13; \quad \kappa^\gamma = 1.2; \quad \kappa^Z = 1.07; \quad \lambda^\gamma = \lambda^Z = 0.1 \tag{5.1}$$

These couplings were defined in section 1.4. They actually deviate from the Standard Model a little more than the most recently quoted bounds from LEP (equation (1.6)). We use the form factors as given in equation (1.5) and we take Λ, the scale of new physics, to be 2 TeV.

Adding anomalous couplings changes the shape of the p_T plot. Figure 5.12 compares the anomalous results plotted in figure 5.11 to the Standard Model results plotted in figure 5.3. The colours follow our normal convention but each anomalous term is plotted as a solid line, with the corresponding Standard Model term as a dotted line.

We see that the $q\bar{q}$ and qg parts are enhanced at large p_T. In particular, adding anomalous terms to the $q\bar{q}$ term causes a huge enhancement, and this term dominates the result, in contrast with the Standard Model case. Neither the qg nor the gg term is significantly increased by the addition of anomalous couplings.

We may also examine the hard scattering cross section as before. From figure 5.13 we see only that the $q\bar{q}$ is substantially enhanced: it dominates the plot. We can

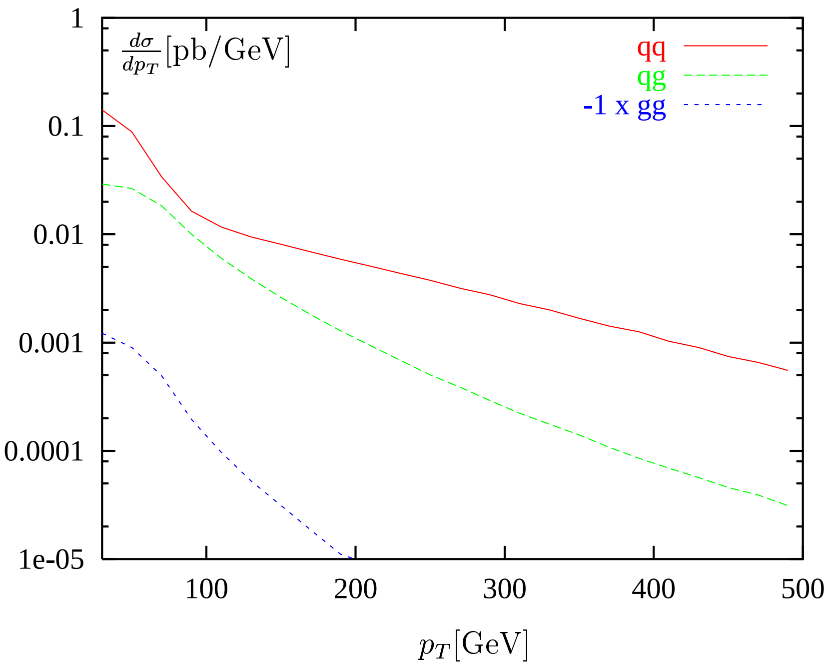

Figure 5.11: $q\bar{q}$, qg and gg contributions to WZ production with anomalous couplings

compare the other terms more easily when plotting to the same scale as figure 5.8: this also makes it easier for us to compare the anomalous case to the Standard Model case given in that figure. This is shown in figure 5.14, where it can be seen that the $q\bar{q}$ hard scattering cross section is massively increased, the qg part somewhat increased and the gg part scarcely changed.

The anomalous results of figure 5.14 are explicitly plotted alongside the Standard Model results of figure 5.8 in figure 5.15. Again the results with anomalous couplings are given in solid lines, and the Standard Model results in dotted.

Not only is the gg term not significantly enhanced by these anomalous couplings, it actually becomes less important as the other terms become larger. We were unable to construct a combination of anomalous couplings that would make the gg contribution important.

In section 1.4, we discussed the search for anomalous couplings, saying that higher order effects tended to occur in the same regions as potential anomalous effects. This was one of the main motivations for calculating the gg term. Having

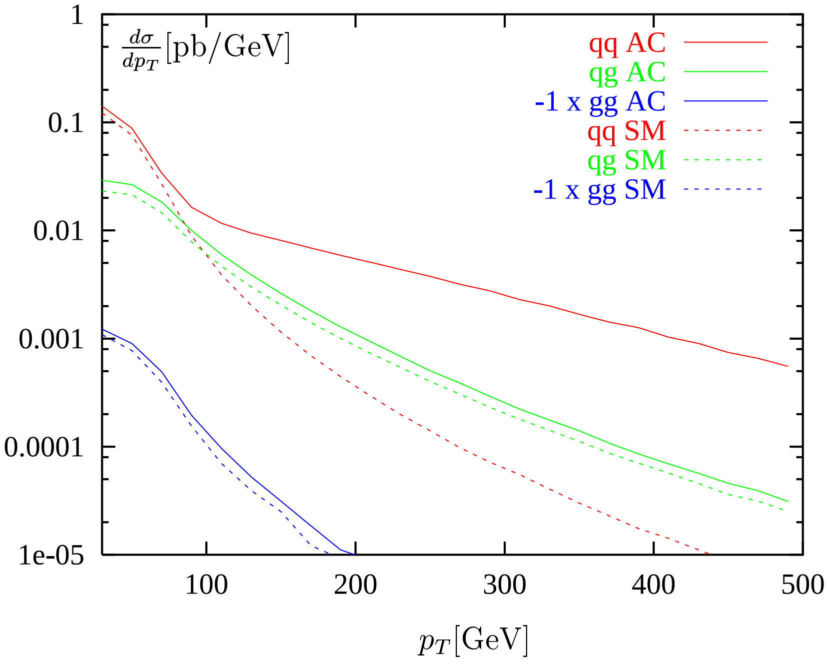

Figure 5.12: Comparing anomalous results of figure 5.11 to Standard Model results of figure 5.3

found that the gg term is always small, we may effectively disregard it in calculations of both the Standard Model and anomalous cases. It can therefore be surmised that if we see deviations from expected (NLO) results, they may be due to anomalous couplings, rather than a large NNLO QCD correction.

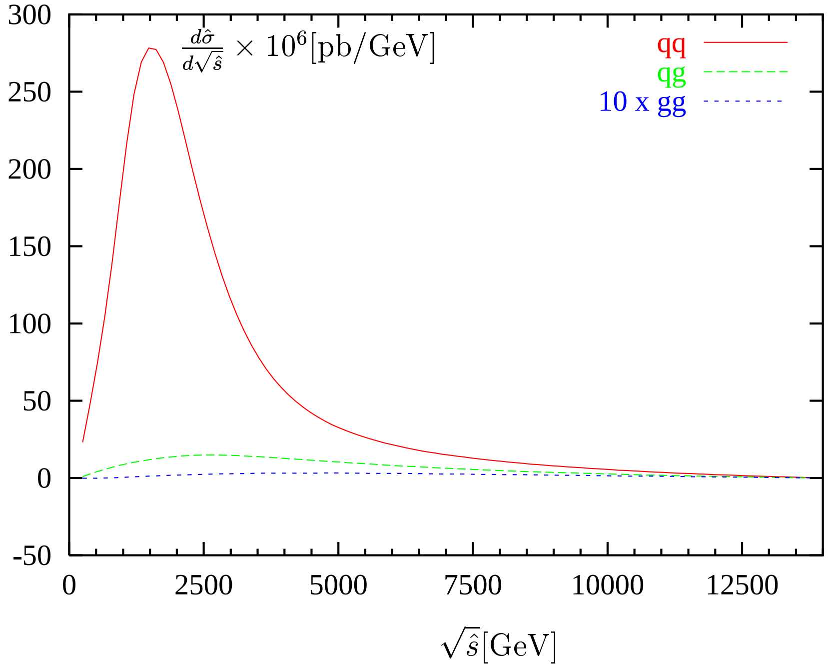

Figure 5.13: Hard scattering for WZ with anomalous couplings

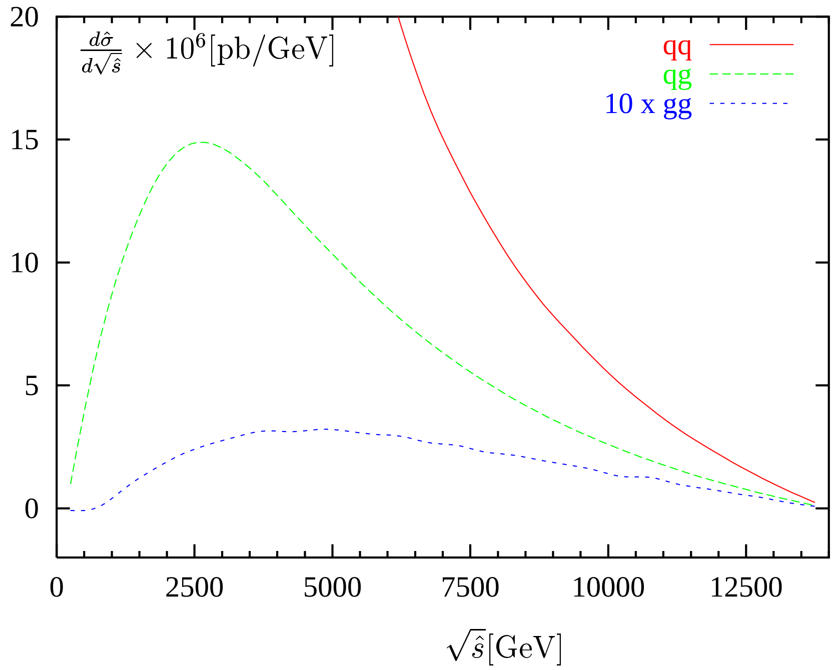

Figure 5.14: Hard scattering with anomalous couplings, scale as in figure 5.8

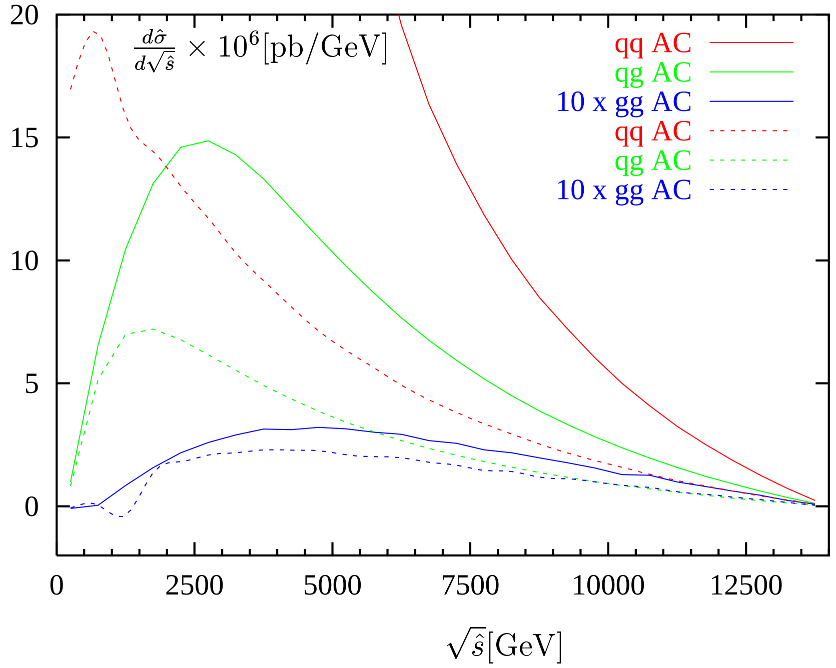

Figure 5.15: Comparing anomalous results of figure 5.14 with Standard Model of figure 5.8

Finally, we look at a hypothetical VLHC: a proton-proton collider at a centre of mass energy of 200 TeV. This is an attempt to see whether higher energies would make the gg part more substantial or whether it would always remain small: we want to look at an extreme case.

Figure 5.16 shows the result for a Standard Model calculation at 200 TeV. Here we can see that the gg term still remains at the 1% level and does not become enhanced at the higher energy. The gg term does not remain negative above p_T=100 GeV but instead becomes positive, though very small. This can be seen in detail in figure 5.17, which, it should be noted, is on a normal plot rather than a log scale and shows the gg term itself rather than -1 times the gg part.

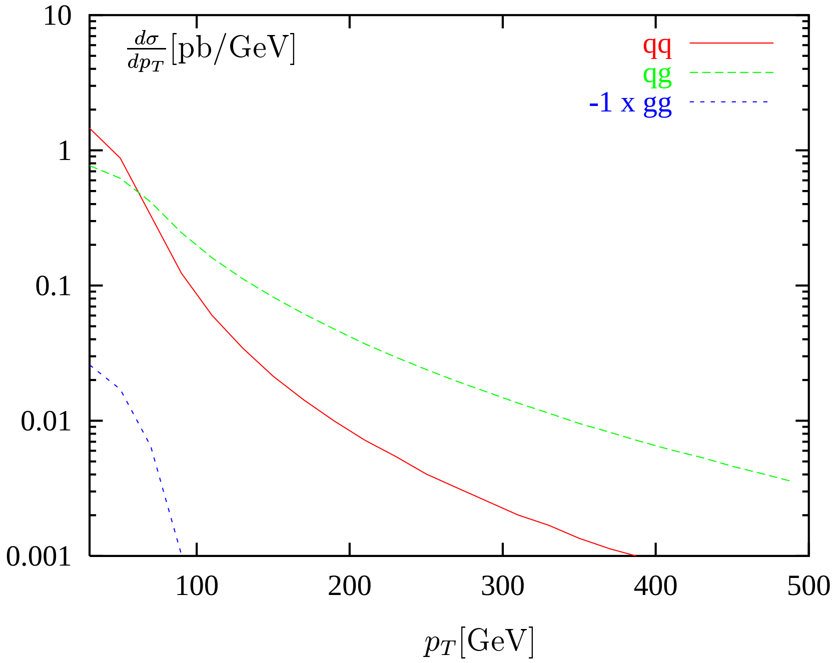

Figure 5.16: $q\bar{q}$, qg and gg contributions to WZ production at VLHC

Our study at VLHC energies was carried out in order to get a qualitative feel for what would happen at high energies and should not be considered to be a realistic prediction for such a machine. We used ordinary parton distributions which presumably would not be valid at such high energies. We used the same cuts on momentum and rapidity as we considered to be appropriate at the LHC. In calculating the Standard Model result, we did not consider the appearance of new particles

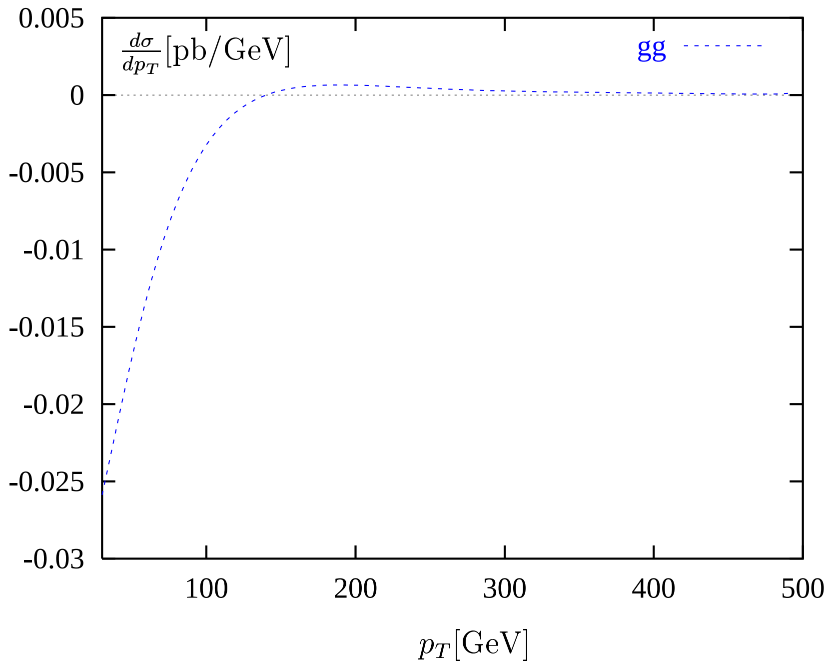

Figure 5.17: gg term at VLHC

or couplings from physics beyond the Standard Model. However, we can say that the gg contribution remained small and gave an overall negative contribution to the cross section. It is unlikely to have a great impact on results even at high energy.

For all the scenarios in this chapter, we concluded that the gg induced term of vector boson pair production is not substantial.

Chapter 6

Conclusion and Outlook

In this thesis, we have discussed the production of pairs of vector bosons: specifically WZ, $W\gamma$ and $Z\gamma$ production. We have extended the known results for vector boson pair production by adding an extra production channel, the gluon-gluon induced term at NNLO.

We initially explained the motivation for this investigation with reference to previous results in the literature. It was known that in vector boson pair production it is common for the NLO terms to be as large or larger than the LO terms, especially in regions such as the high transverse momentum region. It was therefore desirable to calculate NNLO results, and it was thought that the gluon-gluon term ought to be the dominant term in NNLO due to the high gluon density at the LHC. However, it was found instead that a sign change in the gluon-gluon hard scattering, along with the small absolute value of the hard scattering result, leads to a small gluon-gluon induced term. If our assumptions about the small size of other NNLO terms are correct, this implies a good perturbative stability for vector boson pair production.

We gave explicitly the tree level helicity amplitudes for $gg \to V_1 V_2 q\bar{q}$ in the Standard Model. These helicity amplitudes can be applied to any vector boson pair production process, including those not studied here. We added in the appropriate anomalous coupling terms for WZ, $W\gamma$ and $Z\gamma$. All the amplitudes included the decay of the vector bosons into leptons as applicable. We also showed how to obtain the gg induced box loop for Standard Model $Z\gamma$ production from the literature, and calculated the gg induced triangle diagram with an anomalous triple vertex.

We differed from previous studies of vector boson pair production in that we integrated the vector boson pair production process over the whole phase space, rather than requiring two jets to be seen and cutting out the singular regions. This allows us to keep more of the events, rather than losing a large number through a jet veto. We used the subtraction method to cancel singularities analytically. Again, this is a general process for all vector boson pair production processes, though it did not include the singularity caused by the photon becoming collinear, which was treated with Frixione's isolation procedure [86].

The amplitudes were implemented in a Monte Carlo integration using `VEGAS`.

We presented results under a number of conditions, all of which led to the conclusion that the gg induced term of vector boson pair production is small.

We showed p_T plots indicating that the gg induced contribution is small and negative. The size of the gg term was seen to be due to the sign change in the hard scattering at low $\hat{s}$. We also calculated the vector boson pair production with anomalous couplings caused by new physics. Again we found that the gg term was unlikely to be significant, and the same was the case even at very high energies (the hypothetical VLHC).

There are a few obvious extensions to this work that could potentially be carried out.

The tree level amplitudes for gluon induced vector boson pair production could also be used in a calculation of WW or ZZ production. This would just require the calculation of more loop diagrams and is an obvious next step. This would add to the LO and NLO terms from the literature. We would expect these terms also to be small, but the unknown contribution of the loop diagrams would suggest that it would make sense to carry out the calculations explicitly.

A particularly interesting process is the gluon-gluon induced production of two photons, $gg \to q\bar{q}\gamma\gamma$. This is the part of the background to the process $gg \to H \to \gamma\gamma$, which at the LHC is the main decay mode of the production of a light Higgs via gluon fusion. The process of di-photon production was discussed recently by Bern, Dixon and Schmidt [91]. Here they calculated the appropriate loop diagrams for this di-photon background to Higgs production, and used the results of our investigation into WZ and $W\gamma$ production [55] to infer that the tree level process $gg \to q\bar{q}\gamma\gamma$ ought to be small. (They neglected this term in favour of other gluon-gluon induced

NNLO terms, and some newly calculated terms at the next order.) However, an explicit calculation of our tree level term for $\gamma\gamma$ should still be interesting, at least to ensure that there are no 'surprises' in this term.

The next step to take regarding the phase space of vector boson pair production may be to calculate the contribution $qg \to V_1V_2qg$. This is another NNLO contribution. The gg induced contribution turned out to be so small that the qg result, even though suppressed by a power of α_s, might be a bigger contribution. Here the phase space is made more difficult by the possibility of a final state soft gluon: one must combine singularities, allowing soft and collinear singularities to occur together.

Further investigations on the gg induced term would just be checks to ensure that the gg induced contribution to vector boson pair production is always small. Assuming it is found that this contribution is at the 1% level always, as we have found in all our investigations, one may not need to conduct many more investigations on the explicit details of the gg term under all circumstances, as it would be reasonable to leave it out of realistic predictive calculations.

However, the smallness of the gg term should not in any way be seen as a disappointment. It allows us to work just to the known NLO level when making experimental predictions, and be reasonably confident that the QCD corrections are not large. This stability in the QCD predictions suggests that any deviations from the expected (NLO) results could be due to new physics effects rather than this gg induced QCD correction.

We await the LHC results on vector boson pair production with interest.

Appendix A

Colour ordered Feynman rules

These are the rules used to calculate the kinematic parts of Feynman diagrams in the helicity method. Note that we use the conventions of Dixon [52] and in particular that as $\mathrm{Tr}(T^a T^b) = \delta^{ab}$, factors of $\sqrt{2}$ that we might otherwise expect to be associated with colour factors now appear in the Feynman rules.

External particles are given by spinors as described in chapter 2, $|i\pm\rangle$ and $\langle i\pm|$.

Propagators and vertices (with all momenta outgoing) are:

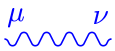

$-i\frac{g_{\mu\nu}}{k^2}$

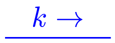

$\frac{i}{\not{k}}$

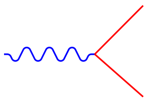

$\frac{i}{\sqrt{2}}\gamma_\mu$

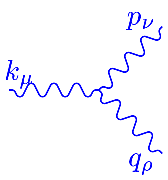

$\frac{i}{\sqrt{2}}(g_{\nu\rho}(p-q)_\mu + g_{\rho\mu}(q-k)_\nu + g_{\mu\nu}(k-p)_\rho)$

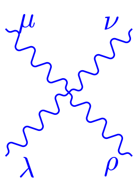

$ig_{\mu\rho}g_{\nu\lambda} - \frac{i}{2}(g_{\mu\nu}g_{\rho\lambda} + g_{\mu\lambda}g_{\nu\rho})$

Appendix B

Helicity amplitudes

B.1 Helicity amplitudes for $gg \to WZq\bar{q}$

Here we present all the helicity amplitudes required for a calculation of $gg \to WZq\bar{q}$.

We give the amplitudes with anomalous couplings included. To obtain the Standard Model result, we would set the anomalous couplings to their Standard Model values, $g_1^Z = \kappa^Z = 1$ and $\lambda^Z = 0$

We need explicit expressions for only 6 amplitudes: the amplitudes for all other helicity configurations can be obtained by some straightforward relations.

The amplitudes that we require are:

$$A_{12}(g_1^+ g_2^+) \quad B_{12}(g_1^+ g_2^+) \quad A_{12}(g_1^+ g_2^-) \quad B_{12}(g_1^+ g_2^-) \quad A_{21}(g_1^+ g_2^-) \quad B_{21}(g_1^+ g_2^-) \tag{B.1}$$

where these are the amplitudes with helicities 1 and 2 as given, and other helicities $l_3^- \, \bar{\nu}_4^+ \, \bar{l}_5^+ \, l_6^- \, q_7^- \, \bar{q}_8^+$. The A amplitudes are those without a triple gauge vertex, while the B amplitudes contain a triple gauge vertex. Hence only the B amplitudes contain anomalous couplings.

The helicity amplitudes without a triple gauge vertex are:

$$A_{12}(g_1^+ g_2^+) = \frac{\langle 73\rangle}{\langle 71\rangle\langle 72\rangle s_{34} s_{56} t_{347}} \left\{ \left(\frac{\langle 72\rangle\langle 6|(7+3)|4\rangle\langle 7|(1+2+8)|5\rangle}{\langle 82\rangle\langle 12\rangle} + \frac{\langle 72\rangle\langle 6|(5+8)(1+2)|7\rangle[34][85]}{t_{568}\langle 12\rangle} \right) \right.$$

$$+\langle 73\rangle[34]\left(\frac{\langle 6|(3+4+7)|1\rangle\langle 7|(2+8)|5\rangle}{\langle 28\rangle u_{1347}}\right.$$
$$\left.+\frac{\langle 6|5+8|2\rangle\langle 7|(3+4)|1\rangle[85]}{t_{568}u_{1347}}\right)\Bigg\} \tag{B.2}$$

$$\begin{aligned}A_{12}(g_1^+g_2^-) &= \frac{1}{s_{12}s_{34}s_{56}}\left\{\frac{\langle 73\rangle\langle 2|(1+8)|5\rangle\langle 6|(3+7)|4\rangle[81]^2}{[82]t_{347}t_{128}}\right.\\
&+\frac{\langle 27\rangle^2\langle 3|(2+7)|1\rangle\langle 6|(5+8)|4\rangle[85]}{\langle 17\rangle t_{127}t_{568}}\\
&+\frac{\langle 37\rangle[81][85]}{[28]u_{1347}}\left(\frac{\langle 72\rangle\langle 6|(1+3+7)|4\rangle}{\langle 17\rangle}-\frac{\langle 2|(3+7)|4\rangle\langle 6|(3+4+7)|1\rangle}{t_{347}}\right)\\
&+\frac{\langle 6|(5+8)|1\rangle[85][37]}{t_{568}}\left(\frac{\langle 27\rangle\langle 2|(1+3+7)|4\rangle}{\langle 17\rangle}\right.\\
&\left.\left.+\frac{\langle 2|(3+7)|4\rangle\langle 2|(3+4+7)|1\rangle}{t_{347}}\right)\right\}\end{aligned} \tag{B.3}$$

$$\begin{aligned}A_{21}(g_1^+g_2^-) &= \frac{1}{s_{12}s_{34}s_{56}}\left\{\frac{\langle 28\rangle\langle 37\rangle[18]\langle 2|(1+8)|5\rangle\langle 6|(3+7)|4\rangle}{\langle 18\rangle t_{347}t_{128}}\right.\\
&+\frac{\langle 27\rangle[71][85]\langle 3|(2+7)|1\rangle\langle 6|(5+8)|4\rangle}{[72]t_{127}t_{568}}\\
&+\frac{[85]\langle 2|(3+7)|4\rangle\langle 6|(5+8)|2\rangle}{t_{568}u_{2347}}\left(\frac{\langle 3|(2+7)|1\rangle}{[72]}+\frac{\langle 37\rangle\langle 2|(3+4+7)|1\rangle}{t_{347}}\right)\\
&+\frac{\langle 2|(1+8)|5\rangle}{\langle 81\rangle u_{2347}}\left(\frac{\langle 3|(2+7)|1\rangle\langle 6|(2+3+7)|4\rangle}{[27]}\right.\\
&\left.\left.+\frac{\langle 37\rangle\langle 2|(3+7)|4\rangle\langle 6|(5+8)|1\rangle}{t_{347}}\right)\right\}\end{aligned} \tag{B.4}$$

These 'A' amplitudes are the sums of diagrams where the W and Z are ordered so that the W is on the same side as the quark, and the Z on the side of the antiquark. To obtain the amplitudes with the opposite ordering of W and Z, we need to reverse the lepton pairs $\{34\} \leftrightarrow \{56\}$. As we have $l_3^-\bar{\nu}_4^+$ but $\bar{l}'^+_5 l'^-_6$, opposite helicities, we have to reverse the order of the pair when swapping the pairs.

- To reverse the ordering of the W and Z on the quark line, change $\{3,4,5,6\}$ in the helicity amplitudes to {6,5,4,3}.

The helicity amplitudes with a triple gauge vertex, including anomalous couplings, are:

$$
\begin{aligned}
B_{12}(g_1^+ g_2^+) \;=\;& 1/(2\langle 12\rangle\langle 17\rangle\langle 28\rangle s_{34}s_{56}u_{3456}) \\
& \{\langle 67\rangle[5|(1+2+8)|7]\langle 3|(5+6)|4\rangle(g_1^Z+\kappa^Z+\lambda^Z) \\
& +\langle 7|(5+6)(1+2+8)|7\rangle\langle 63\rangle[45](g_1^Z+\kappa^Z+\frac{\lambda^Z}{M_Z^2}u_{3456}) \\
& +\langle 6|(3+4)|5\rangle(\langle 73\rangle[4|(1+2+8)7](2g_1^Z+\lambda^Z) \\
& -\frac{\lambda^Z}{M_Z^2}\langle 3|(5+6)|4\rangle\langle 7|(5+6)(1+2+8)|7\rangle)\}
\end{aligned}
\tag{B.5}
$$

$$
\begin{aligned}
B_{12}(g_1^+ g_2^-) \;=\;& \frac{1}{4s_{12}s_{34}s_{56}u_{3456}}\left\{\frac{[18]^2}{t_{128}[82]}\big(-2\langle 76\rangle[5|(1+8)|2]\langle 3|(5+6)|4\rangle(g_1^Z+\kappa^Z+\lambda^Z)\right. \\
& +(\langle 7|(5+6)(1+8)|2\rangle-\langle 7|(3+4)(1+8)|2\rangle[45]\langle 63\rangle(g_1^Z+\kappa^Z+\frac{\lambda^Z}{M_Z^2}u_{3456}) \\
& -2\langle 6|(3+4)|5\rangle(\langle 37\rangle[4|(1+8)|2](2g_1^Z+\lambda^Z) \\
& +\frac{\lambda^Z}{M_Z^2}\langle 3|(5+6)|4\rangle\langle 7|(5+6)(1+8)|2\rangle)\Big) \\
& +\frac{\langle 72\rangle[18]}{\langle 71\rangle[28]}\big(\langle 3|(5+6)|4\rangle\langle 76\rangle[58](g_1^Z+\kappa^Z+\lambda^Z) \\
& +(\langle 7|(5+6)|8\rangle-\langle 7|(3+4)|8\rangle)[45]\langle 63\rangle(g_1^Z+\kappa^Z+\frac{\lambda^Z}{M_Z^2}u_{3456}) \\
& -2\langle 6|(3+4)|5\rangle(\langle 37\rangle[48](2g_1^Z+\lambda^Z) \\
& +\frac{\lambda^Z}{M_Z^2}\langle 3|(5+6)|4\rangle\langle 7|(5+6)|8\rangle)\Big) \\
& +\frac{\langle 72\rangle^2}{\langle 17\rangle t_{127}}\big(2\langle 3|(5+6)|4\rangle[1|(2+7)|6][85](g_1^Z+\kappa^Z+\lambda^Z) \\
& +([1|(2+7)(5+6)|8]-[1|(2+7)(3+4)|8])[45]\langle 63\rangle(g_1^Z+\kappa^Z+\frac{\lambda^Z}{M_Z^2}u_{3456}) \\
& -2\langle 6|(3+4)|5\rangle([1|(2+7)|3][84](2g_1^Z+\lambda^Z) \\
& \left.+\frac{\lambda^Z}{M_Z^2}\langle 3|(5+6)|4\rangle[1|(2+7)(5+6)|8])\Big)\right\}
\end{aligned}
\tag{B.6}
$$

$$
\begin{aligned}
B_{21}(g_1^+ g_2^-) &= \frac{1}{4s_{12}s_{34}s_{56}u_{3456}} \left\{ \frac{[18]\langle 28\rangle}{t_{128}\langle 81\rangle} \big(2\langle 3|(5+6)|4\rangle\langle 67\rangle[5|(1+8)|2\rangle(g_1^Z + \kappa^Z + \lambda^Z) \right. \\
&\quad + (\langle 7|(5+6)(1+8)|2\rangle - \langle 7|(3+4)(1+8)|2\rangle)[45]\langle 63\rangle(g_1^Z + \kappa^Z + \frac{\lambda^Z}{M_Z^2}u_{3456}) \\
&\quad - 2\langle 6|(3+4)|5\rangle(\langle 37\rangle[4|(1+8)|2](2g_1^Z + \lambda^Z) \\
&\quad + \frac{\lambda^Z}{M_Z^2}\langle 3|(5+6)|4\rangle\langle 7|(5+6)(1+8)|2\rangle\Big) \\
&\quad + \frac{1}{[27]\langle 81\rangle} \big(-2\langle 3|(5+6)|4\rangle[1|(2+7)|6][5|(1+8)|2](g_1^Z + \kappa^Z + \lambda^Z) \\
&\quad + ([1|(2+7)(5+6)(1+8)|2] - [1|(2+7)(3+4)(1+8)|2]) \\
&\quad [45]\langle 63\rangle(g_1^Z + \kappa^Z + \frac{\lambda^Z}{M_Z^2}u_{3456}) \\
&\quad + 2\langle 6|(3+4)|5\rangle([1|(2+7)|3][4|(1+8)|2](2g_1^Z + \lambda^Z) \\
&\quad - \frac{\lambda^Z}{M_Z^2}\langle 3|(5+6)|4\rangle[1|(2+7)(5+6)(1+8)2]\Big) \\
&\quad + \frac{\langle 27\rangle[17]}{[27]t_{127}} \big(2\langle 3|(5+6)|4\rangle[1|(2+7)6][85](g_1^Z + \kappa^Z + \lambda^Z) \\
&\quad + ([1|(2+7)(5+6)|8] - [1|(2+7)(3+4)|8])[45]\langle 63\rangle(g_1^Z + \kappa^Z + \frac{\lambda^Z}{M_Z^2}u_{3456}) \\
&\quad + 2\langle 6|(3+4)|5\rangle([1|(2+7)|3][48](2g_1^Z + \lambda^Z) \\
&\quad \left. - \frac{\lambda^Z}{M_Z^2}\langle 3|(5+6)|4\rangle[1|(2+7)(5+6)|7]\Big)\Big) \right\}
\end{aligned} \tag{B.7}
$$

We need some relations to transform all the amplitudes into amplitudes for all other helicity configurations. These relations are the same whether we have an A or a B amplitude.

- To go from $\bar{l}_5'^+ l_6'^-$ to $\bar{l}_5'^- l_6'^+$ we simply swap $5 \leftrightarrow 6$ in the amplitudes above.
- The operation $1 \leftrightarrow 2$ exchanges gluons 1 and 2, though the helicities must be the same, for example $A_{12}(g_1^+ g_2^+)$ to $A_{21}(g_1^+ g_2^+)$

To perform the remaining relation, reversing both gluon helicities simultaneously, we introduce the relation flip$_{WZ}$ where

$$\text{flip}_{WZ} = 3 \leftrightarrow 5, 4 \leftrightarrow 6, 7 \leftrightarrow 8, \langle ab\rangle \leftrightarrow [ab] \tag{B.8}$$

- To reverse both gluon helicities, keeping everything else the same, we use flip_{WZ}. An example:

$$A_{12}(g_1^- g_2^-) = \text{flip}_{WZ}[A_{12}(g_1^+ g_2^+)] \tag{B.9}$$

Of course, we can also combine these relations as required.

B.2 Helicity amplitudes for $gg \to W\gamma q\bar{q}$

Here we present all the helicity amplitudes required for a calculation of $gg \to W\gamma q\bar{q}$.

Initially we will state the independent amplitudes needed for a Standard Model calculation. We will explain how to use the amplitudes to obtain all helicity configurations. We will then give the additional amplitudes needed for the anomalous case.

For the Standard Model case, we need 8 independent amplitudes:

$$\begin{array}{cccc} A_{12}(g_1^+ g_2^+ \gamma_5^+) & B_{12}(g_1^+ g_2^+ \gamma_5^+) & A_{12}(g_1^+ g_2^+ \gamma_5^-) & B_{12}(g_1^+ g_2^+ \gamma_5^-) \\ A_{12}(g_1^+ g_2^- \gamma_5^+) & B_{12}(g_1^+ g_2^- \gamma_5^+) & A_{21}(g_1^+ g_2^- \gamma_5^+) & B_{21}(g_1^+ g_2^- \gamma_5^+) \end{array} \tag{B.10}$$

For each helicity configuration, A is the amplitude with the photon on the same side of the diagram as the antiquark, and B has the photon on the same side as the quark.

The explicit helicity amplitudes for these are given below.

$$\begin{aligned} A_{12}(g_1^+ g_2^+ \gamma_5^+) \quad = \quad & \frac{\langle 36\rangle}{\langle 27\rangle\langle 21\rangle\langle 61\rangle\langle 65\rangle s_{34}}\Big(\frac{\langle 63\rangle[34]\langle 76\rangle}{\langle 57\rangle} + \frac{1}{2(t_{345}-s_{34})}(((\langle 65\rangle[54] \\ & - \langle 63\rangle[34])\langle 6|(1+2+7)|5\rangle - \langle 6|(1+2+7)|4\rangle\langle 6|(3+4)|5\rangle)\Big) \end{aligned} \tag{B.11}$$

$$B_{12}(g_1^+ g_2^+ \gamma_5^+) = \frac{\langle 36\rangle(\langle 6|(3+4)|5\rangle\langle 6|(1+2+7)|4\rangle + \langle 6|(1+2+7)|5\rangle(\langle 63\rangle[34] - [45]\langle 56\rangle))}{2\langle 27\rangle\langle 21\rangle\langle 61\rangle\langle 65\rangle s_{34}(t_{345} - s_{34})} \tag{B.12}$$

$$\begin{aligned} A_{12}(g_1^+ g_2^+ \gamma_5^-) \;=\; & \frac{1}{\langle 61\rangle\langle 62\rangle[65]s_{34}} \\ & \Bigg(\frac{\langle 36\rangle}{t_{346}}\Bigg(\frac{\langle 63\rangle[34]\langle 6|(1+2)|7\rangle[76]}{[75]\langle 12\rangle} + \frac{(s_{16}+s_{26}+s_{76})\langle 5|(3+6)|4\rangle[62]}{\langle 72\rangle\langle 12\rangle} \\ & - \frac{\langle 63\rangle[34]}{\langle 27\rangle[75]t_{257}}(\langle 5|(2+7)|1\rangle(s_{26}+s_{76})[75] + \langle 6|(2+5+7)|1\rangle[72][76]\langle 27\rangle)\Bigg) \\ & + \frac{\langle 26\rangle}{2\langle 27\rangle\langle 21\rangle(t_{345}-s_{34})}(\langle 35\rangle\langle 6|(4+5)|3\rangle\langle 36\rangle[46] \\ & + (s_{56}-s_{46})\langle 35\rangle\langle 6|(3+5)|4\rangle + \langle 56\rangle[45]\langle 53\rangle(s_{16}+s_{26}+s_{76})) \\ & - 2\langle 63\rangle\langle 6|(3+5)|4\rangle[6|(3+4)|5])\Bigg) \end{aligned} \tag{B.13}$$

$$\begin{aligned} B_{12}(g_1^+ g_2^+ \gamma_5^-) \;=\; & \frac{1}{\langle 61\rangle\langle 62\rangle[65]s_{34}} \\ & \Bigg(\frac{\langle 35\rangle\langle 6|(1+2+7)|4\rangle\langle 26\rangle}{\langle 21\rangle\langle 27\rangle} - \frac{\langle 65\rangle\langle 3|(5+6)|1\rangle\langle 6|(2+7)|4\rangle}{\langle 27\rangle t_{156}} \\ & - \frac{\langle 65\rangle[74]}{t_{347}}\Bigg(\frac{\langle 6|(1+2)(4+7)|3\rangle}{\langle 21\rangle} + \frac{\langle 65\rangle\langle 3|(4+7)|2\rangle[51]}{t_{156}}\Bigg) \\ & - \frac{\langle 26\rangle}{2\langle 21\rangle\langle 27\rangle(t_{345}-s_{34})}\rangle(\langle 53\rangle\langle 56\rangle[5|(3+4)|6][46] \\ & + \langle 56\rangle[45]\langle 53\rangle(s_{16}+s_{26}+s_{76}) - \langle 53\rangle s_{56}\langle 6|(3+5)|4\rangle \\ & + 2\langle 36\rangle\langle 6|(3+5)|4\rangle[6|(3+4)|5)\Bigg) \end{aligned} \tag{B.14}$$

$$\begin{aligned} A_{12}(g_1^+ g_2^- \gamma_5^+) \;=\; & 1/(\langle 16\rangle\langle 35\rangle[72]s_{12}s_{34}t_{126}t_{127}) \\ & \Bigg(\frac{1}{\langle 75\rangle t_{257}t_{346}}\{\langle 16\rangle\langle 36\rangle t_{126}(\langle 2|(3+6)|4\rangle t_{127} \\ & (\langle 2|(5+7)|1\rangle\langle 3|(5+7)|1\rangle[72] + \langle 3|(4+6)|1\rangle[17]s_{57}) \end{aligned}$$

$$
\begin{aligned}
&+ \langle 36\rangle\langle 57\rangle\langle 2|(1+7)|5\rangle[64][71]^2 t_{257}) \\
&+ \langle 26\rangle t_{127}t_{346}(\langle 36\rangle t_{126}(\langle 2|(5+7)|4\rangle\langle 3|(5+7)|1\rangle[72] \\
&+ \langle 3|(1+6)|4\rangle[17]s_{57}) + \langle 62\rangle\langle 3|(2+6)|1\rangle\langle 3|(5+7)|4\rangle[72]t_{257})\} \\
&+ \frac{[45]}{(s_{34}-t_{345})}((\langle 16\rangle\langle 63\rangle[71]^2\langle 2|(1+7)(4+5)|3\rangle t_{126} \\
&+ \langle 62\rangle[7|(4+5)|3]t_{127}(\langle 26\rangle\langle 3|(2+6)|1\rangle[72] + \langle 36\rangle[17]t_{126}))\Big)
\end{aligned}
\tag{B.15}
$$

$$
\begin{aligned}
B_{12}(g_1^+g_2^-\gamma_5^+) \;=\;& 1/((\langle 16\rangle\langle 12\rangle\langle 56\rangle s_{34}t_{126})\Big(\langle 26\rangle^3\langle 3|(4+7)|5\rangle[74]/t_{347} \\
&+ \frac{1}{2[72][21]t_{127}(s_{34}-t_{345})}\Big\{\langle 16\rangle\langle 36\rangle[71]^2 t_{126} \\
&((\langle 2|(1+7)|5\rangle(\langle 63\rangle[34]-\langle 65\rangle[54]) + \langle 6|(3+4)|5\rangle\langle 2|(1+7)|4\rangle) \\
&+ \langle 26\rangle^2[72]t_{127}(\langle 3|(2+6)|1\rangle(2\langle 64\rangle[45][74] + \langle 63\rangle([34][75]+[35][74]) \\
&+ [45](\langle 36\rangle[74]\langle 4|(2+6)|1\rangle + 2[75]\langle 35\rangle\langle 62\rangle[21] + \langle 63\rangle[75]\langle 5|(2+6)|1\rangle)) \\
&+ [71]\langle 36\rangle\langle 26\rangle t_{126}t_{127}(\langle 36\rangle([74][35]+[75][34]+[45]\langle|(4+5)|7\rangle)\Big\}\Big)
\end{aligned}
\tag{B.16}
$$

$$
\begin{aligned}
A_{21}(g_1^+g_2^-\gamma_5^+) \;=\;& 1/((\langle 17\rangle\langle 35\rangle[26]s_{12}s_{34}t_{126}t_{127}) \\
&\Big(\frac{1}{\langle 57\rangle t_{157}t_{346}}((\langle 36\rangle\langle 27\rangle[62]\langle 2|(3+6)|4\rangle\langle 3|(5+7)|1\rangle t_{126}t_{127}t_{157} \\
&\langle 27\rangle\langle 36\rangle^2\langle 57\rangle\langle 2|(1+7)|5\rangle[62][64][71]t_{126}t_{157} \\
&+ \langle 3|(2+6)|1\rangle t_{127}t_{346}(\langle 75\rangle\langle 2|(1+7)|5\rangle\langle 3|(2+6)|4\rangle t_{126} \\
&+ \langle 71\rangle\langle 2|(3+6)|4\rangle\langle 3|(5+7)|1\rangle t_{126} + \langle 71\rangle\langle 26\rangle\langle 3|(5+7)|4\rangle[61]t_{157})) \\
&+ \frac{[54]}{(s_{34}-t_{345})}((\langle 3|(4+5)(1+7)|1\rangle t_{126}(\langle 27\rangle\langle 36\rangle[62][71] - t_{127}\langle 3|(2+6)|1\rangle) \\
&- \langle 3|(4+5)|7\rangle\langle 17\rangle\langle 26\rangle\langle 3|(2+6)|1\rangle[61]t_{127})\Big)
\end{aligned}
\tag{B.17}
$$

$$
\begin{aligned}
B_{21}(g_1^+ g_2^- \gamma_5^+) \;=\;& 1/(\langle 17\rangle\langle 35\rangle[26]s_{12}s_{34}t_{126}t_{127}) \\
& \Big(\frac{1}{\langle 65\rangle t_{256}t_{347}}(\langle 17\rangle\langle 26\rangle[74]t_{127}(\langle 36\rangle\langle 2|(5+6)|1\rangle\langle 3|(4+7)|1\rangle[62]t_{126} \\
& + \langle 56\rangle\langle 3|(2+6)|1\rangle(\langle 3|(4+7)|1\rangle[65]t_{126} + \langle 3|(4+7)|5\rangle[61]t_{256})) \\
& + \langle 2|(1+7)|4\rangle t_{126}t_{347}(\langle 56\rangle\langle 3|(2+6)|1\rangle\langle 3|(2+6)|5\rangle t_{127} - \langle 27\rangle\langle 36\rangle[71]t_{256}))) \\
& + \frac{[45]}{(s_{34}-t_{345})}(t_{126}\langle 3|(4+5)(1+7)|2\rangle(\langle 27\rangle\langle 36\rangle[62][71] - t_{127}\langle 3|(2+6)|1\rangle) \\
& - t_{127}\langle 3|(2+6)|1\rangle\langle 3|(4+5)|7\rangle\langle 17\rangle\langle 26\rangle[61]) \Big) \qquad \text{(B.18)}
\end{aligned}
$$

We now want to use the amplitudes above to obtain amplitudes for all possible helicity configurations. We know that the helicities of the leptons and quarks are fixed as $l_3^-, \bar{l}_4^+, q_6^-, \bar{q}_7^+$, but the helicities of gluons and photon can be '+' or '–'.

We introduce the relation $\text{flip}_{W\gamma}$ where

$$
\text{flip}_{W\gamma} = 3 \leftrightarrow 4, 6 \leftrightarrow 7, \langle ab\rangle \leftrightarrow [ab] \qquad \text{(B.19)}
$$

- To reverse gluon and photon helicities, use $\text{flip}_{W\gamma}$. This also reverses gluon ordering and changes A amplitudes to B amplitudes and vice versa.

Examples of the use of $\text{flip}_{W\gamma}$ are:

$$
\begin{aligned}
A_{12}(g_1^- g_2^+ \gamma_5^+) &= \text{flip}_{W\gamma}[B_{21}(g_1^+ g_2^- \gamma_5^-)] \qquad \text{(B.20)} \\
B_{21}(g_1^- g_2^+ \gamma_5^-) &= \text{flip}_{W\gamma}[A_{12}(g_1^+ g_2^- \gamma_5^+)] \qquad \text{(B.21)}
\end{aligned}
$$

The only other relation that we need is to be able to swap the order of gluon 1 and gluon 2. When we do this by swapping $1 \leftrightarrow 2$ in the amplitudes, we also swap the helicity of g_1 for the helicity of g_2. Hence $1 \leftrightarrow 2$ on $A_{12}(g_1^+, g_2^+, \gamma_5^+)$ will give us $A_{21}(g_1^+, g_2^+, \gamma_5^+)$ but $1 \leftrightarrow 2$ on $A_{12}(g_1^+, g_2^-, \gamma_5^+)$ will result in $A_{21}(g_1^-, g_2^+, \gamma_5^+)$.

- To reverse the ordering of the gluons, use $1 \leftrightarrow 2$. This will also exchange helicities 1 and 2.

The two relations above are enough to relate all required helicities to those that are given above.

We now need the anomalous terms to add to these amplitudes. Here we just need four amplitudes, as each combines with both the A amplitude and the B amplitude.

The four independent amplitudes that we need are:

$$\mathcal{A}_{12}^{ac}(g_1^+ g_2^+ \gamma_5^+) \quad \mathcal{A}_{12}^{ac}(g_1^+ g_2^+ \gamma_5^-) \quad \mathcal{A}_{12}^{ac}(g_1^+ g_2^- \gamma_5^+) \quad \mathcal{A}_{21}^{ac}(g_1^+ g_2^- \gamma_5^+) \tag{B.22}$$

and explicit helicity amplitudes for these are given below.

$$\mathcal{A}_{12}^{ac}(g_1^+ g_2^+ \gamma_5^+) = \frac{[54]\langle 6|(1+2+7)|5\rangle \left(\frac{\lambda^\gamma}{M_W^2}\langle 34\rangle\langle 6|(3+5)|4\rangle + \Delta\kappa^\gamma\langle 36\rangle\right)}{2\langle 27\rangle\langle 12\rangle\langle 16\rangle s_{34}(t_{345}-s_{34})} \tag{B.23}$$

$$\mathcal{A}_{12}^{ac}(g_1^+ g_2^+ \gamma_5^-) = \frac{\langle 35\rangle\langle 56\rangle \left(\frac{\lambda^\gamma}{M_W^2}\langle 6|(1+2+7)(4+5)|3\rangle[34] + \Delta\kappa^\gamma\langle 6|(1+2+7)|4\rangle\right)}{2\langle 27\rangle\langle 12\rangle\langle 16\rangle s_{34}(t_{345}-s_{34})} \tag{B.24}$$

$$\begin{aligned}\mathcal{A}_{12}^{ac}(g_1^+ g_2^- \gamma_5^-) = {} & ([45]/(2\langle 16\rangle[27]s_{12}s_{34}t_{126}t_{127}(t_{345}-s_{34})) \\ & \{\langle 26\rangle^2[27][57]t_{127}\left(\frac{\lambda^\gamma}{M_W^2}\langle 34\rangle[4|(3+5)(2+6)|1] + \Delta\kappa^\gamma\langle 3|(2+6)1\rangle\right) \\ & + [17]t_{126}(\langle 16\rangle[17]\langle 2|(1+7)|5\rangle + \langle 26\rangle[75]t_{127}) \\ & \left(\frac{\lambda^\gamma}{M_W^2}\langle 34\rangle[4|(3+5)|6] + \Delta\kappa^\gamma\langle 36\rangle\right)\}\end{aligned} \tag{B.25}$$

$$\begin{aligned}\mathcal{A}_{21}^{ac}(g_1^+ g_2^- \gamma_5^+) = {} & ([45]/(2\langle 17\rangle[26]s_{12}s_{34}t_{126}t_{127}(t_{345}-s_{34})) \\ & \{\langle 27\rangle\langle 2|(1+7)|5\rangle[62][71]t_{126}\left(\frac{\lambda^\gamma}{M_W^2}\langle 34\rangle\langle 6|(5+3)|4\rangle + \langle 36\rangle\Delta\kappa^\gamma\right) \\ & + t_{127}(\langle 17\rangle\langle 26\rangle[61][75] - \langle 2|(1+7)|5\rangle t_{126}) \\ & \left(\frac{\lambda^\gamma}{M_W^2}\langle 34\rangle[4|(3+5)(2+6)|1] + \Delta\kappa^\gamma\langle 3|(2+6)|1\rangle\right)\}\end{aligned} \tag{B.26}$$

These anomalous amplitudes combine with the Standard Model amplitudes to give a complete amplitude for the helicity configuration.

$$A_{12}^{anom}(g_1^+ g_2^+ \gamma_5^+) = A_{12}^{SM}(g_1^+ g_2^+ \gamma_5^+) + \mathcal{A}_{12}^{ac}(g_1^+ g_2^+ \gamma_5^+) \tag{B.27}$$

$$B_{12}^{anom}(g_1^+ g_2^+ \gamma_5^+) = B_{12}^{SM}(g_1^+ g_2^+ \gamma_5^+) - \mathcal{A}_{12}^{ac}(g_1^+ g_2^+ \gamma_5^+) \tag{B.28}$$

All other helicity configurations can be found using the same relations as were required for the Standard Model case, but operating on A^{anom} and B^{anom} rather than the Standard Model A and B.

B.3 Helicity amplitudes for $gg \to Z\gamma q\bar{q}$

Here we present all the helicity amplitudes required for a calculation of $gg \to Z\gamma q\bar{q}$.

We already have the necessary amplitudes for the Standard Model case, as they can be obtained directly from the $W\gamma$ amplitudes given in Appendix B.2.

Here we only need to state the helicity amplitudes for anomalous couplings. We will always use the couplings

$$\tilde{h}_1^{Z/\gamma} = \frac{h_1^{Z/\gamma}}{M_Z^2}; \quad \tilde{h}_2^{Z/\gamma} = \frac{h_2^{Z/\gamma}}{M_Z^4}; \quad \tilde{h}_3^{Z/\gamma} = \frac{h_3^{Z/\gamma}}{M_Z^2}; \quad \tilde{h}_4^{Z/\gamma} = \frac{h_4^{Z/\gamma}}{M_Z^4} \tag{B.29}$$

Though we need amplitudes for every possible helicity configuration of the particles $\left(g_1^{h_1}, g_2^{h_2}, l_3^{h_3}, \bar{l}_4^{h_4}, \gamma_5^{h_5}, q_6^{h_6}, \bar{q}_7^{h_7}\right)$ we can obtain all results from just four explicit helicity amplitudes:

$$\mathcal{A}_{12}^{Z/\gamma,ac}(g_1^+ g_2^+ \gamma_5^+) \quad \mathcal{A}_{12}^{Z/\gamma,ac}(g_1^+ g_2^+ \gamma_5^-) \quad \mathcal{A}_{12}^{Z/\gamma,ac}(g_1^+ g_2^- \gamma_5^+) \quad \mathcal{A}_{21}^{Z/\gamma,ac}(g_1^+ g_2^- \gamma_5^+) \tag{B.30}$$

$\mathcal{A}^{Z,ac}$ has an intermediate Z (a $ZZ\gamma$ vertex) while $\mathcal{A}^{\gamma,ac}$ has an intermediate photon (a $Z\gamma\gamma$ vertex).

The necessary amplitudes can be written explicitly (suppressing the helicities of the quarks and leptons, which are always $l_3^-, \bar{l}_4^+, q_6^-, \bar{q}_7^+$) as:

$$
\begin{aligned}
\mathcal{A}_{12}^{Z/\gamma,ac}(g_1^+,g_2^+,\gamma_5^+) &= \frac{[45]\langle 6|3+4|5\rangle}{4\langle 12\rangle\langle 27\rangle\langle 61\rangle s_{34}}(2(\tilde{h}_1^{Z/\gamma}-i\tilde{h}_3^{Z/\gamma})\langle 63\rangle \\
&\quad -(\tilde{h}_2^{Z/\gamma}-i\tilde{h}_4^{Z/\gamma})\langle 6|(3+4)|5\rangle\langle 53\rangle)
\end{aligned}
\tag{B.31}
$$

$$
\begin{aligned}
\mathcal{A}_{12}^{Z/\gamma,ac}(g_1^+,g_2^+,\gamma_5^-) &= \frac{\langle 56\rangle\langle 53\rangle}{4\langle 12\rangle\langle 27\rangle\langle 61\rangle s_{34}}(2(\tilde{h}_1^{Z/\gamma}-i\tilde{h}_3^{Z/\gamma})\langle 6|(3+5)|4\rangle \\
&\quad +(\tilde{h}_2^{Z/\gamma}-i\tilde{h}_4^{Z/\gamma})[45]\langle 65\rangle t_{345})
\end{aligned}
\tag{B.32}
$$

$$
\begin{aligned}
\mathcal{A}_{12}^{Z/\gamma,ac}(g_1^+,g_2^-,\gamma_5^+) &= \frac{[54]}{4\langle 16\rangle s_{12}s_{34}}\Bigg(\frac{\langle 26\rangle^2[75]}{t_{126}}(2(\tilde{h}_1^{Z/\gamma}-i\tilde{h}_3^{Z/\gamma})\langle 3|(2+6)|1\rangle \\
&\quad +(\tilde{h}_2^{Z/\gamma}-i\tilde{h}_4^{Z/\gamma})\langle 53\rangle[5|(3+4)(2+6)|1]) \\
&\quad +\frac{[71]}{[72]t_{127}}([75]\langle 62\rangle(s_{12}+s_{27})+\langle 12\rangle[71]\langle 6|(1+7)|5\rangle) \\
&\quad (2(\tilde{h}_1^{Z/\gamma}-i\tilde{h}_3^{Z/\gamma})\langle 36\rangle+(\tilde{h}_2^{Z/\gamma}-i\tilde{h}_4^{Z/\gamma})\langle 53\rangle\langle 6|(3+4)|5\rangle)\Bigg)
\end{aligned}
\tag{B.33}
$$

$$
\begin{aligned}
\mathcal{A}_{21}^{Z/\gamma,ac}(g_1^+,g_2^-,\gamma_5^+) &= \frac{[54]}{4s_{12}s_{34}}\Bigg(\frac{\langle 72\rangle[17]\langle 2|(1+7)|5\rangle}{\langle 17\rangle t_{127}}(2(\tilde{h}_1^{Z/\gamma}-i\tilde{h}_3^{Z/\gamma})\langle 36\rangle \\
&\quad +(\tilde{h}_2^{Z/\gamma}-i\tilde{h}_4^{Z/\gamma})\langle 53\rangle[5|(3+4)|6]) \\
&\quad +\frac{1}{[26]\langle 17\rangle t_{126}}(\langle 12\rangle[61]\langle 6|(1+7)|5\rangle+(s_{12}+s_{26})\langle 2|(1+7)|5\rangle) \\
&\quad (2(\tilde{h}_1^{Z/\gamma}-i\tilde{h}_3^{Z/\gamma})\langle 3|(2+6)|1\rangle \\
&\quad (\tilde{h}_2^{Z/\gamma}-i\tilde{h}_4^{Z/\gamma})\langle 53\rangle[5|(3+4)(2+6)1])\Bigg)
\end{aligned}
\tag{B.34}
$$

Once we have these amplitudes, we can obtain all other helicity configurations.

- To reverse helicities of l_3 and $\bar{l}_4$, use $3 \leftrightarrow 4$ in the above amplitudes.
- To reverse helicities of q_6 and $\bar{q}_7$, use $6 \leftrightarrow 7$ in the above amplitudes.

Reversing the helicities of g_1 and g_2 is a little bit more complicated, as here the ordering of the gluons matters. By swapping $1 \leftrightarrow 2$ in the amplitudes, we reverse the ordering of the gluons. If both gluons have the same helicity, then this is just a simple swap from A_{12} to A_{21} or vice versa. However, if the gluons have different helicities, we go from $A_{12}(g_1^+ g_2^-)$ to $A_{21}(g_1^- g_2^+)$ and from $A_{12}(g_1^- g_2^+)$ to $A_{21}(g_1^+ g_2^-)$.

- To exchange g_1 (with helicity 1) for g_2 (with helicity 2), use $1 \leftrightarrow 2$.

These equations give us all helicities with $g_1^+ g_2^+ \gamma_5^+$, $g_1^+ g_2^+ \gamma_5^-$, $g_1^+ g_2^- \gamma_5^+$ and $g_1^- g_2^+ \gamma_5^+$, with either gluon ordering. But we still need to fill in the remaining helicities and to do this we need a 'flip' relation. $\mathrm{flip}_{Z\gamma}$ reverses the helicity of the gluons and photon, while keeping quarks and leptons unchanged, and also reverses gluon ordering.

$$\mathrm{flip}_{Z\gamma} = 3 \leftrightarrow 4, 6 \leftrightarrow 7, \langle ab \rangle \leftrightarrow [ab], \tilde{h}_{1,2}^{Z/\gamma} \to -\tilde{h}_{1,2}^{Z/\gamma} \tag{B.35}$$

An example:

$$A_{21}(g_1^-, g_2^+, \gamma_5^-) = \mathrm{flip}_{Z\gamma}[A_{12}(g_1^+, g_2^-, \gamma_5^+)] \tag{B.36}$$

- To reverse all gluon and photon helicities use $\mathrm{flip}_{Z\gamma}$. This reverses the gluon ordering, but leaves quark and lepton helicities unchanged.

We may also combine the relations to fill in the remaining gaps.

$$A_{12}(g_1^-, g_2^-, l_3^+, \bar{l}_4^-, \gamma_5^-, q_6^+, \bar{q}_7^-) = \mathrm{flip}_{Z\gamma}[A_{12}(g_1^+, g_2^+, l_3^-, \bar{l}_4^+, \gamma_5^+, q_6^-, \bar{q}_7^+)]_{1\leftrightarrow 2, 3\leftrightarrow 4, 6\leftrightarrow 7} \tag{B.37}$$

though of course in this case it helps to combine the relations in advance:

$$A_{12}(g_1^-, g_2^-, l_3^+, \bar{l}_4^-, \gamma_5^-, q_6^+, \bar{q}_7^-) = [A_{12}(g_1^+, g_2^+, l_3^-, \bar{l}_4^+, \gamma_5^+, q_6^-, \bar{q}_7^+)]_{1\leftrightarrow 2, \tilde{h}_{12}^{Z/\gamma} \to -\tilde{h}_{12}^{Z/\gamma}, \langle ab \rangle \leftrightarrow [ab]} \tag{B.38}$$

- To reverse all the helicities of an amplitude at once (also reversing the gluon ordering), use $\tilde{h}_{1,2}^{Z/\gamma} \to -\tilde{h}_{1,2}^{Z/\gamma}$, $\langle ab \rangle \leftrightarrow [ab]$.

Bibliography

[1] U. Baur *et al.*, (2000), hep-ph/0005226.

[2] ATLAS Detector and Physics Performance. Technical Design Report, CERN-LHCC-99-15, 1999.

[3] V. A. Mitsou, (2000), hep-ph/0004161.

[4] K. T. Matchev and D. M. Pierce, Phys. Rev. **D60**, 075004 (1999), hep-ph/9904282.

[5] H. Baer, M. Drees, F. Paige, P. Quintana, and X. Tata, Phys. Rev. **D61**, 095007 (2000), hep-ph/9906233.

[6] ALEPH Collaboration, D. Abbaneo *et al.*, (2001), hep-ex/0112021.

[7] D. Fayolle, (2002), hep-ex/0201035.

[8] J. Ellison and J. Wudka, (1998), hep-ph/9804322.

[9] T. Barklow *et al.*, (1996), hep-ph/9611454.

[10] R. W. Brown, D. Sahdev, and K. O. Mikaelian, Phys. Rev. **D20**, 1164 (1979).

[11] R. W. Brown and K. O. Mikaelian, Phys. Rev. **D19**, 922 (1979).

[12] F. M. Renard, Nucl. Phys. **B196**, 93 (1982).

[13] J. Ohnemus, Phys. Rev. **D44**, 1403 (1991).

[14] S. Frixione, Nucl. Phys. **B410**, 280 (1993).

[15] J. Ohnemus and J. F. Owens, Phys. Rev. **D43**, 3626 (1991).

[16] B. Mele, P. Nason, and G. Ridolfi, Nucl. Phys. **B357**, 409 (1991).

[17] J. Smith, D. Thomas, and W. L. van Neerven, Z. Phys. **C44**, 267 (1989).

[18] J. Ohnemus, Phys. Rev. **D47**, 940 (1993).

[19] J. Ohnemus, Phys. Rev. **D44**, 3477 (1991).

[20] S. Frixione, P. Nason, and G. Ridolfi, Nucl. Phys. **B383**, 3 (1992).

[21] J. F. Gunion and Z. Kunszt, Phys. Rev. **D33**, 665 (1986).

[22] J. Ohnemus, Phys. Rev. **D50**, 1931 (1994), hep-ph/9403331.

[23] J. Ohnemus, Phys. Rev. **D51**, 1068 (1995), hep-ph/9407370.

[24] U. Baur, T. Han, and J. Ohnemus, Phys. Rev. **D57**, 2823 (1998), hep-ph/9710416.

[25] L. J. Dixon, Z. Kunszt, and A. Signer, Nucl. Phys. **B531**, 3 (1998), hep-ph/9803250.

[26] L. J. Dixon, Z. Kunszt, and A. Signer, Phys. Rev. **D60**, 114037 (1999), hep-ph/9907305.

[27] D. de Florian and A. Signer, Eur. Phys. J. **C16**, 105 (2000), hep-ph/0002138.

[28] J. M. Campbell and R. K. Ellis, Phys. Rev. **D60**, 113006 (1999), hep-ph/9905386.

[29] E. Accomando, A. Denner, and S. Pozzorini, (2001), hep-ph/0110114.

[30] L. Ametller, E. Gava, N. Paver, and D. Treleani, Phys. Rev. **D32**, 1699 (1985).

[31] U. Baur and E. W. N. Glover, Nucl. Phys. **B347**, 12 (1990).

[32] K. Hagiwara, R. D. Peccei, D. Zeppenfeld, and K. Hikasa, Nucl. Phys. **B282**, 253 (1987).

[33] K. J. F. Gaemers and G. J. Gounaris, Zeit. Phys. **C1**, 259 (1979).

[34] G. J. Gounaris, J. Layssac, and F. M. Renard, Phys. Rev. **D61**, 073013 (2000), hep-ph/9910395.

[35] K. Hagiwara, J. Woodside, and D. Zeppenfeld, Phys. Rev. **D41**, 2113 (1990).

[36] U. Baur and E. L. Berger, Phys. Rev. **D47**, 4889 (1993).

[37] U. Baur, T. Han, and J. Ohnemus, Phys. Rev. **D48**, 5140 (1993), hep-ph/9305314.

[38] U. Baur, T. Han, and J. Ohnemus, Phys. Rev. **D51**, 3381 (1995), hep-ph/9410266.

[39] U. Baur, T. Han, and J. Ohnemus, Phys. Rev. **D53**, 1098 (1996), hep-ph/9507336.

[40] M. Weber, (2002), hep-ex/0205024.

[41] K. Hagiwara, S. Ishihara, R. Szalapski, and D. Zeppenfeld, Phys. Rev. **D48**, 2182 (1993).

[42] W. J. Stirling and A. Werthenbach, Eur. Phys. J. **C14**, 103 (2000), hep-ph/9903315.

[43] L3, P. Achard *et al.*, Phys. Lett. **B540**, 43 (2002), hep-ex/0206050.

[44] L3, P. Achard *et al.*, Phys. Lett. **B527**, 29 (2002), hep-ex/0111029.

[45] F. A. Berends, R. Kleiss, P. De Causmaecker, R. Gastmans, and T. T. Wu, Phys. Lett. **B103**, 124 (1981).

[46] P. De Causmaecker, R. Gastmans, W. Troost, and T. T. Wu, Nucl. Phys. **B206**, 53 (1982).

[47] R. Kleiss and W. J. Stirling, Nucl. Phys. **B262**, 235 (1985).

[48] R. Gastmans and T. T. Wu, *The Ubiquitous Photon: Helicity method for QED and QCD*, International series of monographs on physics No. 80 (Clarendon, Oxford, UK, 1990).

[49] Z. Xu, D.-H. Zhang, and L. Chang, Nucl. Phys. **B291**, 392 (1987).

[50] J. F. Gunion and Z. Kunszt, Phys. Lett. **B161**, 333 (1985).

[51] M. L. Mangano and S. J. Parke, Phys. Rept. **200**, 301 (1991).

[52] L. J. Dixon, Calculating scattering amplitudes efficiently, In Soper [92], hep-ph/9601359.

[53] R. K. Ellis, W. J. Stirling, and B. R. Webber, *QCD and Collider Physics* (Cambridge University Press, 1996).

[54] S. Wolfram, *Mathematica*, Fourth ed. (Wolfram Research, Inc, Champaign, Illinois, 1999).

[55] K. L. Adamson, D. de Florian, and A. Signer, Phys. Rev. **D65**, 094041 (2002), hep-ph/0202132.

[56] J. J. van der Bij and E. W. N. Glover, Phys. Lett. **B206**, 701 (1988).

[57] E. W. N. Glover and J. J. van der Bij, Phys. Lett. **B219**, 488 (1989).

[58] A. Signer, *Helicity Method for Next-to-Leading Order Corrections in QCD*, PhD thesis, ETH-Zurich, 1995.

[59] Z. Bern, L. J. Dixon, and D. A. Kosower, Nucl. Phys. **B513**, 3 (1998), hep-ph/9708239.

[60] C.-N. Yang, Phys. Rev. **77**, 242 (1950).

[61] K. Hagiwara, T. Kuruma, and Y. Yamada, Nucl. Phys. **B358**, 80 (1991).

[62] M. E. Peskin and D. V. Schroeder, *An Introduction to Quantum Field Theory* (Addison-Wesley, Reading, USA, 1995).

[63] F. Bloch and A. Nordsieck, Phys. Rev. **52**, 54 (1937).

[64] T. Muta, *Foundations of Quantum Chromodynamics*, Lecture Notes in Physics No. 57, Second ed. (World Scientific, 1998).

[65] T. Kinoshita, J. Math. Phys. **3**, 650 (1962).

[66] T. D. Lee and M. Nauenberg, Phys. Rev. **133**, B1549 (1964).

[67] J. C. Collins, D. E. Soper, and G. Sterman, Factorization of hard processes in QCD, in *Perturbative Quantum Chromodynamics*, edited by A. H. Mueller, , Advanced Series on Directions in High Energy Physics No. 5, pp. 1–91, World Scientific, Singapore, 1989.

[68] H. Baer, J. Ohnemus, and J. F. Owens, Phys. Rev. **D40**, 2844 (1989).

[69] W. T. Giele and E. W. N. Glover, Phys. Rev. **D46**, 1980 (1992).

[70] W. T. Giele, E. W. N. Glover, and D. A. Kosower, Nucl. Phys. **B403**, 633 (1993), hep-ph/9302225.

[71] Z. Kunszt, From scattering amplitudes to cross sections in QCD, In Soper [92], hep-ph/9603235.

[72] R. K. Ellis, D. A. Ross, and A. E. Terrano, Nucl. Phys. **B178**, 421 (1981).

[73] Z. Kunszt and D. E. Soper, Phys. Rev. **D46**, 192 (1992).

[74] Z. Bern, L. J. Dixon, D. C. Dunbar, and D. A. Kosower, Nucl. Phys. **B425**, 217 (1994), hep-ph/9403226.

[75] Z. Bern and G. Chalmers, Nucl. Phys. **B447**, 465 (1995), hep-ph/9503236.

[76] Z. Bern, V. Del Duca, and C. R. Schmidt, Phys. Lett. **B445**, 168 (1998), hep-ph/9810409.

[77] Z. Bern, V. Del Duca, W. B. Kilgore, and C. R. Schmidt, Phys. Rev. **D60**, 116001 (1999), hep-ph/9903516.

[78] D. A. Kosower and P. Uwer, Nucl. Phys. **B563**, 477 (1999), hep-ph/9903515.

[79] J. M. Campbell and E. W. N. Glover, Nucl. Phys. **B527**, 264 (1998), hep-ph/9710255.

[80] S. Catani and M. Grazzini, Phys. Lett. **B446**, 143 (1999), hep-ph/9810389.

[81] S. Catani and M. Grazzini, Nucl. Phys. **B591**, 435 (2000), hep-ph/0007142.

[82] S. Catani and M. Grazzini, Nucl. Phys. **B570**, 287 (2000), hep-ph/9908523.

[83] V. Del Duca, A. Frizzo, and F. Maltoni, Nucl. Phys. **B568**, 211 (2000), hep-ph/9909464.

[84] S. Frixione, Z. Kunszt, and A. Signer, Nucl. Phys. **B467**, 399 (1996), hep-ph/9512328.

[85] G. P. Lepage, VEGAS: an Adaptive Multidimensional Integration Program, CLNS-80/447.

[86] S. Frixione, Phys. Lett. **B429**, 369 (1998), hep-ph/9801442.

[87] A. D. Martin, R. G. Roberts, W. J. Stirling, and R. S. Thorne, (2001), hep-ph/0110215.

[88] S. Dittmaier, M. Bohm, and A. Denner, Nucl. Phys. **B376**, 29 (1992), Erratum-ibid.B376 483 (1992).

[89] W. Beenakker *et al.*, (1996), hep-ph/9602351.

[90] D. W. Duke and J. F. Owens, Phys. Rev. **D30**, 49 (1984).

[91] Z. Bern, L. Dixon, and C. Schmidt, (2002), hep-ph/0206194.

[92] D. E. Soper, editor, *QCD and Beyond. Proceedings, Theoretical Advanced Study Institute in Elementary Particle Physics, TASI-95, Boulder, USA, June 4-30, 1995*, World Scientific, 1996.